Global and Planetary Change 73 (2010) 15–113

Contents lists available at ScienceDirect

Global and Planetary Change

journal homepage: www.elsevier.com/locate/gloplacha

Depositional environments and cyclo- and chronostratigraphy of uppermost Carboniferous–Lower Triassic fluvial–lacustrine deposits, southern Bogda Mountains, NW China — A terrestrial paleoclimatic record of mid-latitude NE Pangea

Wan Yang [a,*], Qiao Feng [b], Yiqun Liu [c], Neil Tabor [d], Dan Miggins [e], James L. Crowley [f], Jinyan Lin [c], Stephanie Thomas [d]

[a] Department of Geological Sciences & Engineering, Missouri University of Science & Technology, Rolla, Missouri 65409, USA
[b] College of Geoinformation Science and Engineering, Shangdong University of Science and Technology, Qingdao, China
[c] Department of Geology, Northwestern University, Xian, China
[d] Department of Geological Sciences, Southern Methodist University, Dallas, Texas, 75275, USA
[e] Denver Argon Geochronology Laboratory, U.S. Geological Survey, Denver Federal Center, Box 25046, MS 974, Denver, Colorado, 80225, USA
[f] Department of Geosciences, Boise State University, Boise, Idaho, 83725, USA

ARTICLE INFO

Article history:
Received 3 March 2008
Accepted 26 March 2010
Available online 11 June 2010

Keywords:
Permian–Early Triassic
Stratigraphy
Continental climate
Fluvial–lacustrine
China

ABSTRACT

Two uppermost Carboniferous–Lower Triassic fluvial–lacustrine sections in the Tarlong–Taodonggou half-graben, southern Bogda Mountains, NW China, comprise a 1834 m-thick, relatively complete sedimentary and paleoclimatic record of the east coast of mid-latitude NE Pangea. Depositional environmental interpretations identified three orders (high, intermediate, and low) of sedimentary cycles. High-order cycles (HCs) have five basic types, including fluvial cycles recording repetitive changes of erosion and deposition and lacustrine cycles recording repetitive environmental changes associated with lake expansion and contraction. HCs are grouped into intermediate-order cycles (ICs) on the basis of systematic changes of thickness, type, and component lithofacies of HCs. Nine low-order cycles (LCs) are demarcated by graben-wide surfaces across which significant long-term environmental changes occurred. A preliminary cyclostratigraphic framework provides a foundation for future studies of terrestrial climate, tectonics, and paleontology in mid-latitude NE Pangea.

Climate variabilities at the intra-HC, HC, IC, and LC scales were interpreted from sedimentary and paleosol evidence. Four prominent climatic shifts are present: 1) from the humid–subhumid to highly-variable subhumid–semiarid conditions at the beginning of Sakamarian; 2) from highly-variable subhumid–semiarid to humid–subhumid conditions across the Artinskian-Capitanian unconformity; 3) from humid–subhumid to highly-variable subhumid–semiarid conditions at early Induan; and 4) from the highly-variable subhumid–semiarid to humid–subhumid conditions across the Olenekian-Anisian unconformity. The stable humid–subhumid condition from Lopingian to early Induan implies that paleoclimate change may not have been the cause of the end-Permian terrestrial mass extinction. A close documentation of the pace and timing of the extinction and exploration of other causes are needed. In addition, the semiarid–subhumid conditions from Sakamarian to Artinskian–Kungurian (?) and from middle Induan to end of Olenekian are in conflict with modern mid-latitude east coast meso- and macrothermal humid climate. Extreme continentality, regional orographic effect, and/or abnormal circulation of Paleo-Tethys maybe are possible causes. Our work serves as a rare data point at mid-latitude NE Pangea for climate modeling to seek explanations on the origin(s) of climate variability in NE Pangea from latest Carboniferous to Early Triassic.

1. Introduction

The pace and cause(s) of end-Permian mass extinction have been in debate (e.g., Erwin, 1993, 2002; Knoll et al., 1996; Isozaki, 1997; Ward et al., 2005). A global cause would have had a significant impact on both marine and terrestrial climate and ecologic conditions. In fact, impact on the terrestrial environments would have been more severe than that on the marine environments because of the lack of oceanic buffering on land. In addition, a progressive cause could have left a record of progressive changes over the time span much longer than the end-Permian. Hence, a continental climate history of the entire Permian is critical to understanding the causes and dynamics of mass extinction. However, the rarity of continuous Permo–Triassic continental records, especially in the mid- to high-latitude of northern

* Corresponding author.
E-mail address: wan.yang@wichita.edu (W. Yang).

0921-8181/$ – see front matter © 2010 Elsevier B.V. All rights reserved.
doi:10.1016/j.gloplacha.2010.03.008

Pangea, has limited the documentation of climatic variability of Pangea (e.g., Stollhofen, et al., 2000; Yin et al., 2001; Scheffler, et al., 2006; Tabor et al., 2007; Ward et al., 2005; Montañez, et al., 2007; Fielding et al., 2008). This paper summarizes the up-to-date observations and interpretations of the cyclostratigraphy and paleoclimate variability of two superbly-exposed uppermost Carboniferous–Lower Triassic sections in NW China. The sections provide a relatively continuous sedimentary and paleoclimatic record in the mid-latitude of NE Pangea. Depositional environmental interpretations from field and laboratory observations established a three-order cyclostratigraphic framework. Preliminary climatic interpretations from lithology, paleosols, and depositional systems within the framework identified four levels of climate variability at 0.1–100-m scales. The results establish a foundation for future detailed reconstruction of latest Carboniferous–Early Triassic continental climate and ecologic evolution in the mid-latitude NE Pangea.

1.1. Geological background

The study area covers ~88 km^2 and is ~15 km north of Daheyan in the southern foothills of Bogda Mountains, Xinjiang Uygur Autonomous Region, NW China (Fig. 1A, B). It is largely occupied by a west-plunging syncline (Fig. 1C). The Bogda Mountains are a giant anticline, contain Devonian to Quaternary sedimentary and igneous rocks, and separate the Turpan–Hami Basin to the south from the Junggar Basin to the north–northwest (Zhang, 1981). Permo–Triassic fluvial and lacustrine deposits are exposed along the foothills of Bogda Mountains (Liao et al, 1987; Cheng and Lucas, 1993; Carroll et al., 1995; Wartes et al., 2002; Greene et al., 2005; Yang et al., 2007a; Metcalfe et al., 2008). They were deposited in the greater Turpan–Junggar rift basin on the uppermost Carboniferous (based on newest ages in this study, see below) volcanic-arc basement formed by collision between the Junggar and Northern Tianshan plates (Fig. 1D; Allen et al., 1995; Yang, 2008; cf. Carroll et al., 1995; Shao et al., 1999; Greene et al., 2005). Lake expansion and contraction and source uplift to the south (e.g., Shao et al., 2001; Wartes et al., 2002; Greene et al., 2005) had occurred episodically in the region during the Permian to Early Triassic. Continental rifting was probably caused by regional sinistral shearing (Allen et al., 1995; Sengor and Nat'lin, 1996). Yang (2008) speculated that the Permo–Triassic paleogeography of the greater Turpan–Junggar basin is similar to that of the Quaternary Basin and Range Province of western US, both with active alluvial and lacustrine sedimentations in many small grabens and half grabens (Fig. 1D; see also Allen et al., 1995; Sengor and Nat'lin, 1996). Rapid lateral facies and thickness changes in the study area with reference to the stratal and basin geometries on seismic sections in nearby Turpan–Hami Basin (Fig. 1D; Yang, 2008; Yang et al., 2009) suggest that the uppermost Carboniferous–Lower Triassic strata were deposited in a half graben (named here as Tarlong–Taodonggou half graben). Finally, recent plate tectonic reconstruction places the study area near the NW coast of the Paleo-Tethys at the easternmost Kazakhstan Plate, which had migrated northward from ~40 to 50°N paleo-latitude during Kungurian–Wuchiapingian time (Sengor and Nat'lin, 1996; Ziegler et al., 1997; Scotese, 2001). Thus, a humid east-coast meso- and macro-thermal climate is expected in the greater Turpan-Junggar basin.

1.2. Stratigraphy

The Carboniferous–Triassic chronostratigraphy in the greater Turpan–Junggar basin is poorly constrained mainly by biostratigraphy of invertebrates (mainly ostracods and choncostracans), plants, spores and pollens, and vertebrates (Fig. 2; Zhang, 1981; Liao et al., 1987; Cheng and Lucas, 1993; Zhou et al., 1997; Liu, 2000; Wartes et al., 2002; Zhu et al., 2005; Metcalfe et al., 2008; and references within). A relatively detailed biostratigraphy is only available for short intervals about the Permo–Triassic boundary at limited locations, such as Taodonggou in the study area (Liao et al., 1987; Cheng et al., 1996; Zhou et al., 1997; Liu, 2000).

The previously-reported Permo–Triassic litho- and chronostratigraphy in the Taodonggou area (e.g., Zhang, 1981; Liao et al., 1987; Cheng et al., 1996; Liu, 2000; Wartes et al., 2002) was extended to the Tarlong area through physical tracking and cyclostratigraphic correlation in this study (Fig. 2). Eight ages from five sample sites were obtained through $^{40}Ar/^{39}Ar$, SHRIMP, and/or IDTIMS geochronological analyses in this study (Fig. 2; Appendix). Biotite and sanidine from the ash-flow tuff underneath the Daheyan–Taoxigou unconformity in Taodonggou are dated as 301.61 and 300 Ma, respectively, through $^{40}Ar/^{39}Ar$ geochronological analysis. The ages constrain the Taoxigou Group (Liao et al, 1987) as no younger than late Gzhelian. Zircons in an ash-fall tuff in the uppermost lower Daheyan LC yield an age of 301.26 Ma (IDTIMS) and a less accurate age of 295.5 Ma (SHRIMP). The four ages do not constrain the duration of the unconformity, but lower the base of the lower Daheyan LC from Kungurian to late Gzhelian and, using the IDTIMS age of 301.26 Ma, the top of the lower Daheyan is also lowered to late Gzhelian (Fig. 2).

The middle Daheyan, upper Daheyan, Lucaogou, and Hongyanchi LCs are constrained to a late Gzhelian–Artinskian age by an age of 281.42 Ma obtained from a volcanic ash in profundal shale in the uppermost Hongyanchi in SE Tarlong (Fig. 2; Appendix). The shale was cut by a meandering stream of the overlying Quanzijie LC. Correlation with the NE and SW Tarlong and Taodonggou sections indicates that the ash-bearing interval in SE Tarlong correlates to a surface ~38 m below the top of the Hongyanchi LC in NE Tarlong, suggesting significant erosion had occurred in SE Tarlong. Hence, the age is likely that of the middle–upper Hongyanchi LC. No absolute radiometric dates are available to constrain the individual ages of middle and upper Daheyan, Lucaogou, and Hongyanchi LCs (cf. Zhu et al., 2005). The thickness of the LCs in NE Tarlong section, the age (301 Ma) at the uppermost lower Daheyan LC, and the age (281.42 Ma) at the surface ~38 m below the top of the Hongyanchi LC are used to calculate an average sedimentation rate, which is used to calculate the duration of individual LCs in proportion to their thicknesses. These crude estimates place the middle Daheyan LC between the upper Gzhelian and basal Sakamarian (301–294 Ma), the upper Daheyan LC between basal Sakamarian and lower–middle Sakamarian (294–291 Ma), the Lucaogou LC between lower–middle Sakamarian and basal Artinskian (291–284 Ma), and the Hongyanchi LC between basal and middle Artinskian (284–280 Ma). The radiometric dates indicate the great uncertainty of previous biostratigraphy-based chronostratigraphy for the Lower Permian. For example, the interval from lower Daheyan to Hongyanchi LCs spans maximum ~10 m.y. previously but minimum 21 m.y. after the revision (Fig. 2).

Fig. 1. (A) Paleotectonic and paleogeographic reconstruction of Pangea at Late Permian (255 Ma) of Scotese (2001), showing the study area (star) in the easternmost Kazakhstan Plate which migrated from ~40 to 50°N during Kungurian to Wuchiapingian time (Ziegler et al., 1997). (B) Map showing the study area in Xinjiang, NW China. (C) Geological map of the study area showing location of NE Tarlong, Taodonggou, and other sections (thick black lines) in a syncline in southern Bogda Mountains. Basemaps are 1:10,000-scale topographic maps. Modified from Yang et al. (2007a). (D) An interpreted 2-D seismic section ~70 km ESE of the study area in Tainan Depression of the Turpan–Hami Basin, showing stratal and structural geometries of small half grabens developed above the Carboniferous–Devonian basement and capped by Unconformity 1 during the rifting phase, and enlarged half grabens developed between unconformities 1 and 2 during the early drifting phase. Blue dashed lines outline some depositional systems. Red lines are faults. The other lines are sequence boundaries of varying orders. Seismic sequence stratigraphic interpretation indicates that the sediment fills in the small and large half grabens are of a Permo–Triassic age. Modified from Yang (2008).

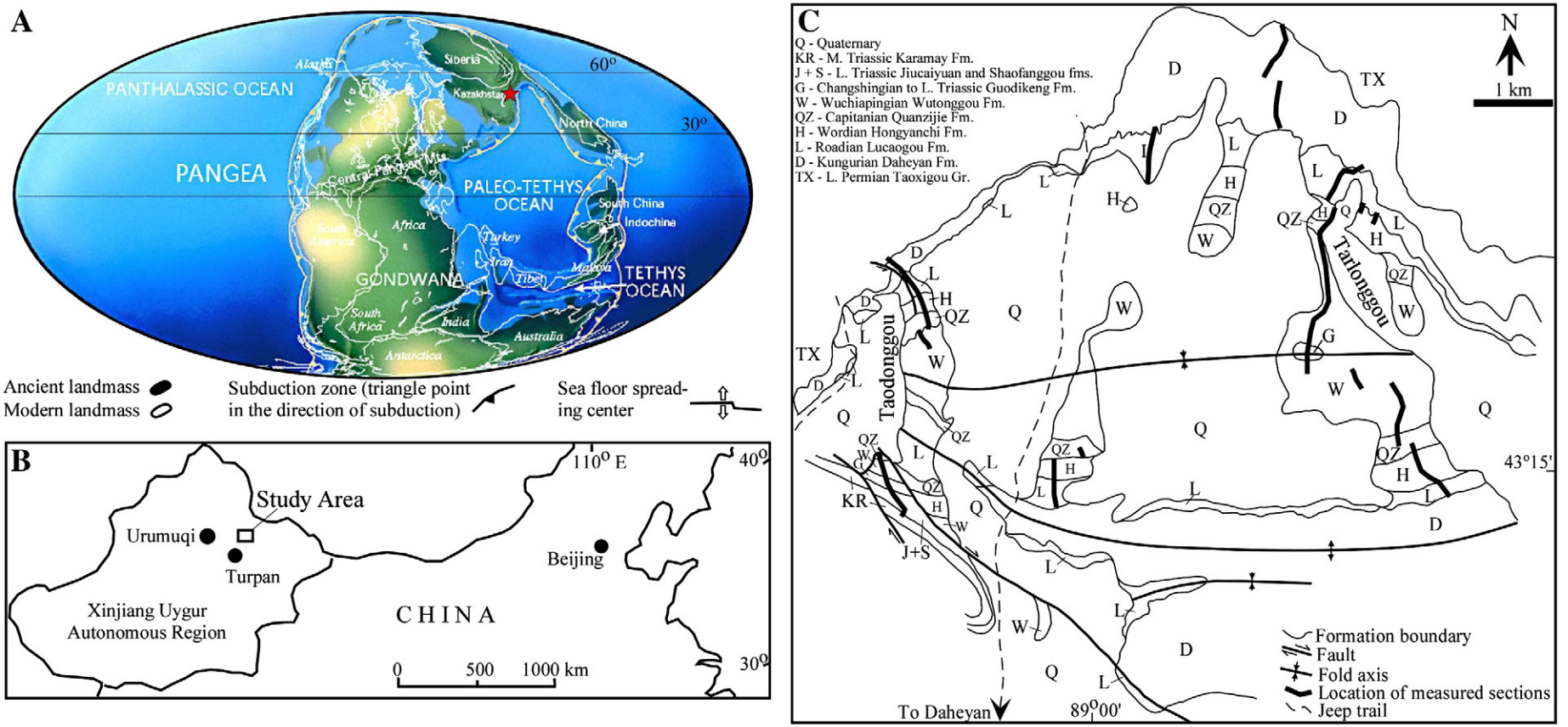
A
PANTHALASSIC OCEAN
PANGEA
PALEO-TETHYS OCEAN
TETHYS OCEAN
GONDWANA
Siberia
Kazakhstan
North China
South China
Indochina
Africa
Turkey
Iran
Tibet
Malaya
India
Australia
Antarctica
South Africa
South America
Central Pangean Mts
60°
30°
Ancient landmass
Modern landmass
Subduction zone (triangle point in the direction of subduction)
Sea floor spreading center
B
Study Area
Urumuqi
Turpan
Beijing
Xinjiang Uygur Autonomous Region
CHINA
110° E
40°
30°
0 500 1000 km
C
Q - Quaternary
KR - M. Triassic Karamay Fm.
J + S - L. Triassic Jiucaiyuan and Shaofanggou fms.
G - Changshingian to L. Triassic Guodikeng Fm.
W - Wuchiapingian Wutonggou Fm.
QZ - Capitanian Quanzijie Fm.
H - Wordian Hongyanchi Fm.
L - Roadian Lucaogou Fm.
D - Kungurian Daheyan Fm.
TX - L. Permian Taoxigou Gr.
N
1 km
Taodonggou
Tarlonggou
To Daheyan
89°00'
43°15'
Formation boundary
Fault
Fold axis
Location of measured sections
Jeep trail
D
SSW
NNE
1
2
Carboniferous-Devonian basement
1 km
1 sec. (2-way travel time)

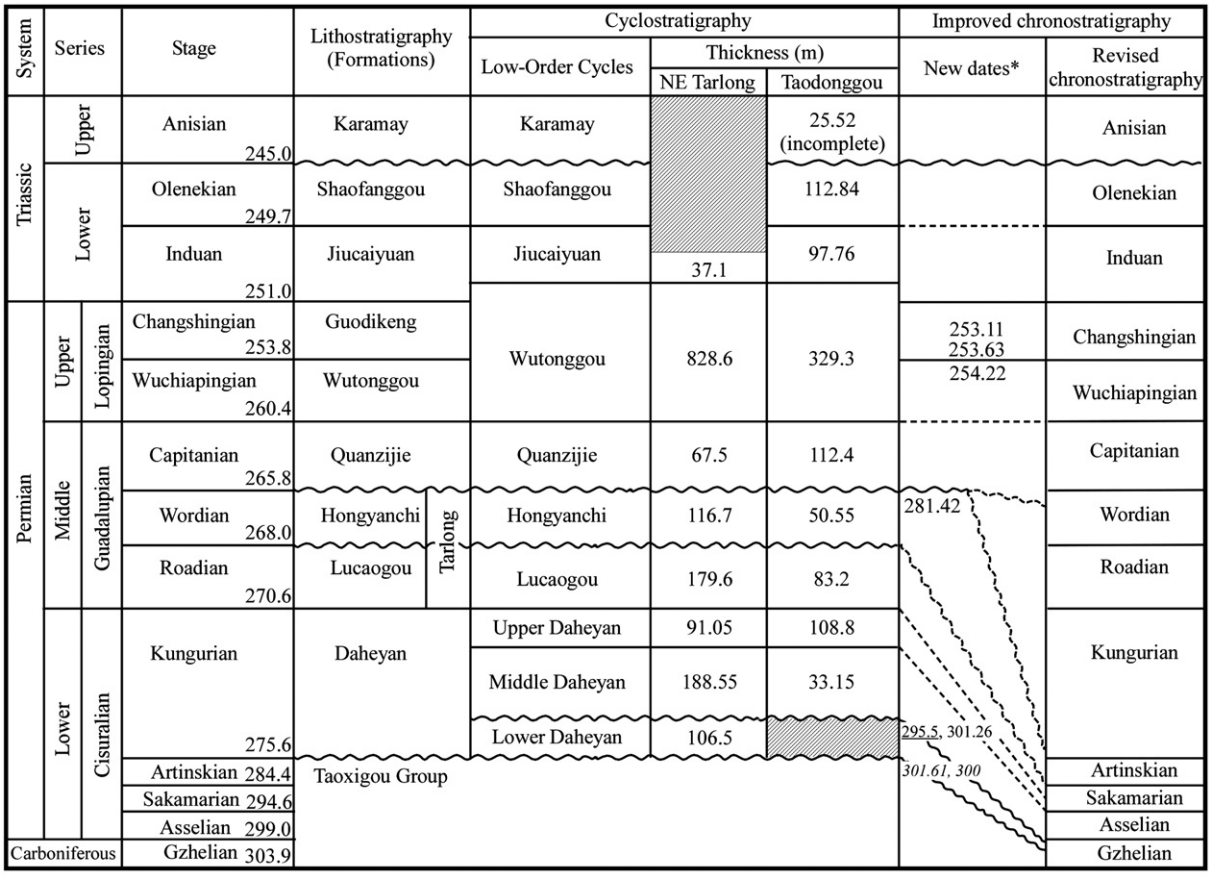

*Underlined numbers - dates from SHRIMP analysis; italic numbers - dates from Ar^{40}/Ar^{39} analysis; plain numbers - dates from IDTIMS analysis.

Fig. 2. Chrono-, litho-, and cyclostratigraphy of Permian–Triassic strata in the NE Tarlong and Taodonggou sections. Absolute ages at stage boundaries from Gradstein et al. (2004); lithostratigraphic and chronostratigraphy synthesized from Zhang (1981), Liao et al. (1987), Wartes et al. (2002), and Zhu et al. (2005). Hachured areas indicate missing strata. Wavy lines are major unconformities. Dashed lines indicate uncertain age correlations.

The age of the top of the Hongyanchi LC is important to determine the duration of the Hongyanchi–Quanzijie unconformity. The previous chronostratigraphy places the base of the Quanzijie LC at the base of Capitanian (265.8 Ma; Fig. 2); the unconformity would span a maximum of ~14 million years encompassing the Kungurian, Roadian, and Wordian stages. However, because of the uncertainty of previous chronostratigraphy, the actual duration may be significantly shorter if the top of Hongyanchi extends upward into Kungurian or younger age and the base of Quanzijie is lowered into Wordian or older age.

The age of the Wutonggou LC ranges from Lopingian to early Induan based on previous chronostratigraphy (Fig. 2). The placement of Permo–Triassic boundary is a work in progress. Liao et al. (1987) placed the boundary in the upper Guodikeng Formation (i.e., upper Wutonggou LC) in Taodonggou on paleontologic evidence (Fig. 2). A cluster of three cm-thick tuffaceous sandstones ~28 m below the top of Wutonggou LC and the first occurrence of invertebrate bones ~15 m above the top in Taodonggou were correlated to Tarlong to constrain the Permo–Triassic boundary in NE Tarlong. An age of a bentonite ~241 m below the top of the Wutonggou is 253.12 Ma; two ages of a bentonite ~249 m below the top are 253.65 and 254.26 Ma (Fig. 2; Appendix), confirming the basal Changshingian age of the upper Wutonggou LC. Correlation between Taodonggou and NE Tarlong using these stratigraphic and age constraints places the Permo–Triassic boundary in a 90 m-thick interval in the NE Tarlong section (see Section 4.7).

Last, the age of Jiucaiyuan and Shaofanggou LCs is from middle Induan to Olenekian according to previous chronostratigraphy; some (e.g., Wartes et al., 2002) tentatively placed Jiucaiyuan as middle–late Induan and Shaofanggou as Olenekian, which is the scheme adapted in this study (Fig. 2). The chronostratigraphy will be improved through future geochronological analysis of numerous volcanic rocks, bentonites, and tuffaceous sandstones in the studied sections.

1.3. Methodology and data

Eleven stratigraphic sections of a total thickness of ~3400 m were measured at a cm–dm scale in this study (Fig. 1C). Among them, the NE Tarlong and the Taodonggou sections are the most complete (Fig. 2). In addition, the pedo-types and morphologies of ~30 paleosols were described mainly in the Upper Permian and Lower Triassic intervals of the two sections. Thus, data from the NE Tarlong and Taodonggou sections are discussed in detail in this paper (see journal online supplements for detailed description and interpretation of the two sections).

Fig. 3. Lithology, sedimentary structure, and interpretation of five basic types of high-order cycles. A) Braided stream cycle; B) meandering stream cycle; C) lacustrine deltaic cycle; D) fluctuating profundal mixed siliciclastic and carbonate cycle; E) lakeplain–littoral siliciclastic cycle. Each cycle type has several varieties because commonly not all the component lithofacies are present in a particular cycle. No vertical scale intended. Interpretation begins with depositional environment, lake type (speculative for non-lacustrine cycles), tectonics, and ends with climate. Dashed lines for speculative or alternative interpretations. See Fig. 4A for explanations.

Facies Description

A. Braided stream cycles

Calcisol or argillic Spodosol on mudrock parent rock. Erosional top. Overbank.

Conglomeratic lithic wacke to arenite and conglomerate, crudely fining upward, large planar & x-beds, locally reverse or normal graded, many internal erosional surfaces, clasts imbricated. Uppermost part may contain illuviated sands and calcitic nodules (as Calcisols). Low-relief erosional base. Channel fill.

Matrix-supported conglomerate, rare, clasts randomly oriented, massive no or crude upward coarsening trend, sharp non-erosional base, uppermost part may be stratified due to fluvial reworking. Debris flow deposits.

B. Meandering stream cycles

Calcisol, calc. Argillisol, or Argillisol, Spodosol, Histosol, on mudrock & ss parent rocks. Calcisol: pedogenic calcitic nodules. Spodosol: common Fe-oxide pisoids in Bs horizon. Argillisols: illuvial clay sheets or tubules. Histosol, sub-bituminous to bituminous coal interbedded with carbonaceous shale, petrified woods. Floodplain.

Shale, silty sh, sltst, well laminated to platy, local ss lenses. As the fine-grained upper interval of the overall upward-fining and thinning succession. Proximal overbank. Absent/thin in coarse-grained streams.

Lithic wacke, subarenite, arenite, conglomeratic, conglomerate at base, upward-fining. As the coarse portion of the overall upward-fining trend. Large tabular and trough x-beds, locally graded. Concentrated plant remains on bedding plane. Clasts imbricated in conglomerate. High-relief erosional base. Rapid lateral facies changes. Commonly accretionary. Channel lag and point bar.

C. Lacustrine deltaic cycles

Calcisol or Spodosol/Histosol, mudrock and ss parent rocks. Spodosol may contain iron-oxide pisoids and overlie Histosol. Deltaplain.
Interbedded laminated mudrock and ss, with variable plant remains and root molds. Delta plain.

Lithic wacke, subarenite, arenite, and conglomerate, upward-coarsening (m sd to pebble) and thickening. L. part well laminated and bedded, rare burrows; u. part large x-beds with local channel fill. Locally concentrated plant remains on bedding plane. Delta front, distributary channel fill, channel mouth bar.

Shale, well laminated, upward-increasing sltst & thin ss. Many disseminated plant remains; may contain fish fossils. Prodelta.

Lithic arenite to subarenite, f-vc, laminated to x-bedded, rare HCS. Persistent. L. part may have imbricated "shoreline" pebbles. Lake shore.

D. Fluctuating profundal mixed siliciclastic and carbonate cycles

Calcisol with calcitic nodules and sparse-common root mottles in mudrocks. Lakeplain.

Dolomitic sh and dolomite, sub-mm laminated, some disrupted with recrystallized calcite. Littoral to lakeplain.
Limestone, micritic, stromatolitic/cryptalgal laminite, skeletal, oolitic, or rarely palustrine. Shallow to deep littoral.

Shale, sub-mm laminated, organic rich with type I and II kerogens. Abundant fish fossils. Local sandy and silty intervals at base and discontinuous limestone lenses. Rare dropstones. Profundal.

Lithic arenite to subarenite, f-vc, laminated to x-bedded, rare HCS. Persistent. L. part may have imbricated "shoreline" pebbles. Lakeshore to shallow littoral.

Sh, silty sh, sltst, thick-laminated. Persistent. Lakeplain.

E. Lakeplain-littoral siliciclastic cycles

Calcisol, calcareous Argillisol, or Argillisol, Spodosol, Gleysol. Parent rocks are mudrock and thin lithic wacke. Common illuvial or carbonaceous rootlets. Lakeplain.

Shale. siltstone, sandstone, sub-mm to mm laminated, x-laminated. Ostracods and/or plant remains. Fining upward. Sublittoral to littoral.

Lithic arenite-subarenite, f-vc, Laminated, x-bedded, rare HCS. Rip-up clasts. L. part may have thin imbricated "shoreline" pebbles. Ripple-marked top. Sparse to abundant ostracods. Coarsening upward. Persistent. Lakeshore to littoral.

Sh, silty sh, sltst, thick-laminated. May contain Histosol. Persistent. Lakeplain.

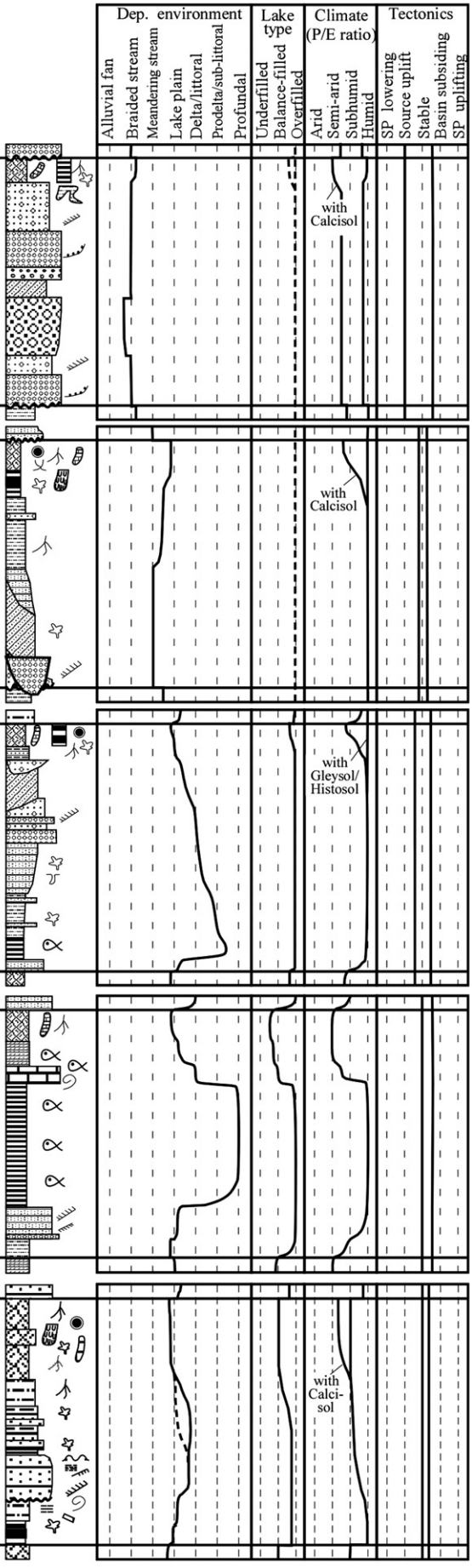

Cyclostratigraphic analysis and correlation in this study were carried out in four general steps. First, depositional environments of lithofacies were interpreted on the basis of lithology, sedimentary texture and structure, fauna and flora, and stratal geometry and boundary relationship. In addition, nine paleosol types are identified through field observations of lithology, soil texture and structures, color, and soil morphology. Mineralogy, texture, and fauna and flora of ~100 thin-sections of sandstones, limestones, mudrocks, and paleosols were documented. The paleosol and petrographic data were used to substantiate environmental interpretations but will be fully reported in future publications.

Second, three orders of sedimentary cycles were delineated on the basis of repetitive depositional environment changes. A high-order cycle (HC) signifies a cycle of environmental shift associated with lake transgression/expansion and regression/contraction or a cycle of fluvial erosion and deposition (Fig. 3). It is the basic cyclostratigraphic entity recognized in the outcrop. The stacking of HCs commonly shows a longer trend of environment shifts associated with transgression and regression to comprise an intermediate-order cycle (IC). An IC is termed as a stratigraphic sequence, which may consist of transgressive, condensed section, highstand, and regressive systems tracts, each of which is composed of one or more HCs (Yang et al., 2007b). Finally, thick intervals of many ICs showing similar overall environments define low-order cycles (Figs. 4–11).

Third, the hierarchical cycles were correlated among measured sections. A process–response strategy using not only the type, thickness, and stacking patterns of cycles but also the interpreted controlling processes on cyclic sedimentation were used in the correlation (Yang et al., 2009). The procedure requires interpretation of a variety of autogenic and allogenic processes. Finally, the correlation established a hierarchical cyclostratigraphic framework, within which paleoclimatic variability was interpreted.

2. Lithofacies and their depositional environments

The fluvial and lacustrine fills in the Tarlong–Taodonggou half-graben contain 15 basic types of lithofacies. Their characteristics and depositional environmental interpretations form the basis of sedimentary cycle delineation and paleoclimatic interpretation (Table 1).

2.1. Clast-supported and matrix-supported conglomerate lithofacies

The conglomerates are characterized by the dominantly andesitic and basaltic clasts, which range from granule to boulder size. Sedimentary clasts are uncommon but increase in the Upper Permian and Lower Triassic. Many of them have similar textures to underlying pene-contemporaneous Permian conglomerate, shale, sandstone, and limestone and were probably derived from local horsts, whereas some limestone clasts have marine fossils and were probably derived from Carboniferous marine rocks in northern Tianshan. Large plant remains and petrified wood fragments are sparse and locally concentrated. The maximum clast size and the abundance of conglomerates decrease up section, indicating a reduced relief of northern Tianshan and enlargement of the catchment basin.

The clast-supported conglomerates are of several origins. First, many conglomerates are lenticular and 10–100 cm thick. They are fining upward with interbedded sandstones in the upper part. Clasts are subangular to well-rounded, imbricated, and moderately to well-sorted. Plane and graded beds, trough and tabular cross-beddings, and basal and internal erosional surfaces are common. The conglomerates were interpreted as braided stream channel and bar deposits where they have a low-relief (1–10 cm) erosional base and are not overlain by thick mudrocks (Figs. 3A, 4B), or as channel lag and lower point bar deposits of meandering streams where they fill channel forms with a high-relief (10–100 cm) erosional base and are overlain by thick muddy deposits (Figs. 3B, 6B, 8B, C, 9B, C). Second, some conglomerates occur in upward-coarsening and thickening successions of shale, sandstone, and conglomerate with a non-erosional base and top. They were interpreted as delta-front channel-mouth-bar deposits. Last, some other conglomerates are thin (10 cm thick) but laterally persistent for 10–100 m. They are well-sorted, rounded, and imbricated, and have a sharp to slightly erosional base and a sharp to gradational top. They commonly overlie paleosols and underlie well-bedded and sorted arenites. They were interpreted as well-washed beach and littoral deposits (i.e. shoreline pebbles) (Figs. 3C, 6C and 11B).

Matrix-supported conglomerate is rare. Clasts are very poorly sorted, lack preferred orientation and vertical grain size trend. The lithofacies is massive and, in some cases, cross-bedded in the upper 10s of cm, and has a sharp nonerosional base and no internal erosional surfaces. It is 1–10 m thick and 10–100 m long, and occurs as isolated units in thick braided stream deposits in Daheyan LCs and as thick volcaniclastic units in Taoxigou Group (Figs. 3A and 4C, D, E). The lithofacies was interpreted as debris flow deposits.

2.2. Sandstone lithofacies

The sandstones include compositionally immature and texturally immature to mature lithic wacke, subarenite, and arenite. Igneous grains dominate; sedimentary grains are uncommon but increase up section. An exception are the abundant limestone grains in sandstones vertically and laterally adjacent to lacustrine limestones in the Lucaogou and Hongyanchi LCs (Yang et al., 2008), which were derived from contemporaneous limestone crusts. Feldspars are commonly <25% and quartz <5%, and both increase up section. Framework grains range from coarse-silt to very coarse sand, angular to well-rounded, and very poorly to very well-sorted. Overall, grain size decreases from dominantly gravelly very coarse to coarse sand in the uppermost Carboniferous to Middle Permian to dominantly coarse to very fine in the Upper Permian to Lower Triassic. Sorting and rounding also improve up section. The increasing textural maturity indicates a reduced relief of the source area and enlargement of the catchment basin.

The complex sandstone lithofacies are subdivided according to their environmental origins. Environmental interpretations are based on stratal geometry, boundary relationship, vertical textural, structural, and thickness trends, fossil content, and facies associations, in addition to the composition, texture, and structure of individual sandstones (Table 1).

2.2.1. Fluvial subfacies

Sandstones in upward-fining conglomerate-sandstone–mudrock successions commonly are angular to sub-rounded, poorly to moderately well-sorted subarenites to wackes, containing large-scale tabular and trough cross-beddings and plane and graded beds. Some are accretionary in high-relief channel forms, and were interpreted as point bar deposits in meandering streams (Figs. 3B, 6B, 8B, C, 9B, C). Sandstones in the upper part of upward-fining successions are thin (10s of cm), laterally persistent wackes. They are laminated or massive and interbedded with mudrocks, and commonly contain plant remains and root molds, and were interpreted as overbank deposits. Finally, some gravelly coarse to very coarse subarenites and arenites occur in crudely fining-upward conglomerate-sandstone successions. They are plane bedded or large-scale cross-bedded and fill in channel forms with a low-relief erosional base. They were interpreted as braided stream deposits. Some braided stream sandstones are massive and contain nodular or tabular micrites and were interpreted as Calcisols (see Section 2.5 "Paleosols"). Braided stream deposits occur mainly in the Lower Permian (Table 1).

2.2.2. Lakeshore and littoral subfacies

Lithic arenite and subarenite dominate this subfacies. Quartz and feldspar are more common than in other sandstone subfacies.

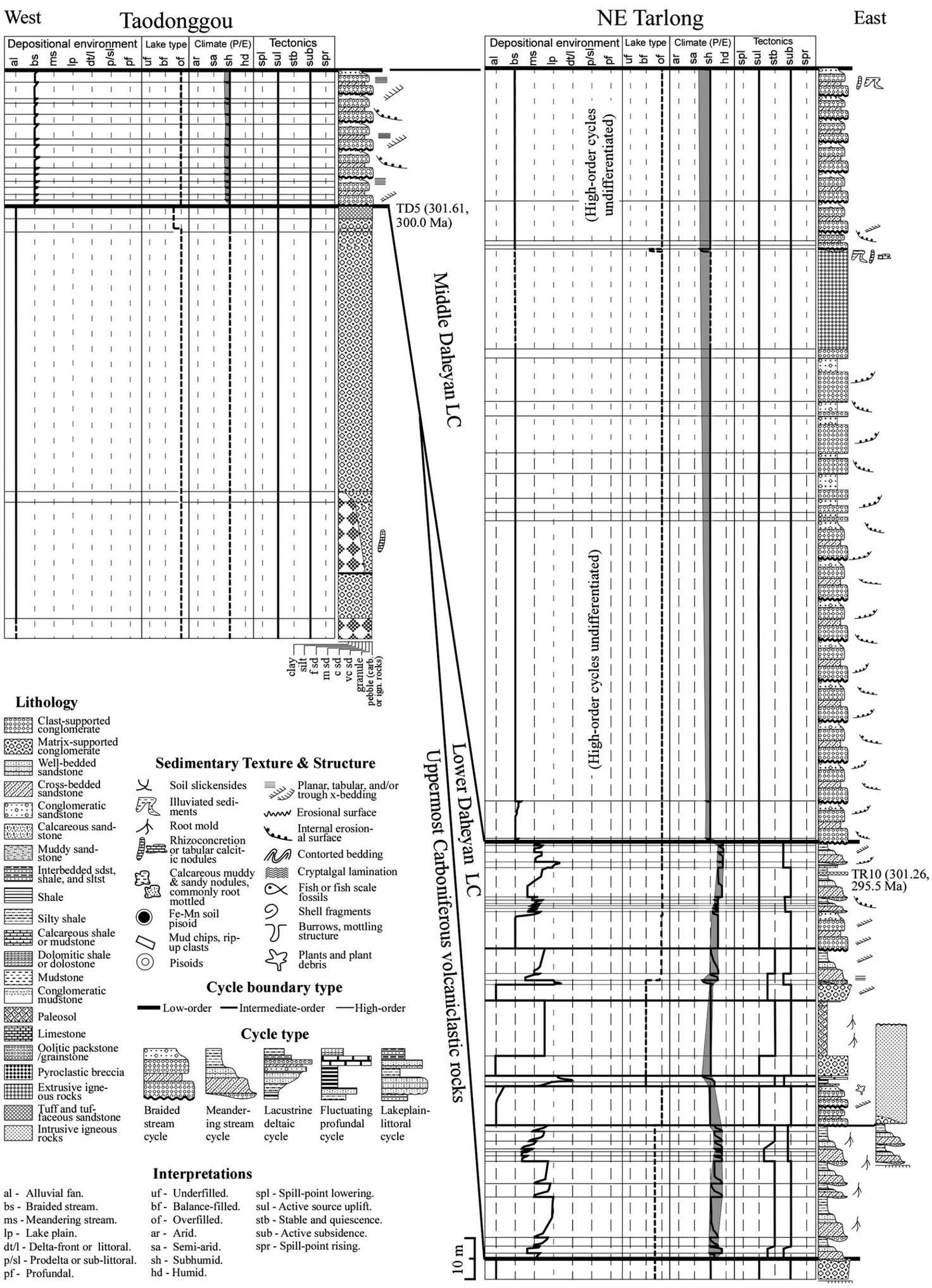

Fig. 4. (A) Highly simplified lithology and sedimentary structure, interpreted depositional environment, lake type, climate, and tectonic movement of source area and depositional site, and cyclostratigraphy of the uppermost Carboniferous volcaniclastic deposits of Taoxigou Group and upper Gzhelian lower Daheyan and upper Gzhelian–Asselian middle Daheyan low-order cycles (LCs). Dashed lines are tentative interpretations or correlations. The measured litho-columns are mostly replaced by simplified cycle types, because the cm-scale field measurements cannot be displayed legibly in the figure. Readers are referred to detailed litho-columns and descriptions of the sections in the data repository. Sample names and radiometric ages are labeled next to the litho-column. The gray-colored portion of the climate curve is constructed by connecting the most arid and most humid points of adjacent high-order cycles, to qualitatively outline long-term climate variations at the intermediate- and low-order cycle scales. (B) Field photo of an upward-fining braided stream cycle outlined by two dashed lines in middle Daheyan LC, Taodonggou. Person is 1.7 m tall. (C) Field photo of a debris flow deposit, upper middle Daheyan, NE Tarlong. Person is 1.7 m tall. (D) An unconformity (dashed line) separating volcaniclastic debris flow deposits of the Taoxigou Group from overlying braided stream deposits of the middle Daheyan LC, NW Tarlong. People (circled) are 1.7 m tall. (E) Field photo showing a vertically-jointed ash-flow tuff (outlined by dashed lines) separating volcaniclastic debris flow deposits of the Taoxigou Group from overlying middle Daheyan LC, Taodonggou. Sample TD5 from the tuff is dated as ~300 Ma. Person is 1.7 m tall. Stratigraphic-up to left/south. (F) Field photo showing a loose layer of black angular basalt clasts in an oolitic grainstone in upper lower Daheyan LC, NE Tarlong. Short scale bar is 1 cm long.

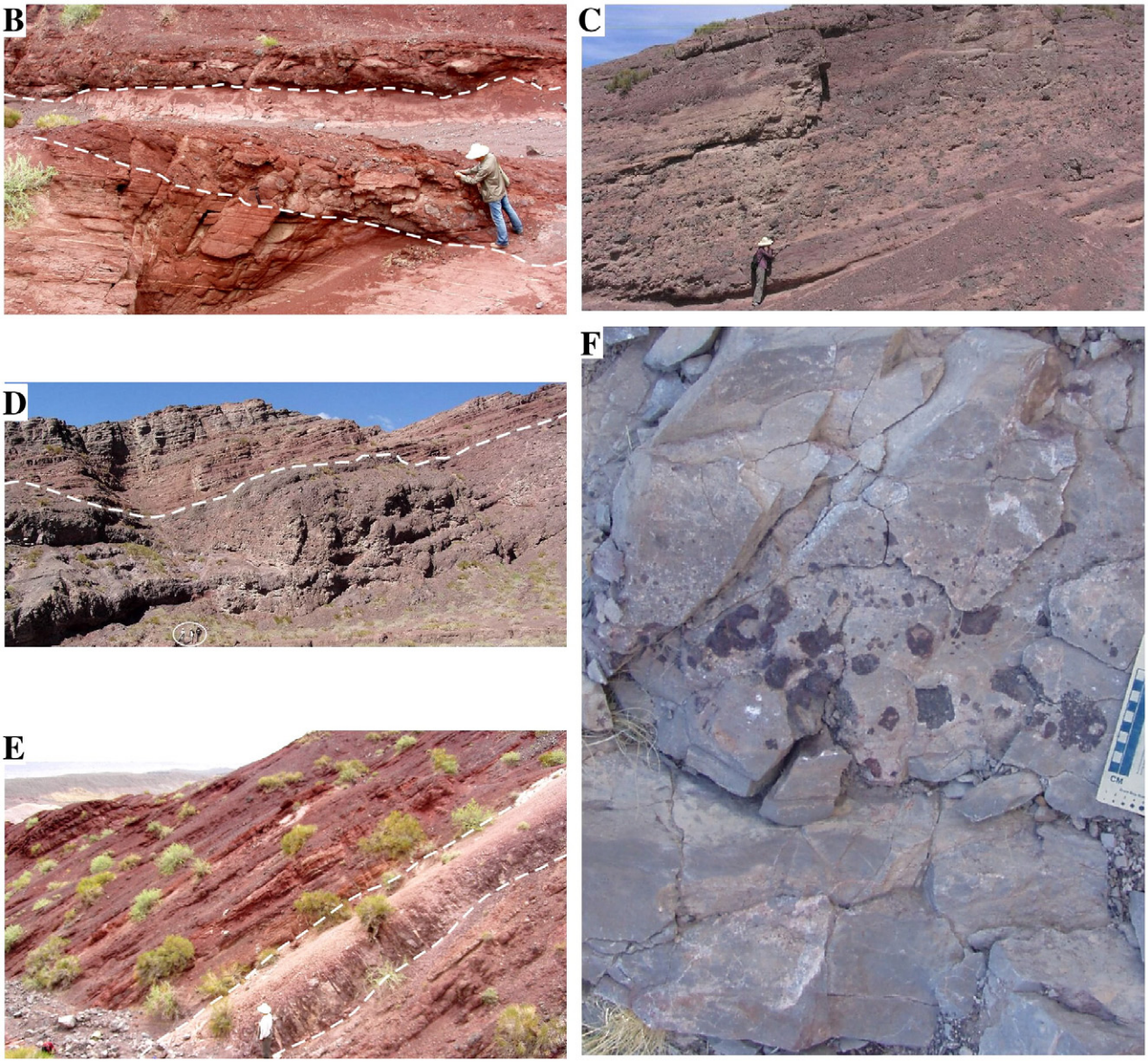

Fig. 4 (*continued*).

Skeletal and peloidal carbonate grains and superficial ooids are common, especially where adjacent to limestones. Reworked mud clasts are common where the sandstones overlie paleosols (Fig. 11C). Grains are variable in size, well-sorted, and sub-rounded to well-rounded. Plane beds, high-angle tabular cross-beddings, climbing ripple cross laminations, ripple marks, and in some cases, hummocky cross stratifications, are common. The basal contacts are sharp to slightly erosional. This subfacies are thin (1–100 cm thick), tabular, and laterally persistent for 100s of m, and were interpreted as well-washed beach to littoral deposits (Figs. 3E, 6C, 11B, C; Table 1). In some cases, the uppermost part has a disrupted bedding and abundant grayish green, mm-diameter root molds, suggesting pedogenic alteration during subsequent exposure (Fig. 11D).

2.2.3. Deltaic subfacies

This subfacies includes lithic wacke, subarenite, and arenite forming upward-coarsening and thickening successions. It overlies shale with a gradational, flat to contorted contact. Grains are fine to very coarse, moderately to well-sorted. Disseminated plant remains are common on bedding planes. Climbing ripple cross-laminations change upward to large low-angle tabular and trough cross-beddings or convolute beddings. In some cases, ripple marks and/or hummocky cross stratifications are present, indicating wave reworking. The subfacies commonly is lenticular with a concave base and a convex top, 1–10 m thick, and laterally persistent for 100s of m. Several successions may stack vertically. Some pronounced clinoform packages were observed, where individual sigmoidal clinoforms are 1–100 cm thick with a dip angle up to 20° (Fig. 6G; Yang et al., 2008). This subfacies was interpreted as delta-front deposits (Figs. 3C, 6D, 9E; Table 1).

2.2.4. Turbidite subfacies

This lithofacies occurs as fine to medium, moderately to well-sorted lithic subarenites in middle Hongyanchi LC, and is conspicuous in a 10 m interval in SE Tarlong. Individual beds are normal graded to well-laminated, 1–30 cm thick, and have a sharp base and a sharp to gradational top. They are interbedded with or encased in black sub-mm-laminated black shale. Individual beds are laterally persistent for ~200 m and the entire interval is only present in Tarlong. This subfacies was interpreted as turbidites deposited in the graben center (Table 1).

2.2.5. Other subfacies

First, tuffaceous sandstones occur as thin (1–10 cm), laterally persistent beds in shale-rich intervals throughout the studied sections. They have a sharp to diffuse base and top and bright orange, yellow, or red colors. Fine to medium, very angular to sub-rounded quartz, feldspar, volcanic fragment, and sparse biotite are present. The subfacies was interpreted as reworked tuffs, which are best preserved in low-energy lacustrine and overbank deposits. Second, a 3 m-thick reddish brown arenite in the middle Daheyan LC in Taodonggou is coarse to medium-grained, well-sorted, and subangular to sub-rounded. Uniform tabular cross-beds are ~1 m high and 3–4 m long, with a 10–15° slope. In addition, discrete normal-graded thin laminae are parallel to the bedding plane and thicken slightly down slope, interpreted as grain flow deposits. The sandstone has a low-relief erosional base and is truncated by a braided stream channel at the top. It was interpreted as an eolian dune deposit.

2.3. Mudrock lithofacies

The mudrock lithofacies is complex and of diverse origins. Six subfacies were identified in the field. Their depositional environments were interpreted on the basis of composition, texture, structure, fossil content, and associations with adjacent lithofacies (Table 1).

2.3.1. Shale and siltstone subfacies

This subfacies is variably calcareous and thickly laminated. Those in the lower part of the upward-coarsening and thickening successions are gray to dark gray, several meters thick, and contain abundant disseminated plant remains and sparse ostracods and choncostracods. They change upward from pure or silty shale to siltstone with increasing intercalated thin sandstones, and were interpreted as prodeltaic deposits (Figs. 6D and 9E). Some other thin (10s of cm) shale and siltstone contain abundant ostracods, chonchostracods, and gastropods, and are dark gray to blackish gray and rich in plant remains. They commonly contain angular sand-size mud clasts where overlying muddy paleosols. The clasts are probably reworked rip-ups from the paleosols, as suggested by the sharp to slightly erosional bases. In addition, the subfacies commonly underlie beach to littoral sandstone and conglomerate. They were interpreted as lake-margin littoral to marsh deposits during transgression (Fig. 9D). Finally, some other shale, siltstone, and sandy shale are brown to reddish brown and contain sparse to rich plant remains but no microfossils. They are sandy, platy, or mottled and contain intercalated thin sandstones and paleosols. The subfacies are 0.1–1 m thick and occur in the upper part of upward-fining and thinning successions. They were interpreted as fluvial overbank deposits (Fig. 9B, C).

2.3.2. Organic-rich shale subfacies

This subfacies is dark gray to blackish gray, very well mm-to-sub-mm laminated, and 1–100 cm thick. Fish scales, microfossils, and microscopic plant remains are sparse to common and locally concentrated. They are variably calcareous and contain rare siltstone and fine sandstone laminae. The total organic content (TOC) ranges from 5 to 20%; and kerogens are types I and II, indicating an algal or mixed algal and plant origin for the organic matter. Isolated cobble to sand-sized grains distort or rupture underlying laminae and are overlain by continuous laminae (Fig. 6F; see also Yang et al., 2007a). They were interpreted as dropstones deposited when seasonal lake ice melted. However, diagenetic dolomitic or carbonate nodules with similar features are also locally abundant and need to be carefully identified. Microscopically, the lithofacies contains alternating clayey and silty laminae, which may have been deposited under highly seasonal climate, where clay-rich laminae were deposited during dry or icy seasons and silt-rich laminae in wet or warm seasons. It commonly overlies littoral sandstones and underlies limestone, dolomite, and dolomitic shale (Fig. 6E), and in some cases, is interbedded with thin turbidite sandstones. This subfacies was interpreted as a sub-littoral to profundal anoxic deposit in under- to balance-filled lakes (Carroll and Bohacs, 1999). Carroll (1998) had a similar interpretation in his biomarker study of similar lithologies to the west of the study area.

2.3.3. Dolomitic shale subfacies

Dolomitic shales are gray to dark gray or yellowish brown, dense, and variably calcareous and dolomitic. Thin, parallel and algal laminations are dominant; mud cracks are rare. Fish scales and skeletons and microfossils are common and locally concentrated. Calcite is microcrystalline; dolomite is euhedral to anhedral and 10s of μm in size. Rare elongate gypsum crystals and calcified nodules are present. Organic content is high with a TOC of 10–22% and types I and II kerogens. Microscopically, calcareous and dolomitic laminae alternate with clayey or silty organic-rich laminae. Mud and organic-rich laminae suggest increased mud influx, probably during wet seasons, whereas dolomitic laminae suggest reduced mud influx and increased evaporation (e.g., Carroll, 1998), probably during dry seasons (see Talbot and Allen, 1996 for alternative interpretations). Dropstones similar to those in the organic-rich shale facies are present. The subfacies commonly overlies limestone and is interbedded with dolomite (Fig. 6E). It was probably deposited in a low-energy evaporative under-filled lake.

2.3.4. Bentonite subfacies

Bentonites occur as thin (1–20 cm) beds in shale or carbonate-rich intervals throughout the studied sections. They are pale gray, dark blackish gray, or grayish and pinkish white, ductile, and intensely slickensided. Sparse biotite, quartz, feldspar, and zircon are present. They are altered volcanic ash-fall deposits in low-energy lake and overbank environments.

2.3.5. Carbonaceous shale and coal subfacies

This subfacies is black to blackish gray and variably silty and sandy. It is well-laminated to massive, 1–50 cm thick, and has a sharp to gradational base and top. Ostracods, choncostracans, and gastropods are absent to locally concentrated. Coals are mainly lignitic and rarely bituminous. The subfacies are laterally persistent for 0.1–1 km. Some are interbedded with overbank shale, siltstone, and sandstone and, in a few cases, filling abandoned channels (Fig. 9B), interpreted as floodplain deposits. Others commonly underlie beach-littoral sandstones and overlie pedogenically-altered deposits or paleosols with a sharp to slightly erosional contact (Fig. 9D). They contain a variable amount of microfossils and sandstone laminae. They were interpreted as marginal swamp and mud-flat deposits associated with an approaching shoreline and raised groundwater table during early transgression. Coal occurs only in the Wutonggou LC (Table 1).

2.3.6. Massive mudstone subfacies

Two types of massive mudstones are present. First, dark gray mudstones contain abundant disseminated plant remains, gastropods, ostracods, choncostracans, and unidentified bivalves, and are extensively mottled. They were interpreted as bioturbated deposits in low-energy oxygenated shallow embayment. Second, variegated mudstones contain abundant pedogenic features. They are described in Section 2.5 “Paleosols”.

2.4. Carbonate lithofacies

Carbonate lithofacies include limestone and dolomite subfacies and are volumetrically insignificant (Table 1). They occur mainly in the Lucaogou and Hongyanchi LCs.

2.4.1. Limestone subfacies

Grainstone, packstone, wackestone, and lime mudstone all are present. Allochems include skeletal fragments, ooids, intraclasts, peloids, and minor pisoids and oncoids. Lithic, feldspar, and quartz

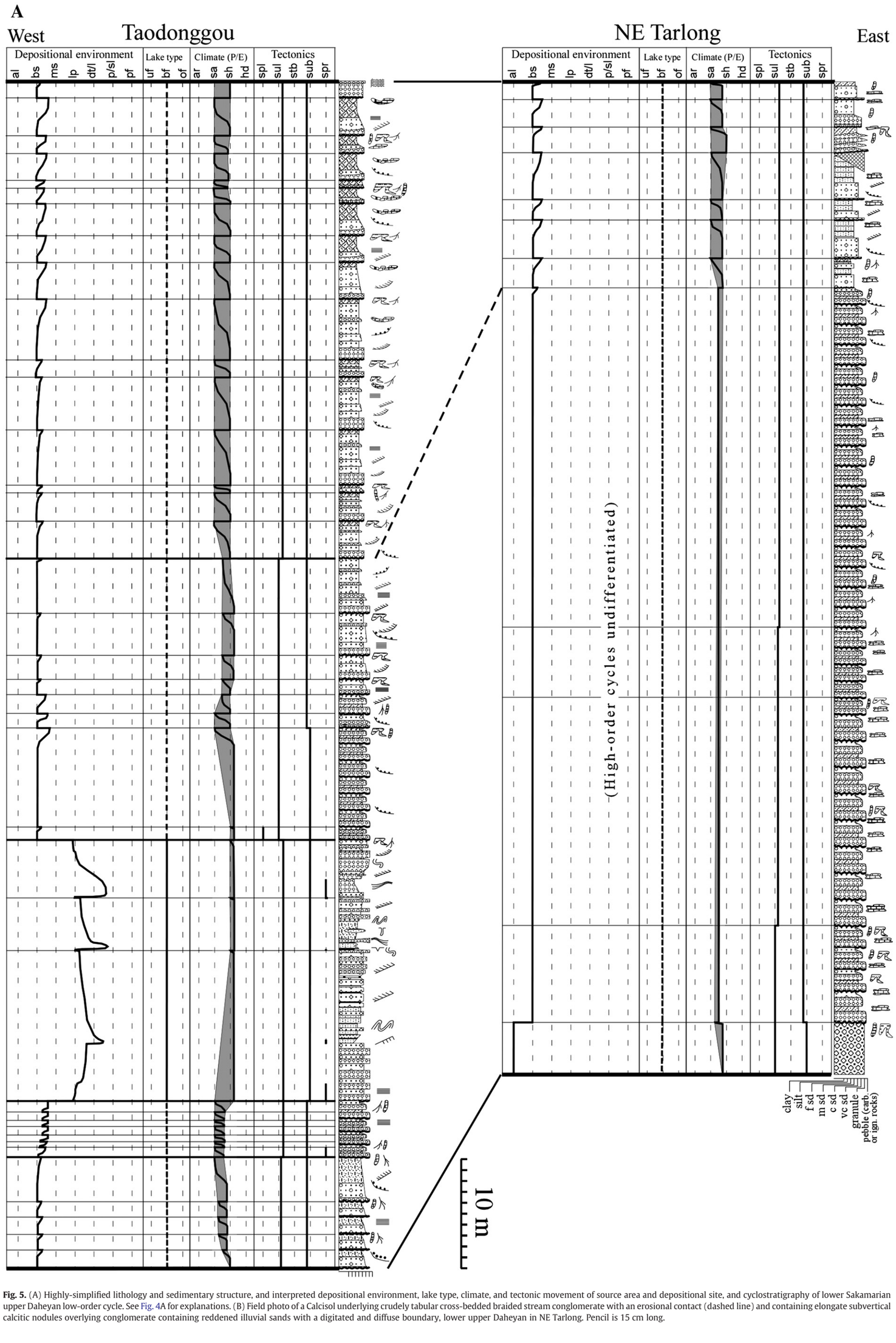

Fig. 5. (A) Highly-simplified lithology and sedimentary structure, and interpreted depositional environment, lake type, climate, and tectonic movement of source area and depositional site, and cyclostratigraphy of lower Sakamarian upper Daheyan low-order cycle. See Fig. 4A for explanations. (B) Field photo of a Calcisol underlying crudely tabular cross-bedded braided stream conglomerate with an erosional contact (dashed line) and containing elongate subvertical calcitic nodules overlying conglomerate containing reddened illuvial sands with a digitated and diffuse boundary, lower upper Daheyan in NE Tarlong. Pencil is 15 cm long.

Fig. 5 (*continued*).

grains range from 5–50%; and siliciclastic mud is common in wackestones and lime mudstones. Ooids have radial and/or concentric cortices and mostly lithic cores. Intraclasts and peloids of a silt to pebble size are commonly blackened and locally concentrated in scour-and-fill structures. Well-sorted pisoids rarely form thin (1–10 cm thick) rudstones and were interpreted as high-energy littoral deposits. Pisoids are also scattered in highly altered wackestones or lime mudstones, interpreted as pedogenic. Oncoids are algae-coated, disc-shaped, and 1–20 cm in diameter. They are locally concentrated in well-laminated lime mudstones at the toes of limestone clinoforms in the basal Lucaogou LC in NE Tarlong (Yang et al., 2008). Organic matter is common, as indicated by brown stains and asphalt along bedding planes and fractures. TOC ranges from 5 to 11% in seven samples, with types I and II kerogens. Fish scales and skeletons are common; well-preserved bivalves are locally abundant; and plant remains are sparse to common.

Most limestones are altered to a variable extent through micritization, recrystallization, silicification, and dolomitization, during pedogenesis and diagenesis. Irregular laminae of highly-contorted calcite nodules with microscopic thinning and thickening occur in several wackestones and mudstones in the Lucaogou LC (Fig. 6H). The contortion and disruptive bedding suggest deformation under a semi-consolidated state probably by dehydration of original gypsum nodules, which were later calcified. Lenticular gypsum crystals are scattered in some wackestones and lime mudstones. Finally, highly recrystallized limestones contain cm-size angular organic-rich shale clasts, suggesting dissolution of primary gypsum laminae and brecciation of shale partings in the limestones.

A variety of sedimentary structures are present. Faint cross and horizontal laminations, crude tabular cross-beddings, and scour-and-fill structures are common in grainstones and packstones. Root molds, color mottling, micro-karsts, and dissolution channels occur in the upper part of some limestones, indicating pedogenic alteration. Animal burrows are common in unaltered limestones and, in some cases, producing a nodular texture. Algal laminations are common in muddy algal laminites and stromatolites, which contain thrombolitic clots forming 1–10-cm-thick laminae. Algal laminites are 5–30 cm thick, and contain alternating organic-rich, micritic, and dolomitic laminae. Laterally-linked to discrete hemispheric stromatolitic beds have knobby top surfaces with a relief up to 30 cm. Last but not the least, Cone-in-cone and micro-brecciation structures are well-developed in highly-recrystallized limestones.

Limestones are well-bedded and laterally persistent, ranging from 1–50 cm thick. A 5 m-thick northward-prograding clinoform package in basal Lucaogou LC extends ~5 km from east to west along strike and ~200 m from south to north in northern Tarlong (Fig. 6G; Yang et al., 2008). The clinoforms are couplets of skeletal lithic arenite in the lower part and arenaceous grainstone or packstone in the upper part. Individual clinoforms are 0–40 cm thick and sigmoidal with a maximum dip angle of 20°. The package indicates northward progradational infilling by lakeshore and littoral carbonate deposits. Two coquinas in the upper part of Wutonggou LC in Taodonggou are lenticular, laterally continuous, and 5–15 cm thick. They contain articulated to broken bivalves, ostracods, choncostracans, gastropods, and, in places, plant remains, in a sandy matrix. They were interpreted as shell hashes accumulated on the beach.

Skeletal limestones were probably deposited in shallow well-oxygenated lakes; oolites in high-energy littoral to shore environment; stromatolitic and algal laminites in very shallow quiet environment; and finely laminated organic-rich micrites in sub-littoral profundal environment. The highly altered and mottled muddy limestones are probably palustrine or pedogenically-altered lacustrine deposits (Table 1).

2.4.2. Dolomite subfacies

Dolomites are yellowish to reddish brown, dense, parallel or algal laminated or fissile, and react slowly with dilute hydrochloric acid. They are composed of dolomite mud or microspars, a minor amount of organic matter similar to that in the limestones, siliciclastic mud, and rare gypsum crystals. Well-preserved fish scales and skeletons are locally abundant. Beds are 1–20 cm thick and, in some cases, contain limestone, dolomitic limestone, and dolomitic shale laminae. Mud cracks, fenestrae, and color mottling are not common.

Dolomite and dolomitic shale are commonly interbedded, both of which overlie wackestone and lime mudstone or organic-rich shale (Fig. 6E). They were probably deposited in quiet, shallow, and hypersaline under-filled lakes at the contraction stage.

2.5. Paleosols

Seven general types of paleosols were identified on the basis of soil structure (such as ped shape, size, and surface characteristics), chemical and physical accumulations in the soil profile, and stratigraphic changes of structures and products (Table 2; Mack et al., 1993). They are Protosol, Gypsisol, Calcisol, Vertisol, Argillisol, Gleysol, and Histosol. The landscape (including soil drainage, environmental, and topographic) and climatic (in terms of the ratio between precipitation and evaporation) conditions at the sample sites were speculated using modern and ancient analogs (e.g., Retallack, 1990; Mack and James, 1994).

2.5.1. Protosol

Protosols are characterized by a massive structure and a lack of well-developed soil horizons. Some contain poorly-developed blocky peds. They are variegated with red, brown, purple, yellow, and orange colors, showing diffuse to discrete color mottles. The parent lithologies are dominantly sandstones and mudrocks, some conglomerates, and rare limestones, which are gray or red to brown. The gray color of parent lithologies suggests a somewhat poorly-drained lowland environment, whereas the red or brown color suggests an oxidized environment with variable drainage conditions. Climatic conditions cannot be confidently interpreted for Protosols because of the lack of distinctive climate indicators. Protosols are common in the studied sections, as a result of the fluvial-lacustrine origin of the deposits.

2.5.2. Gypsisol

Gypsisols were speculated from indirect field and petrographic evidence. They contain blocky peds and common bladed carbonate nodules. The parent rocks mainly are mudrock and, in some cases, limestone. The nodules are muddy and display a rosette form,

suggesting calcite replacement of original gypsum nodules (Thomas et al., 2007). Evaporate minerals were observed in B horizons but there is no evidence of translocation of evaporate minerals. Micritic dolomite crusts are commonly autobrecciated and cracked. The fractures are mm to sub-mm wide and mm–cm long and are filled with lithic silts from overlying or other allochthonous sources. They were interpreted as desiccation cracks. Scattered lenticular gypsum crystals and calcified gypsum nodules (Fig. 6H) are present in dolomitic and calcitic matrix of the Lucaogou and Hongyanchi LCs. The speculated Gypsisols may have developed in the exposed muddy sediments of playa lakes under an arid climate. They occur mainly in the Lower–Permian Lucaogou and Hongyanchi and Lower–Triassic Jiucaiyuan and Shaofanggou LCs.

2.5.3. Calcisols

The well-developed blocky peds and the presence of equant, elongate, to tabular, autobrecciated micritic nodules define Calcisols. The parent lithologies include mudrock, sandstone, conglomerate, and limestone. The nodules are discrete in most cases and contain scattered lithic grains and patchy mud and, in some cases, discontinuous concentric micritic laminae. Sparry calcite-filled rounded molds are common. Elongate nodules are 1–100 cm long and 0.1–10 cm in diameter, subvertical, and downward branching and tapering (Figs. 5B and 11E), and were interpreted as rhizoliths. Tabular nodules are 3–20 cm thick and up to 3 m long, bedding parallel, mainly in conglomerates, and commonly below equant and elongate nodules, and were interpreted as calcite precipitation about the groundwater table. Reddened sandstone matrix is massive and cemented by calcite and iron oxide, with an irregular or digitated base, suggesting illuviation (Fig. 5B). Microscopic dissolution channels/cracks containing dislodged clasts and surrounding patchy pisoids also suggest downward illuviation and re-precipitation from soil water. Muddy matrix has weekly to moderately calcareous peds that are platy, prismatic, or equant, angular to rounded, and ~2–30 mm in size. Slickensides are small and uncommon. Color mottles are rare to abundant, rounded, and have diffused to sharp boundaries. Limestone alteration in the Lucaogou and Hongyanchi LCs is indicated by autobrecciation, color mottling, patchy oxidation, micritic crusts containing lithic grains, and locally concentrated pisoids. Downward-tapering burrows or rootlets filled with silt and sand are common but micro-karstic features are rare. Soil profiles are 10 cm to 2 m thick with well-developed Bk, Bt, and BC horizons; and stacked profiles are not uncommon. The Calcisols developed in well-drained sediments accumulated in floodplain, lakeplain, and exposed playa environments under an arid to semi-arid climate. They occur throughout the studied section, but are concentrated in Lower–Permian Daheyan, Lucaogou, Hongyanchi, and Lower–Triassic Jiucaiyuan and Shaofanggou LCs.

2.5.4. Vertisol

The common feature among a variety of Vertisols in the studied sections is the well-developed prismatic to wedge-shaped peds. Slickensides are abundant. They are 1–10 cm long and coated with oriented clays. Well-developed antiformal–synformal structures are uncommon. The parent lithologies are dominantly mudrocks. Several types of Vertisols are present. Some Vertisols contain common but a varying amount of carbonate nodules, and were interpreted as calcic Vertisols formed on low-relief lake-margin and floodplain landscape. An example is the stacked paleosols at the top of the Hongyanchi LC that contain large-scale antiformal–synformal structures where slickensides are lined with tabular calcitic nodules (Fig. 7C). Some Vertisols contain a varying amount of Fe–Mn nodules and concretions and were interpreted as ferric Vertisols formed in a subhumid climate. Last, some other Vertisols are gray to dark gray and underlie transgressive lake deposits; they were interpreted as gleyed Vertisols. Vertisols indicate a climate with strong precipitation seasonality (Mack and James, 1994). The calcic Vertisols are concentrated in Lucaogou, Hongyanchi, and Jiucaiyuan LCs; the ferric and gleyed Vertisols in the Wutonggou LC.

2.5.5. Argillisol

Argillisols are defined by accumulation of abundant illuvial clays (argillans; Retallack, 1990; Mack et al., 1993) in and on the surfaces of blocky peds. The parent lithologies are dominantly sandstone and, in some cases, mudrock and conglomerate. The argillans form sub-mm thick shiny continuous sheets on ped surfaces or fill mostly subvertical–vertical tubules of mms in diameter (Fig. 9G). Soil matrix in gray to blackish gray Argillisols is noncalcareous and, in some cases, rich in disseminated plant remains. Carbonaceous films may be present as linings of clay-filled tubules or as remains of decayed roots (Fig. 9H). Matrix in reddish brown Argillisols is moderately to highly calcareous and commonly contain calcareous clay-filled tubules and, rarely, calcareous rhizoliths or thin twigs (Fig. 11D). They developed on fluvial and lacustrine sediments, especially the sandy ones, in upland or topographic highs under a humid climate. Argillisols occur throughout the studied sections, especially in the Wutonggou LC.

2.5.6. Gleysol

Gleysols are dark gray to blackish gray with a blocky to prismatic structure. The parent lithology is dominantly mudrocks, which commonly occur underneath transgressive surfaces or lignites. They may contain carbonized rootlets ranging from 1–10 cm long. Horizons with Fe–Mn pisoids are common (Fig. 9C, F). The pisoids are brown, discrete, non-calcareous, rounded, and 3–15 mm in diameter. Cortices are discontinuous, wavy, concentric laminae 10–100 s of microns thick, composed of Fe and Mn oxides with scattered sand and silt grains; cores are dense ferruginous claystone. The pisoids-bearing horizons are dark gray, brown, or variegated, 30–200 cm thick with pisoids concentrated in the middle, and commonly overlain by a 10-cm thick argillaceous horizon. Muddy matrix is non-calcareous and contains no or minimal organic carbon. Common color mottles are rounded and mm in diameter; elongate, downward-tapering mottles are cm long and locally concentrated. Some mottles have a dark-colored central spot, interpreted as steles. Peds are mostly rounded, equant to prismatic, 2–10 mm in size. Soil horizons are vague, except where pisoids-bearing horizons are present. Individual soil profiles are 1–2 m thick and commonly stacked. They also commonly overlie paleosols of other types, and can be differentiated from the underlying paleosols by their dark gray color and sharp basal contacts, although their ped structures may not be significantly different from the underlying paleosols. The dark gray color, preservation of plant organic matter, abundant Fe–Mn pisoids, and stratigraphic position of Gleysols suggest that they formed in humid, water-logged, low-land environments probably associated with a raised groundwater table caused by transgression and presence of lake margin swamps (Table 2). They are most common in the Wutonggou LC.

2.5.7. Histosols

Histosols include coals and intercalated carbonaceous shale and highly mottled mudstone. Coals are lignitic to sub-bituminous, 1–40 cm thick. They occur as in-situ accumulation of plant materials in the transgressive swamps or abandoned fluvial channels (Figs. 9B, D). In rare cases, a succession of gray blocky mudstone containing calcitic nodules underlies a coal accumulation. The nodules are abundant and irregular to equant without preferred orientations. The calcitic nodules may be precipitates in alkaline soil waters. The combined coal and underlying mudstone was interpreted as calcic Histosol. The thick coals and underlying thick calcitic nodule-rich mudstone in the upper Wutonggou LC in NE Tarlong is a good example of such Histosol. Histosols formed in poorly to very poorly-drained low-land lake margin or floodplain environments under a humid climate. They occur exclusively in the Wutonggou LC.

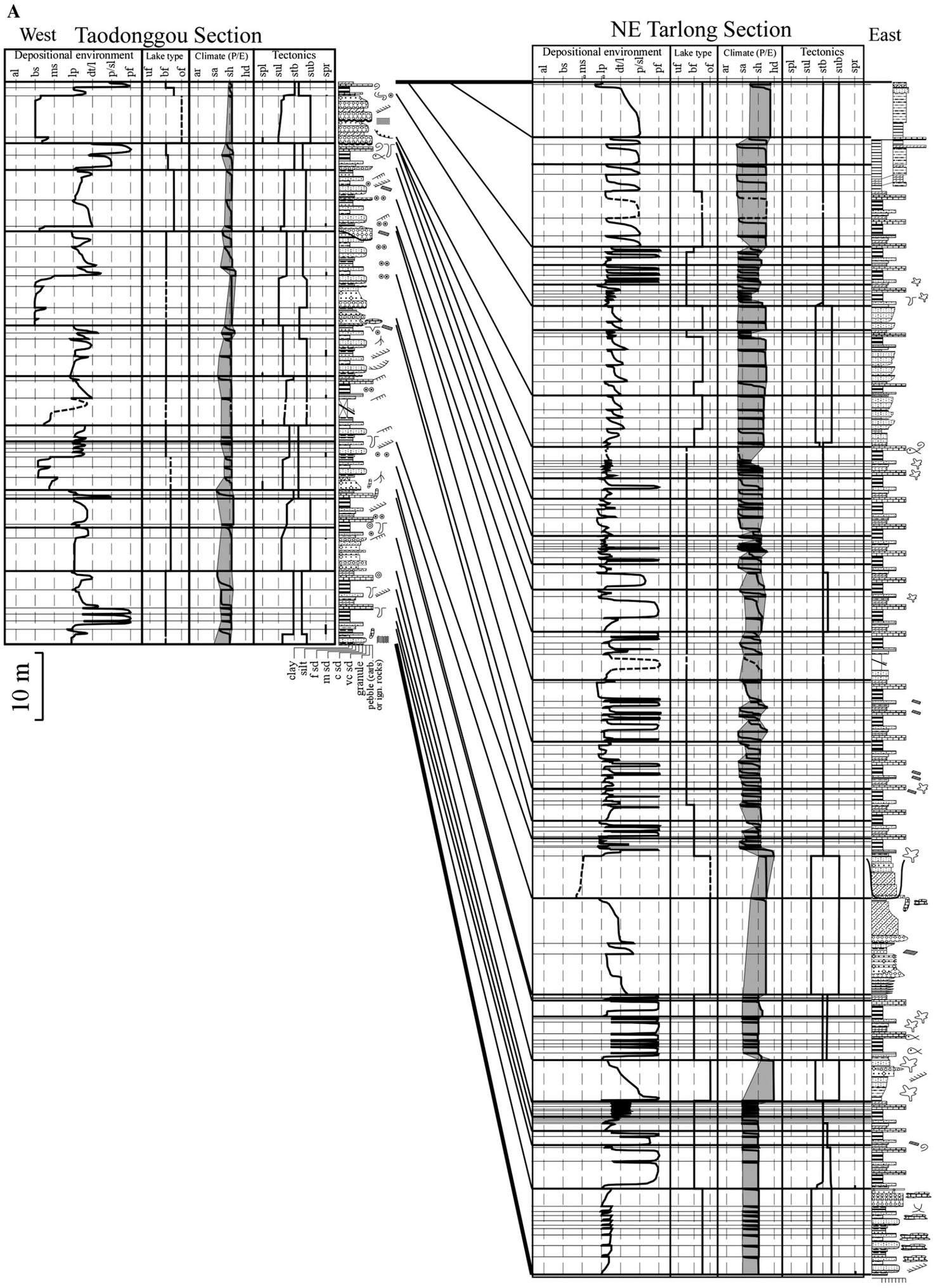

Fig. 6. (A) Highly-simplified lithology and sedimentary structure, and interpreted depositional environment, lake type, climate, and tectonic movement of source area and depositional site, and cyclostratigraphy of upper Sakamarian Lucaogou low-order cycle (LC). Correlation is selectively adapted from Yang et al. (2009). See Fig. 4A for explanations. (B) Field photo showing a meandering stream channel cutting (short dashed line) into profundal deposits. Stratigraphic-up to right. Taodonggou. Person as scale. (C) Field photo of a persistent, thin conglomerate (shoreline pebbles) overlying a Calcisol with a slightly erosional contact (dashed line), which separates underlying upper Daheyan from overlying Lucaogou LCs. The medium-coarse, well-sorted lithic arenite above the conglomerate is a persistent and well-washed lakeshore transgressive deposit. Taodonggou. Small bars are 1 cm long. (D) Field photo of a deltaic succession marked by a triangle showing the upward-coarsening and thickening trend. It is 6 m thick and encased in a thick succession of fluctuating profundal mixed carbonate and siliciclastic high-order cycles in the background, lower Lucaogou, NE Tarlong. (E) Field photo of two fluctuating profundal high-order cycles composed of transgressive littoral–sub-littoral fine-grained sandstone, siltstone, and silty shale (a), maximum-transgressive profundal organic-rich shale (b), regressive limestone (c), and laminated dolomite and dolomitic shale (d). Dashed lines are cycle boundaries, middle Lucaogou, NE Tarlong. Pencil (circled) is 15 cm long. (F) Field photo of an angular limestone clast disrupting underlying thinly laminated shale and draped by similar shale on top, interpreted as a dropstone deposited when lake ice melted, upper Lucaogou, NE Tarlong. White bar is 1 cm long. (G) Field photo of northward prograding limestone clinoforms in basal Lucaogou LC, NE Tarlong. Dashed line marks the sharp transgressive ravinement surface overlain by a deltaic system. Person is 1.8 m tall. (H) Microphotographs of highly-deformed sparry calcitic nodules in a dolomitic mud matrix. Extensive thinning and thickening of the nodules suggest deformation under a semi-consolidated state. They were interpreted as calcified gypsum nodules. Plain light. Sample TR56-6 of middle Lucaogou, NE Tarlong.

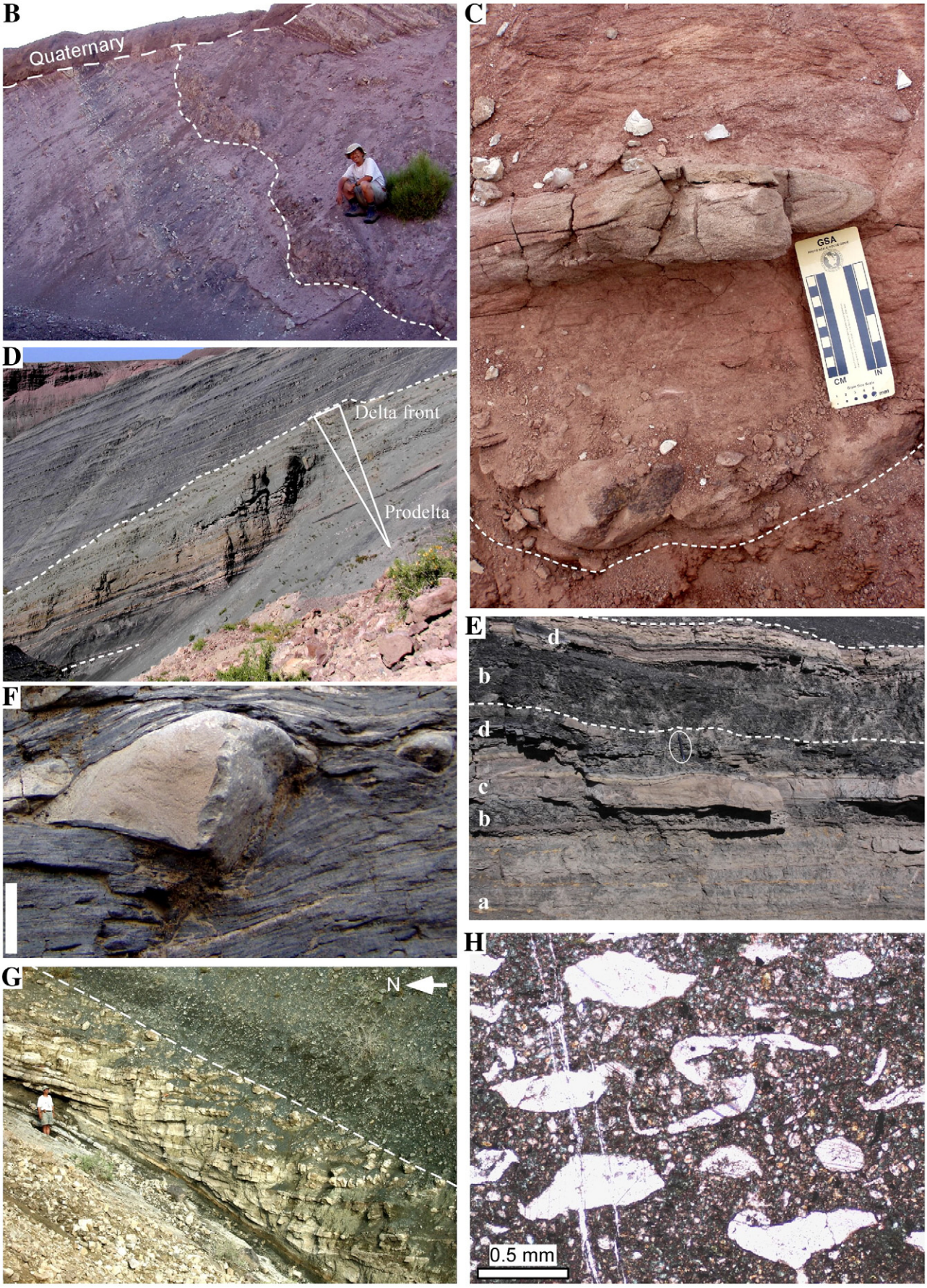

Fig. 6 (*continued*).

3. Depositional systems and sedimentary cycles

A depositional system is composed of component lithofacies that are genetically linked by sedimentary processes within a depositional environment (Brown and Fisher, 1977). Hence, repetitive lateral environmental shifts at a locality result in repetitive vertical stacking of depositional systems in stratigraphic records. These stratigraphic repetitions of depositional systems define sedimentary cycles, reflecting repetitive environmental shifts and associated changes in environmental conditions and sedimentary processes at a locality. It is well known that fluvial–lacustrine records are strongly cyclic (Talbot and Allen, 1996) because fluvial–lacustrine sedimentation is sensitive to frequent environmental changes. Five depositional systems are interpreted in this study: braided stream, meandering stream, and lacustrine deltaic, fluctuating profundal, and lakeplain–littoral systems.

Two general types of sedimentary cycles are defined as erosion–deposition and environmental cycles, representing two types of cycles of sedimentation. An erosion–deposition cycle has an erosional base and an overlying depositional system, representing oscillations between phases of erosion/nondeposition and deposition. Environments during the phase of deposition may not change repetitively, such as a braided stream cycle. An environmental cycle is composed of a succession of depositional systems formed during a cycle of environmental shifts, such as lake expansion and contraction. A phase of erosion may or may not occur before deposition. Many sedimentary cycles are environmental cycles with an erosional/nondepositional base, as a combination of the two basic types. Sedimentary cycles at a dm–m scale are commonly recognized in outcrop observations. They are regarded as basic cyclostratigraphic entities and termed as high-order cycles (HCs) in this study, because they provide a framework to facilitate interpretations of processes and factors controlling erosion, nondeposition, deposition, and environmental changes in the field. 986 HCs are delineated in the Taodonggou and NE Tarlong sections. They are grouped into five types on the basis of types of depositional systems and facies associations (Fig. 3).

3.1. Braided stream high-order cycles

Braided stream cycles are the erosion–deposition type, and contain an upward-fining succession of clast-supported conglomerate (lithofacies 1a in Table 1) and sandstone (lithofacies 2a) on a low-relief erosional base (Fig. 3A). They are 1–11 m thick (Fig. 4B). Most cycles in the upper Daheyan LC are capped by a Calcisol (Figs. 3A and 5A, B), indicating a more stable paleo-landscape than cycles without Calcisols.

The paleoclimate conditions under which a braided stream cycle formed were interpreted from climate-sensitive sedimentary features, if present. The caveat for the interpretation is that the sedimentary imprints of other processes controlling cyclic sedimentation must be removed. This may not be possible in cases where climatic interpretation of a sedimentary feature is non-unique (e.g., Garner, 1959), climatic signals are masked or obliterated by other processes, and the effects of other processes on sedimentation are non-unique or not interpreted accurately. Hence, the paleoclimatic interpretations in this paper are preliminary and of the first order.

Tectonic influence on intermontane sedimentation is significant (Talbot and Allen, 1996 and references within). Thus, the movement of source areas and lake spill-point, subsidence at the depositional site, and their possible effects on lithofacies and depositional environment changes were interpreted and filtered prior to climate interpretation (Fig. 3). Lake type was interpreted as overfilled, balance-filled, or under-filled, on the basis of facies associations and stacking patterns as proposed by Carroll and Bohacs (1999). Lake type is speculated for non-lacustrine cycles, assuming a lake was nearby. The interpretations of lake type, climate, and tectonics started at the HC scale, which were used to construct long-term trends. Finally, climate was interpreted qualitatively with respect to the precipitation (P)/evaporation (E) ratio as arid ($P/E \ll 1$), semiarid (<1), subhumid (>1), and humid ($\gg 1$) in this study.

Braided stream cycles with capping Calcisols probably formed in a semiarid–subhumid climate (Table 2; Retallack, 1990; Mack and James, 1994). Initial erosion and ensuing deposition were followed by a prolonged period of nondeposition, landscape stability, and pedogenesis. Intra-cycle variation from a more humid condition during basal erosion and deposition to a more arid condition during pedogenesis may be present but not necessary. An erosion–deposition cycle may be caused by episodic source uplift or lateral migration of braided streams. The absence of Calcisols in braided stream cycles suggests a more continuous deposition and a more humid climate than those with Calcisols. Alternatively, the continuous deposition could have been caused by accelerated subsidence of depositional site and source uplift. Finally, rare ferric Gleysol-capped braided stream cycles in the Wutonggou LC probably formed in a subhumid–humid climate (Table 2).

It should be noted that the environmental curve of a cycle (Figs. 3–13) correlates with the stratigraphic column in thickness, whereas the climate curve correlates with the cycle in time, including hiatuses of nondeposition and erosion at the cycle boundary. For example, the semiarid condition at the uppermost part of a Calcisol-capped braided stream cycle (Figs. 3A and 5B) may actually represent the condition during the period of nondeposition and pedogenesis after braided stream deposition had ceased, not necessarily the condition when the uppermost part of the sediments was deposited. This dilemma of graphically presenting the two curves together exists in all cycle types for climate interpretation based on sedimentary features that were not formed syndepositionally.

3.2. Meandering stream high-order cycles

Meandering stream cycles are the erosion–deposition type, and contain channel-fill conglomerate and sandstone (lithofacies 1a and 2a in Table 1) on a high-relief erosional base and overbank sandstone, mudrock, and paleosol (lithofacies 3a, 3e, 3f, and 5; Fig. 3B). Two general sub-types were identified. The first sub-type is the coarse-grained cycles with thick channel-fill and thin overbank deposits (similar to the wandering stream systems of Miall, 1996). Channel-fill deposits are conglomerate and conglomeratic sandstone; overbank deposits are sandstone and mudrock. These cycles are 2–8 m thick. The second sub-type is the classic meandering stream cycles where the channel-fill deposit has a similar or smaller thickness than the overbank deposit. Channel-fill deposits include channel-lag conglomerate and accretionary point-bar sandstone, where conglomerate is much less abundant than that of coarse-grained cycles (Fig. 8B, C). Overbank deposits are dominantly mudrocks (Fig. 9B, C). They are 2–12 m thick and common in the Wutonggou and Jiucaiyuan LCs (Figs. 9A and 10A).

Meandering streams develop in catchment of a low topographic gradient and require a perennial flow. Thus, meandering stream cycles indicate a large catchment basin and a subhumid–humid climate. This interpretation is supported by common plant remains, petrified woods, and capping humid paleosols (Fig. 3B), and is especially applicable to some “super” systems (thicker than 10 m) in the Wutonggou LC, which suggest a large perennial river flow in a large catchment basin, intense source denudation and weathering under a humid climate (Miall, 1996). However, cycles capped by Calcisols or calcareous Argillisols may have formed in a semiarid–subhumid climate or the upland of the catchment (Table 2). Alternatively, they may indicate an intra-cycle variation between subhumid–humid during stream deposition and semi-arid conditions during non-deposition and pedogenesis. Finally, systematic upward

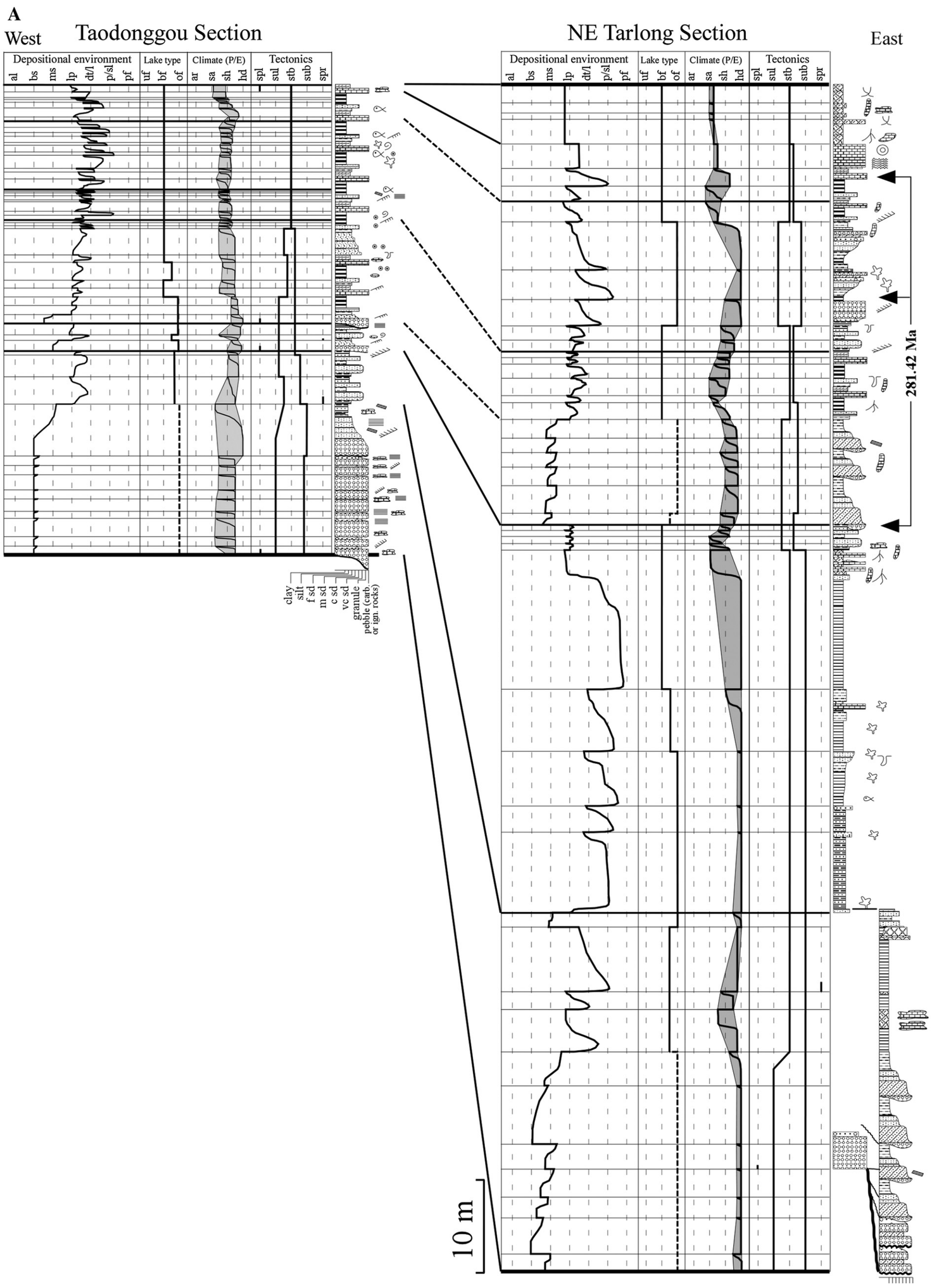

Fig. 7. (A) Highly-simplified lithology and sedimentary structure, interpreted depositional environment, lake type, climate, and tectonic movement of source area and depositional site, and cyclostratigraphy of Artinskian Hongyanchi low-order cycle (LC). See Fig. 4A for explanations. (B) Field photo and measured section of five thin fluctuating profundal mixed siliciclastic–carbonate high-order cycles (HCs), upper Hongyanchi, Taodonggou. In the photo, dashed lines are cycle boundaries; dotted lines facies boundaries. See Fig. 4A for explanations. (C) Field photo of two calcic Vertisols in the uppermost Hongyanchi LC (long dashed line - top of paleosols and the Hongyanchi–Quanzijie unconformity; short dashed line — contact between paleosols and skeletal limestone). Field view is ~100 m across. Inset: Close-up of the two stacked calcic Vertisols. Dashed lines are the top of the well-defined Bk horizons. The lower Vertisol has well-developed slickensides filled with pedogenic calcite and antiforms, NE Tarlong. Person as scale. (D) Field photo showing an unconformity (long-dashed line) separating fluctuating profundal HCs in the Lucaogou LC (left) from braided stream and coarse-grained meandering stream HCs of the Hongyanchi LC (right, outlined by short-dashed lines), NE Tarlong. People (circled) are 1 m tall. Stratigraphic-up to the right.

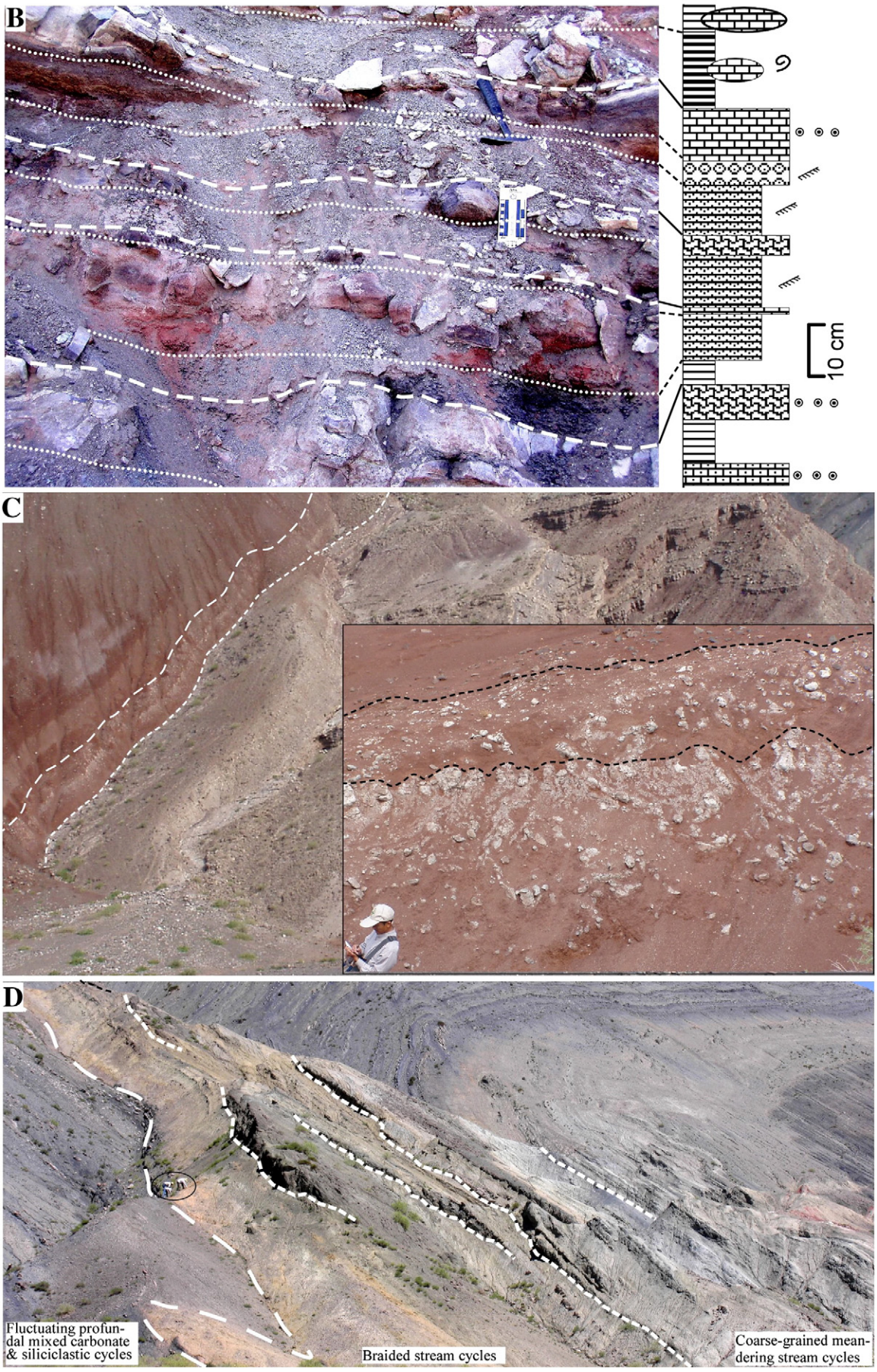

Fig. 7 (*continued*).

stacking of braided, coarse meandering, and classic meandering stream systems is not uncommon (e.g., Fig. 7D). It indicates stream evolution during catchment peneplanation, source denudation and retreat, and increased stream discharge caused by an enlarged catchment and/or an increasingly humid climate (Miall, 1996).

3.3. Lacustrine deltaic high-order cycles

Lacustrine deltaic cycles are the environmental type and generally consist of two depositional systems deposited during lake expansion and contraction, respectively (Fig. 3C). The lower system contains a basal thin transgressive lake-margin deposit of well-washed conglomerate or sandstone (lithofacies 1a or 2b in Table 1) with a sharp or broad, slightly erosional base. In some cases, common in the Wutonggou LC, the deposit is underlain by an interval of upward Gleysol, carbonaceous Argillisol, Histosol, and ostracod and choncostracan-bearing shale (lithofacies 3a, 3e, and 5) with a sharp base. The interval is 1–100 cm thick, interpreted as subaerial lake-margin deposits associated with an approaching shoreline and a rising groundwater table (e.g., Fig. 9D). The uppermost part of the lower system is commonly overlain by 1–10 cm thick thinly laminated shale with common ostracods (lithofacies 3a and 3b) and, in some cases, scattered fish scales. The shale has a sharp to gradational base, which, in rare cases, is mantled with cm-thick oxidized pisoids and oncoids, suggesting a period of starved sedimentation. It was interpreted as the maximum-transgressive condensed deposit. The upper system of the deltaic cycle is a thick, upward-coarsening and thickening succession of prodeltaic–delta–front shale, siltstone, sandstone, and/or conglomerate (lithofacies 3a, 2c, and 1a) in the lower part (Figs. 6D and 9E), and distributary channel-fill and interdistributary deltaplain sandstone, conglomerate, mudrock, and paleosols in the upper part (lithofacies 2a, 1a, 3a, 3e, 3f, and 5). The upper system indicates progradational infilling. The deltaic cycles are 1–13 m thick.

Delta formation requires a large influx of river water and sediments, which likely occur in an over-filled lake (Carroll and Bohacs, 1999) and a humid climate, although lake transgression may be of a tectonic, climatic, and/or autogenic origin. Common disseminated plants in prodeltaic and delta-front facies and carbonaceous shale, Histosol, and Gleysol in deltaplain facies suggest a continuing humid condition throughout a deltaic cycle. Some cycles, however, contain Calcisols in the deltaplain facies, and suggest intra-cycle variations from humid during lake expansion and delta progradation to semiarid conditions at the end or after deltaic deposition (Figs. 3C and 5A).

3.4. Fluctuating profundal mixed carbonate and siliciclastic high-order cycles

Fluctuating profundal mixed carbonate and siliciclastic cycles are the environmental type, representing an overall trend of lake expansion/deepening and contraction/shallowing. They are 0.2–3 m thick and exclusively in the Lower Permian (Figs. 3D, 6A, E and 7A, B). The basal part is composed dominantly of fine subarenite to arenite and rare conglomerate (lithofacies 2b and 1a in Table 1) with a sharp to slightly erosional contact, suggesting a high-energy lake shore to littoral environment during lake expansion. Organic-rich shale (Lithofacies 3b) overlies the sandstones, indicating a starved profundal environment during maximum expansion. This is followed by an upward succession of calcareous shale, limestone, and dolomitic shale and dolomite (lithofacies 4a, 3c, and 4b), indicating increasingly saline and evaporative lake water in low-energy littoral, playa, to mud flat environments (Fig. 6E; see also Carroll, 1998). The cycle may be capped by Calcisols, calcic Vertisols, or possible Gypsisols. Primary gypsum may have occurred as interlaminae or nodules in the succession. Grainstone and packstone facies commonly are associated with arenite and subarenite (Fig. 7B) and, in some cases, calcareous shale, indicating a high-energy littoral and lakeshore environment. The facies associations in the fluctuating profundal cycle indicate large fluctuation of lake level and associated environmental shifts. One or more of the component lithofacies are commonly absent in a specific cycle (Fig. 3D). Nevertheless, a deepening–shallowing trend is always represented by the succession of component lithofacies.

The absence of thick coarse-grained facies and presence of evaporate minerals and arid paleosols suggest limited river inflow, an under-filled or balance-filled lake, tectonic quiescence in the source area, and a semi-arid to arid climate. Lake expansion–contraction suggests possible low-magnitude intra-cyclic climatic variations from subhumid–semiarid during lake expansion to semi-arid to arid during lake contraction (Fig. 3D). Finally, calcic Vertisols and interlaminations of organic-rich, silt-rich and dolomitic shales, limestone, and dolomite suggest strong precipitation seasonality; common dropstones suggest seasonally frozen lakes.

3.5. Lakeplain–littoral siliciclastic high-order cycles

The lakeplain–littoral cycles are the environmental type, similar to the fluctuating profundal cycles. They contain shoreline and littoral well-washed sandstone and conglomerate (lithofacies 2b and 1a in Table 1) and sub-littoral shale (lithofacies 3a) and overlying lakeplain muddy and sandy paleosols (lithofacies 3e and 5; Fig. 3E). They may be capped by a variety of arid to subhumid paleosols. Some cycles have a basal interval composed upward of thin (1–10 cm) Gleysol, carbonaceous Argillisol, Histosol, or ostracod and chocostracan-bearing shale (lithofacies 3a and 3e), interpreted as subaerial transgressive deposits. Sharp or broad, slightly erosional base and top are common. Some cycles lack the basal well-washed coarse-grained facies, indicating a low-energy transgressive environment. The lakeplain–littoral cycles are generally thin, ranging from 10 to100 cm thick.

The absence of thick coarse-grained deposits and the small magnitude of environmental shift suggest limited influx of river water and sediments, subdued source uplift, a balance-filled lake, or alternatively a depositional site away from depositional loci. The small cycle thickness suggests moderate subsidence at the depositional site. The climate probably varied from subhumid to semiarid. It was humid enough to cause a river inflow large enough so that the lake water was too fresh and/or turbid for carbonate and evaporite to accumulate, but was arid enough to limit the influx of river water and sediments so that deltas could not form extensively. Intra-cyclic climatic variations may be great if both the basal humid and capping arid paleosols are present in a cycle. Cycles in the Wutonggou LC lack the capping arid paleosols, whereas those in the Jiucaiyuan and Shaofanggou LCs lack the basal humid paleosols. Both cases suggest intra-cyclic climatic variations from a relatively wet during lake expansion to a relatively dry condition during lake contraction and subaerial exposure.

3.6. Multi-order cyclicity

Stratigraphic stacking of HCs into ICs and LCs reflects that the geologic processes controlling environmental changes had operated with varying dominance and at multi-order temporal and spatial scales. Sequence stratigraphic analysis of nonmarine strata is challenging due to rapid lateral facies and thickness changes, common erosional surfaces, poor biostratigraphic resolution, and multiple sediment sources, transport regimes, and depocenters (Shanley and McCabe, 1994; Miall, 1996, 2006; Talbot and Allen, 1996; Olsen, 1997; Gierlowski-Kordesch and Kelts, 2000). It has been experimented in the study area (Yang et al., 2007b, 2008, 2009; Yang, 2008). However, principles and procedures of sequence stratigraphy are not the focus here and only described briefly below and summarized in Table 3.

An intermediate-order cycle or sequence is composed of a succession of HCs that shows an upward trend of deepening and

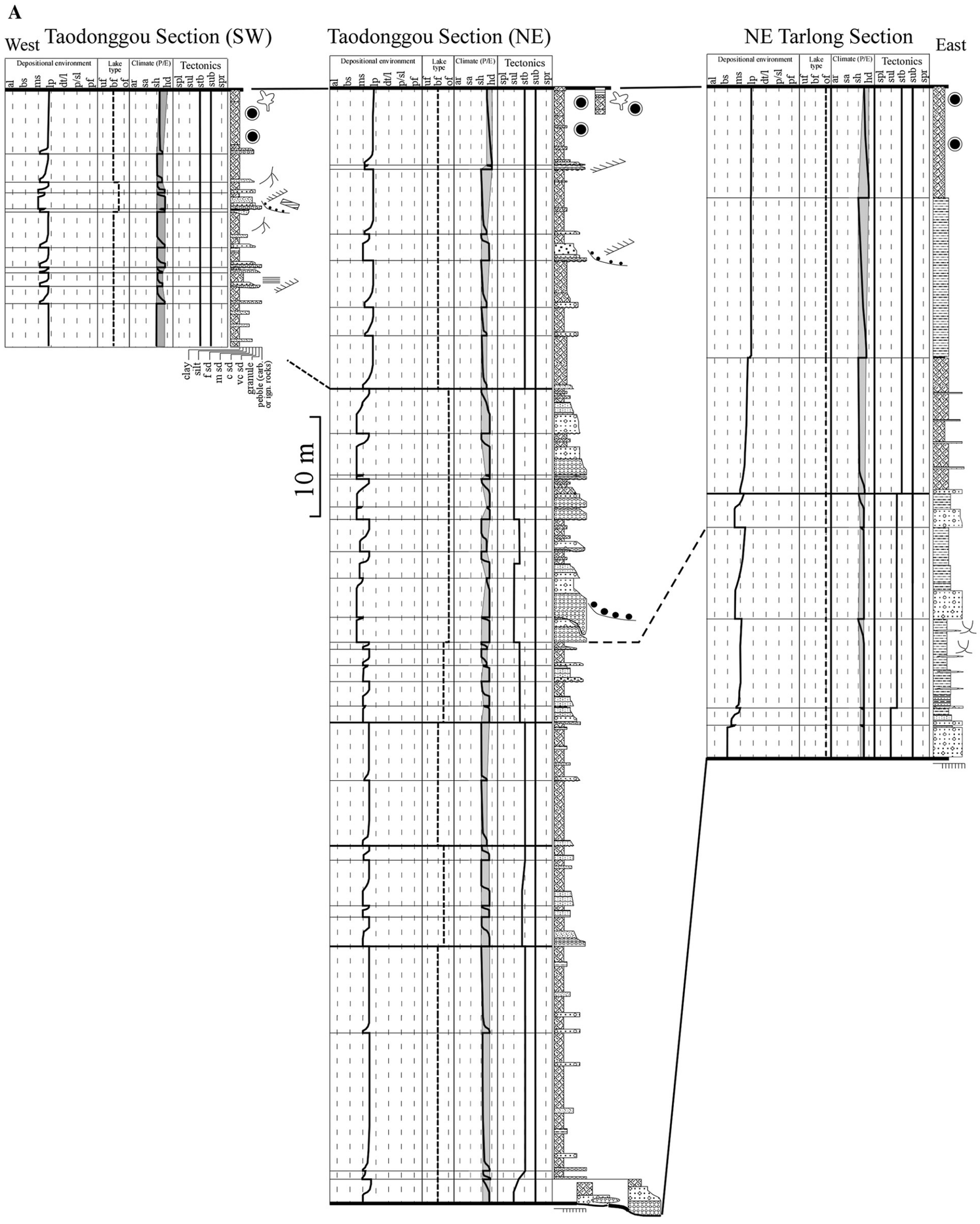

Fig. 8. (A) Highly-simplified lithology and sedimentary structure, and interpreted depositional environment, lake type, climate, and tectonic movement of source area and depositional site, and cyclostratigraphy of Capitanian Quanzijie low-order cycle (LC). See Fig. 1C for section locations and Fig. 4A for explanations. (B) Field photo showing a meandering channel (thick long-dashed line) cutting into underlying Argillisol. Lenticular channel-lag conglomerates are outlined by thin short-dashed line and high-angle and low-angle cross-bedded are outlined by thin short-dashed lines in the lower and upper point-bar conglomeratic sandstones and sandstones, forming an upward-fining succession, upper Quanzijie, Taodonggou. Hammer is 35 cm long. (C) Field photo showing gray stacked channel-fill conglomerates encased in red overbank siltstone and silty shale, lower Quanzijie, Taodonggou. Strata are overturned with stratigraphic-up to lower left. Person is 1.9 m tall. (D) Field photo of two red and black ash-fall tuffs (white arrows) in profundal shales of Hongyanchi LC, which is cut by a meandering stream at the base of Quanzijie LC. The lower ash is dated as 281 Ma. Dashed line is the Hongyanchi–Quanzijie unconformity. SE Tarlong. Hammer is 35 cm long.

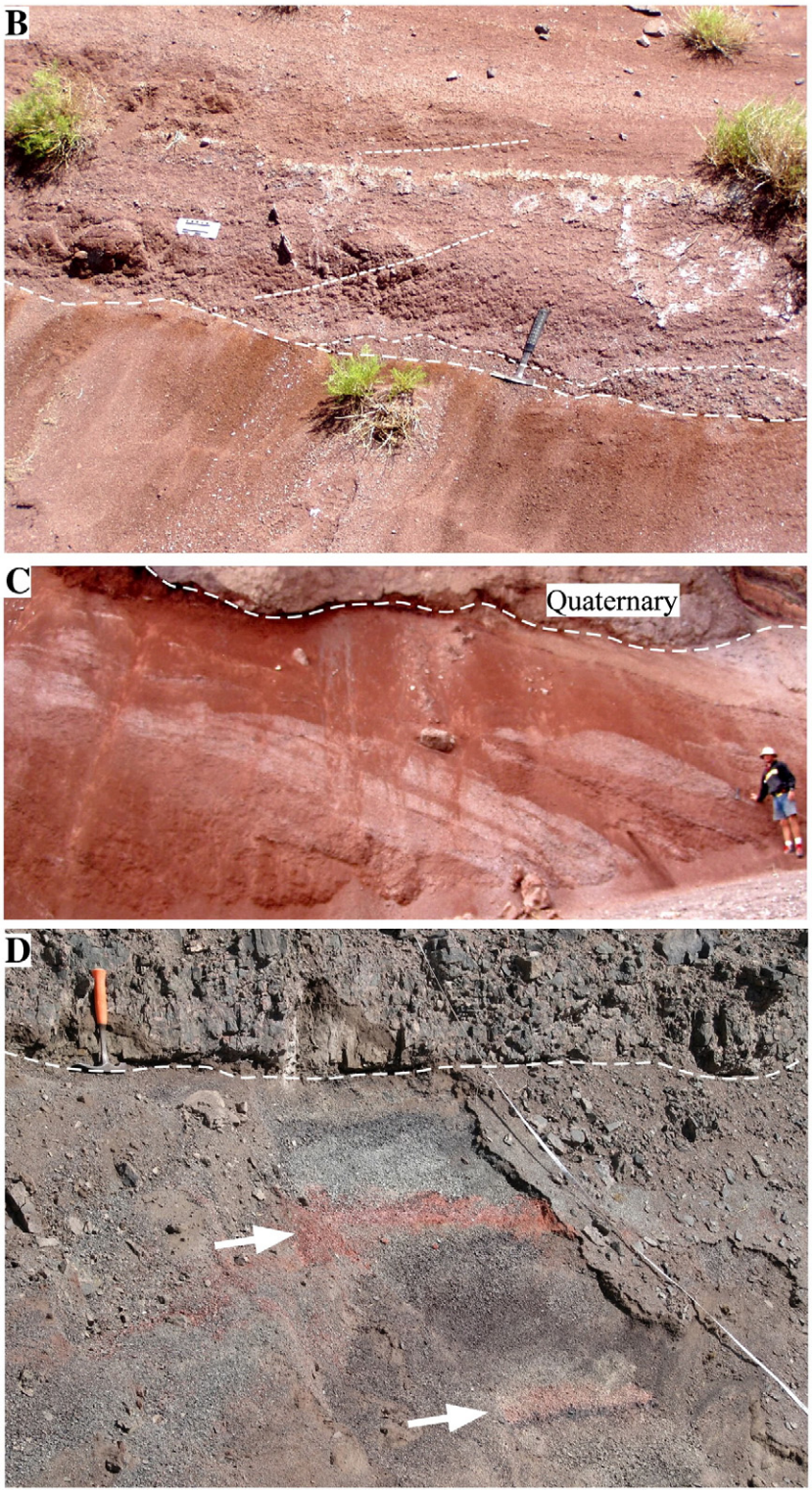

Fig. 8 (*continued*).

shallowing of depositional environments, indicating an intermediate-term of lake expansion and contraction. In an ideal sequence, the basal interval consists of fluvial HCs in an erosional contact with underlying lacustrine deposits, signifying a low lake level and maximum lake contraction. It is termed lacustrine lowstand systems tract (LLST; Fig. 12). The overlying HCs contain relatively thick transgressive deposits; and their maximum-transgressive deposits become progressively deeper and thicker. They signify a period of progressive lake expansion and deepening, and comprise the transgressive systems tract (LTST). One or two thin HCs with a significant portion of profundal lithofacies overlie the LTST, and comprise the condensed section (LCS). The LCS is, in turn, overlain by a succession of thick HCs containing progressively shallower-water lithofacies, indicating progradational infilling of a lake basin, and is the highstand systems tract

(LHST). The uppermost part of a sequence consists of a succession of thin HCs with a significant proportion of paleosols that indicate frequent subaerial exposure and limited accommodation space, signifying the final infilling of a lake basin. This succession is the regressive systems tract (LRST). In the studied sections, the type, number, and thickness of HCs in a systems tract varies depending on the depositional settings and lake types; LLST and LCS are rare (Fig. 12 and Table 3). Nevertheless, as a whole, a sequence represents a cycle of initial to maximum lake expansion, followed by lake contraction and disappearance due to sediment infilling and/or lake level fall. The intermediate-order sequence and its systems tracts are similar to a depositional sequence and associated systems tracts as defined in marine settings (Mitchum and Van Wagoner, 1991). Yang et al. (2007b, 2009) recognized that, however, the type and mechanism of controlling processes in the fluvial–lacustrine setting are quite different from those in the marine settings.

Low-order cycles are defined on the basis of similarity in types of HCs and ICs, which reflects the long-term trend of environmental changes and long-term stability of tectonic and/or climatic conditions. Low-order cycles are demarcated by regional unconformities and/or conformities, across which major changes in environment and tectonic and/or climatic conditions occurred. The nature and magnitude of environmental shift across a LC boundary vary within the Tarlong–Taodonggou half graben (e.g., Jeffrey et al., 2010). Hence, the changes are apparently abrupt across unconformities but gradational across conformities. The great contrasts in lithofacies, types of HCs and ICs, and controlling processes, and regionally traceable boundaries of low-order cycles facilitate reliable correlation in the study area.

4. Characteristics of low-order cycles and climatic variability

Climatic variabilities at intra-HC, HC, IC, and LC scales were identified in the studied sections (Fig. 13). Most climate cycles coincide with sedimentary cycles, but not in all cases because climate is not the sole control on cyclic sedimentation and climate signals other than P/E ratio, such as temperature and wind, were not interpreted in this study. For example, changes in P/E ratio may be insignificant within a Histosol/Gleysol-capped deltaic HC. Climate changes within HCs vary in magnitude but are gradual in shift. Changes across HC boundaries are commonly abrupt (Figs. 3–13), which may be in part due to the hiatus at cycle boundaries (see also Section 3.1). Climatic changes are commonly abrupt and of a moderate to large magnitude across IC boundaries and moderate to large within ICs.

Climate variability interpreted at the LC scale is the most reliable among the four levels. This is because: 1) long-term climate interpretation utilizes all available evidence that may not be present in individual HCs and ICs; 2) long-term tectonic signals are relatively easy to be identified and, then, removed during climate interpretation; and 3) signals of autogenic processes are commonly erratic in time and space and can be eliminated through lateral correlation and cycle stacking, as a result, cause minimal distortion to the long-term trend. Hence, the climate variability at the LC scale is discussed below in detail in the context of major characteristics of individual LCs.

4.1. Lower Daheyan low-order cycle

The lower Daheyan LC contains 6 ICs and 36 HCs, and is 106.5 m thick in NE Tarlong. It is absent from NW Tarlong to Taodonggou (Table 4). Both its base and top are graben-wide unconformities (Figs. 2, 4A). Classic meandering stream HCs dominate. Two thin fluctuating profundal HCs contain arenaceous lime mudstone and peloidal or oolitic wackestone to grainstone and no profundal shale. A 9 m-thick braided stream HC may be alternatively interpreted as reworked beach conglomerate and sandstone deposits because of the presence of well-rounded and imbricated clasts, abundant low-angle tabular cross-beds, well-preserved desiccation cracks, and the lack of internal erosional surfaces.

The rapid thickness change of the lower Daheyan LC suggests a highly variable depositional topography atop the Taoxigou volcaniclastics, upon which meandering streams developed in local alluvial valleys (Figs. 1C, 4A). Temporary ponding of streams formed small balance-filled lakes. Tectonic uplift in the source areas, including distant mountains and local horsts, was probably episodic and subsidence of the valley floor persistent. Meandering streams with well-developed floodplains and lake-margin mud flat suggest perennial river flux. Red to purple, calcareous and ferruginous Argillisols with root molds indicate a dominantly subhumid climate with thin humid intervals (Fig. 4A and Table 4). A 35 cm-thick oolitic grainstone contains a loosely-defined layer of very angular to angular basaltic pebbles and cobbles in the middle part (Fig. 4F). They are randomly oriented and float in the ooid sand. The clasts may have been shed on to lake ice from nearby hillslope during winter storms and dropped in and mixed with ooids when ice melted, or transported by a spring stream flowing on lake ice. This interpretation implies a seasonally-frozen lake.

4.2. Middle Daheyan low-order cycle

The Middle Daheyan LC contains 15 HCs in 1 IC in Taodonggou and at least 15 HCs and 1 IC in NE Tarlong where high-order cycles are not fully delineated due to low-quality exposure (Fig. 4A and Table 4). It is 188.55 m thick in NE Tarlong and 33.15 m thick in Taodonggou. Its base is an unconformity; and the top is a sharp, locally erosional surface. Braided stream HCs dominate and are thin in Taodonggou and thick in NE Tarlong. A 27.5 m-thick interval of basaltic flows in NE Tarlong thins to the east, south, and west and is absent in Taodonggou.

The lack of lacustrine deposits and abundant pebble–boulder braided stream deposits suggest the development of an alluvial fan complex and steepening of depositional topography in the study area. The thickness is the greatest in NE Tarlong, medium in southern Tarlong, and the thinnest in Taodonggou, indicating a depocenter in the vicinity of NE Tarlong. The thickness variation also suggests a highly-variable topography, great source uplift, and fast subsidence in the depositional site. Two thin Calcisols are present, one in a local depression on top of the basalt flow and the other at the top of the LC in NE Tarlong (Fig. 4A). The monotonic stacking of numerous braided stream HCs suggests fast alluvial sedimentation and a dominantly subhumid climate.

4.3. Upper Daheyan low-order cycle

The upper Daheyan LC contains 39 HCs in 5 ICs in Taodonggou and at least 12 HCs in NE Tarlong (Fig. 5A and Table 4). It is slightly thinner (91.05 m) in Tarlong than in Taodonggou (108.8 m). Its base is sharp to locally erosional; and its top is sharp to erosional with overlying wave-reworked conglomerate, sandstone, or pisolitic rudstone. Braided stream HCs dominate and grade upward into coarse-grained meandering stream HCs. An overall upward-fining trend of an increased amount of sandstone is present; and the deposits in Taodonggou are finer than those in Tarlong (Fig. 5A). Three deltaic HCs in the lower Taodonggou section contain well-stratified and well-washed conglomerates and sandstones and are lack of prodeltaic deposits and plant materials, indicating a wave-dominated braidplain delta. Calcisols cap almost all HCs (Fig. 5A, B). They contain abundant calcitic nodules and illuvial oxidized sandy matrix, and become thicker and better developed up section.

The dominance of braided stream HCs and overall upward-fining indicate peak development of the alluvial fan complex followed by gradual cessation. Calcisols suggest prolonged hiatuses between episodes of fluvial sedimentation. Thickening in Taodonggou

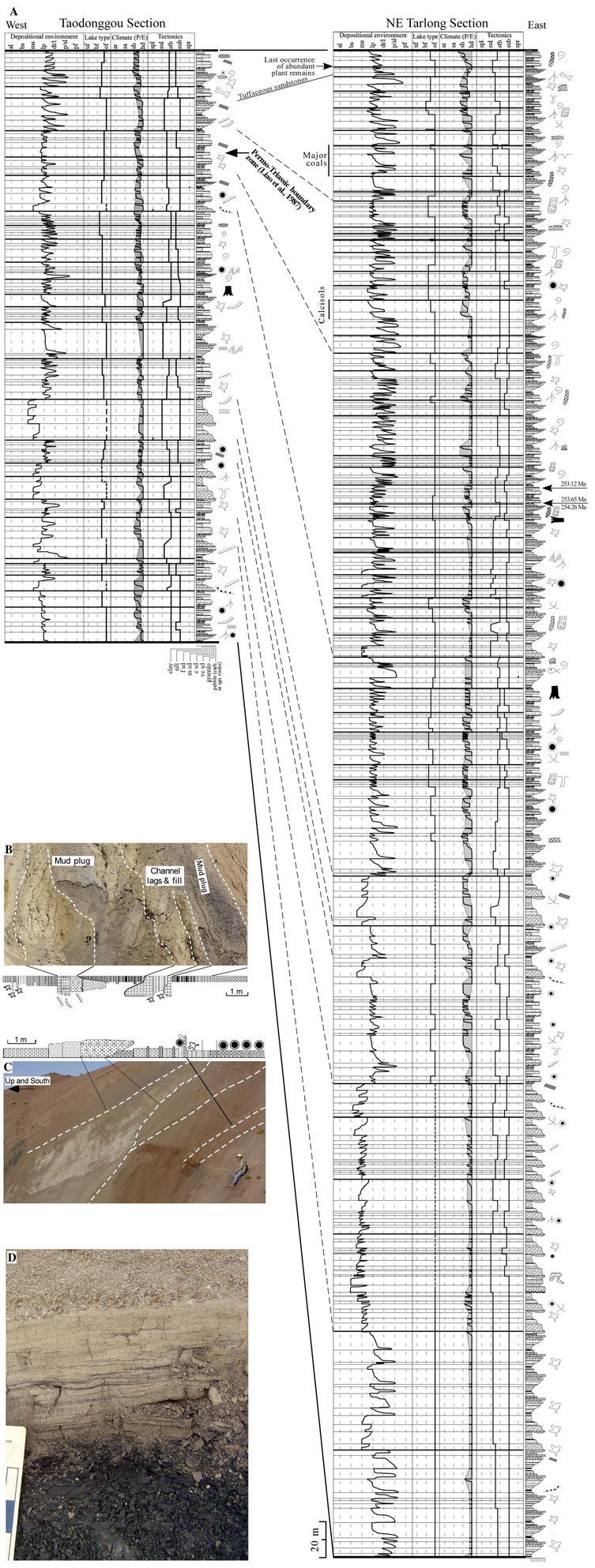

Fig. 9. (A) Highly-simplified lithology and sedimentary structure, and interpreted depositional environment, lake type, climate, and tectonic movement of source area and depositional site, and cyclostratigraphy of Wuchiapingian–lower Induan Wutonggou low-order cycle (1C). See Fig. 4A for explanations. (B) Field photo and measured section of an upward-coarsening deltaic system, a distributary channel sand, mud, and coal fills (mud plug), overlain by a meandering stream system, lower Wutonggou, SW Taodonggou. Stratigraphic-up is to the right. See Fig. 4A for explanations. (C) Field photo and measured section of a meandering stream channel cutting into a lakeplain–littoral high-order cycle. The top of Fe–Mn pisoids-bearing Gleysol is the base of Wutonggou LC, NE Taodonggou. See Fig. 4A for explanations. (D) Field photo of a transgressive succession composed upward of coal and carbonaceous siltstone as subaerial transgressive deposits, a ripple-laminated, laterally persistent fine-medium arenite as a transgressive littoral/lakeshore deposit, and a shale rich in disseminated plant remains as maximum-transgressive prodeltaic deposits, middle Wutonggou, NE Tarlong. Scale bar is 2.5 cm. (E) Field photo of a coarsening upward shale-sandstone deltaic succession. Dashed lines outline delta-front sandstones, upper Wutonggou, NE Tarlong. Stratigraphic-up is to the upper right. Person is 1.7 m tall. (F) Close up of a Bc(g) horizon of a Gleysol (Table 2) containing abundant Fe–Mn pisoids, lower Wutonggou, NE Taodonggou. (G) Close-up of a soil ped containing abundant dark gray, vertical–subvertical tubules filled with illuvial clays (argillans; black arrows), interpreted as clay-filled root molds, upper Wutonggou, NE Tarlong. Scale bar is 1 cm long. (H) Close-up of vertical–subvertical, downward-tapering clay-filled tubules with black remnant carbon films, interpreted as root molds, upper Wutonggou, NE Tarlong. Pen is 0.8 mm wide.

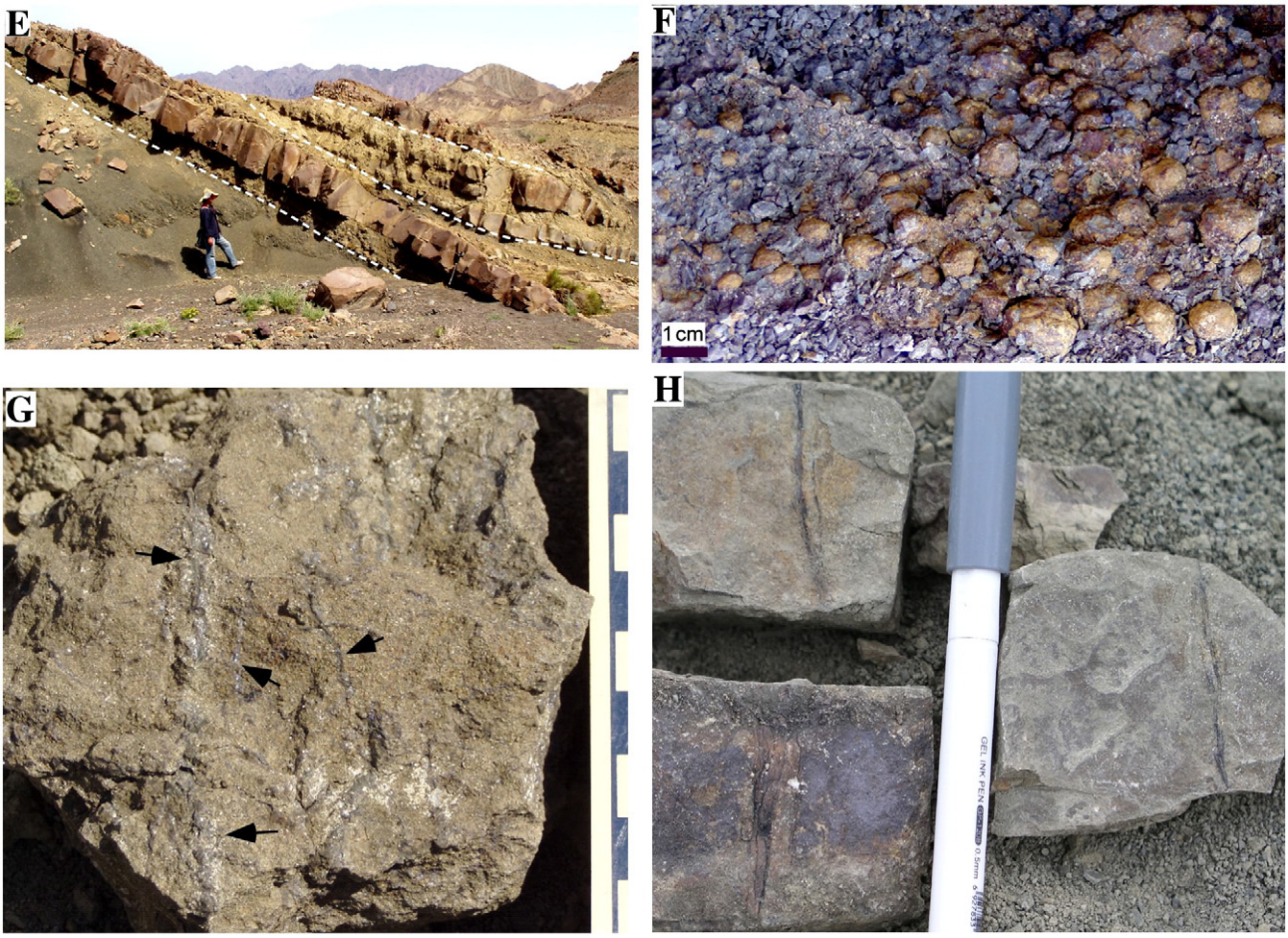

Fig. 9 (*continued*).

indicates that fluvial and deltaic deposits were filling topographic lows and a short-lived balance-filled lake in the vicinity of Taodonggou. The above evidence suggests a gradual lowering of the source area(s) and enlargement of the catchment basin. Abundant Calcisols indicate a persistent subhumid–semiarid condition throughout the upper Daheyan LC well into the uppermost Hongyanchi LC (see below), and signify a major shift from the subhumid conditions in the lower and middle Daheyan LCs. The drier climate may have contributed to a more stable landscape and reduced fluvial influx.

4.4. Lucaogou low-order cycle

The Lucaogou LC contains 137 HCs in 31 ICs in NE Tarlong and 45 HCs in 12 ICs in Taodonggou (Fig. 6A and Table 4). It is thin in Taodonggou (83 m), SE and SW Tarlong, thick in NE Tarlong (180 m), and the thickest in north-central Tarlong (Yang et al., 2009). Its base is a sharp erosional surface mantled with a thin layer of well-washed and well-sorted conglomerate, arenite, or pisolitic rudstone, interpreted as lag deposits on a graben-wide transgressive surface. Its top is a high-relief fluvial channel base in Taodonggou and NE Tarlong, and well-washed beach conglomerate and arenite in southern Tarlong, signifying a major regression. The northern and SE Tarlong sections contain dominantly fluctuating profundal HCs intercalated with lakeplain–littoral and deltaic HCs, whereas the Taodonggou section contains a mixture of fluctuating profundal, lakeplain–littoral, and braided stream HCs with a few deltaic HCs; and the SW Tarlong section contains dominantly deltaic HCs (Jeffrey et al., 2010).

The contrasts in thickness and cycle type between Tarlong and Taodonggou (Fig. 6B, D, E, G) suggest that northern Tarlong is both the depositional and subsidence centers, where profundal sedimentation was dominant, interrupted by episodic deltaic progradation; and northern Taodonggou and SW Tarlong were at the ramp margin of the half-graben (Yang et al., 2009). This interpretation is supported by a 10 m interval of northward-prograding limestone and overlying deltaic clinoforms (Yang et al., 2008) in the basal Lucaogou LC in northern Tarlong. The lake was mainly balance-filled, only over-filled during periods of major deltaic progradation. Source uplift was episodic as indicated by sporadic coarse deposits and erosion; and subsidence was great in northern Tarlong but small in the other parts of the half-graben, as indicated by the thickness variations. Sequence stratigraphic analysis of Yang et al. (2009) depicted mobile depocenters in the early Lucaogou time which became stabilized in middle and late Lucaogou. The highly variable lacustrine cycles suggest large and frequent fluctuations of lake depth and depositional environments, some of which may be caused by episodic uplift or lowering of spill points.

The climate oscillated dominantly between subhumid to semiarid conditions, characterized by large intra-HC variations (Fig. 6A). Short intervals of humid and semiarid–arid conditions are present in the NE Tarlong section, where stratigraphic resolution is high. Deltaic deposits with abundant plant remains suggest large river inflow and precipitation. Possible Gypsisols, Calcisols, and evaporitic deposits suggest semiarid–arid conditions. In most intervals, the absence of plant-rich deltaic deposits and arid paleosols suggests subhumid to semi-arid conditions, under which fluctuating profundal HCs were

deposited. Finally, dropstones in profundal shales (Fig. 6F) suggests that the lakes were seasonally frozen.

4.5. Hongyanchi low-order cycle

The Hongyanchi LC contains 45 HCs in 5 ICs in NE Tarlong and 53 HCs in 6 ICs in Taodonggou (Fig. 7A and Table 4). It thins rapidly away from NE Tarlong (117 m) to Taodonggou (51 m) as well as SE and SW Tarlong. Its base is a high-relief fluvial channel base in NE Tarlong and Taodonggou (Fig. 7D), and a highly-contorted deltaic base in SE and SW Tarlong. Its top is a disconformity on highly-mature stacked vertic Calcisols in NE and SW Tarlong and Taodonggou (Fig. 7C), and a meandering stream channel base in SE Tarlong (Fig. 8D). All types of HCs occur, although fluctuating profundal HCs dominate, and range widely from 0.15 to 16 m thick (Fig. 7A and Table 4).

The thickness pattern suggests a paleogeography similar to that of the underlying Lucaogou LC (Figs. 6A, 7A), where NE Tarlong was the subsidence and depositional center. A similar depositional environmental trend is present at different parts of the graben, despite of the rapid thickness changes. There are more HCs and ICs in the shorter Taodonggou section than in the much thicker NE Tarlong section. The discrepancy is mainly caused by many undocumented thin (1–10 cm) HCs in the thick profundal shales in the lower Hongyanchi in NE Tarlong (also in SE Tarlong; Fig. 7A). These HCs are couplets of sandy turbidites and profundal shales. Fluvial and deltaic environments change upward into deep-profundal, then lake margin and fluctuating profundal environments. This trend suggests an early episode of major lake contraction and fluvial incision and deposition followed by lake expansion, then contraction, and final exposure and landscape stabilization. Lake type changes upward from dominantly overfilled to balance-filled. A catastrophic spill-point lowering may have occurred across the Lucaogou and Hongyanchi boundary, causing major fluvial incision (Jeffrey et al., 2010). Source uplift and basin subsidence were probably active in early Hongyanchi, then gradually stabilized.

The climate in the early Hongyanchi time was humid, as suggested by thick fluvial and deltaic deposits, lack of Calcisols, abundant plant remains, and lake expansion. The climate in the middle-late Hongyanchi fluctuated widely from subhumid–semiarid to humid–subhumid at both the HC and IC scales and shifted gradually to a semiarid condition culminating at the end of Hongyanchi (Fig. 7A, C).

4.6. Quanzijie low-order cycle

The Quanzijie LC contains 35 HCs in 5 ICs in Taodonggou and at least 8 HCs in 2 ICs in the poorly-exposed NE Tarlong section (Fig. 8A and Table 4). The NE Tarlong section is 67.5 m thick, thinner than the Taodonggou (112.4 m) and SE and SW Tarlong sections which have similar thicknesses. The base of Quanzijie is a disconformity on top of mature Calcisols in NE and SW Tarlong and Taodonggou, but a channel base in SE Tarlong. The top is a sharp to gradational contact with deltaic deposits of the Wutonggou LC. Meandering stream HCs dominate. Upward-decreasing abundance and maximum clast size of conglomerates indicate an overall fining-upward trend. The most conspicuous feature is the thick red-brown-colored overbank deposits composed of siltstones and silty mudstones (Figs. 7C, 8B, C). They are mostly structureless, poorly lithified, non-calcareous, and lack of any fossils and distinctive pedogenic structures. All rocks in the Quanzijie are variably tuffaceous. Laterally persistent volcanic ash-fall deposits are abundant and 1–100 cm thick. In several cases in SW Tarlong, well-laminated shale or upward-coarsening and thickening shale-sandstone successions are bounded at the base and top by thick tuffs. They were interpreted as littoral–sub-littoral and deltaic deposits, respectively, in volcanics-dammed lakes. Finally, the uppermost Quanzijie (~10 m thick) contains one to two well-developed Gleysols containing Fe–Mn pisoids (2a in Table 2).

The onset of graben-wide meandering stream deposition signifies a major change from lacustrine to fluvial environments. This change may have been caused by a catastrophic spill-point lowering event, a climate change across the Hongyanchi–Quanzijie unconformity, and/or uplift of the source area and catchment basin. The overall fining-upward trend suggests gradual tectonic stabilization; the preservation of thick fluvial deposits suggests fast subsidence in the graben (Fig. 8A). The thickness pattern and short-lived lakes in SW Tarlong suggest the catchment area was tilted to the southwest and the depocenter shifted away from NE Tarlong. Finally, thick mudrocks and Gleysols in the uppermost Quanzijie indicate an extensive mud flat and rising groundwater table, suggesting an approaching lake shoreline to the study area.

Diagnostic sedimentary evidence of climatic conditions is limited. The extensive meandering stream deposits suggest perennial river flow and intense weathering in the source area, pointing to a humid–subhumid condition. This interpretation is supported by the lack of arid paleosols and the pervasive red-brown color of the Quanzijie which suggests intensive oxidation and leaching. On the other hand, the lack of plant materials, clay-size sediments, and humid paleosols does not support the interpretation of a subhumid–humid condition. The thick structureless siltstones are enigmatic in their origin. Nevertheless, the thick mudrocks and Gleysols in the uppermost Quanzijie signify a shift to humid–subhumid conditions. Hence, the climate during the Quanzijie time was tentatively interpreted as subhumid to humid.

4.7. Wutonggou low-order cycle

The Wutonggou LC contains 121 HCs in 27 ICs in Taodonggou and 328 HCs in 49 ICs in NE Tarlong (Fig. 9A and Table 4). It is 329.3 m thick in Taodonggou, much thinner than that in NE Tarlong (828.6 m) and SE Tarlong (733.5 m). Its base is sharp, where deltaic deposits overlie lake-plain deposits. Its top is sharp in Tarlong but is a fluvial channel base in Taodonggou. The cycle is distinctively gray to greenish gray. Abundant deltaic HCs, minor meandering stream and lakeplain–littoral HCs, and rare braided stream HCs occur in NE and SE Tarlong; but lakeplain–littoral HCs dominate in Taodonggou. An overall fining-upward trend is shown by a decrease in grain size and the abundance of conglomerates. Histosols, Gleysols, and Argillisols are abundant (Fig. 9A, B, C, D, F, G). Calcisols occur in two successive HCs over a 10-m interval in upper Wutonggou in Tarlong (Fig. 9A). In addition, the upper Wutonggou contains sparse calcitic nodules in some HCs and overall becomes increasingly calcareous upward.

The persistent deposition of sandy and gravelly sediments throughout the Wutonggou suggests ample clastic supply from a persistently uplifting source area. The upward decrease in grain size and conglomerates suggests a gradually decreasing topographic gradient of the catchment (Guan et al., 2010). The thick sediment accumulation requires fast graben-wide subsidence. The contrast in thickness and types of HCs between Tarlong and Taodonggou indicates NE and SE Tarlong areas were both the subsidence and depositional centers, where meandering streams flew and deltas prograded into overfilled lakes. The Taodonggou area was away from the depocenter where lake-margin sedimentation dominated.

The climate was dominantly humid to subhumid (Fig. 9A), as indicated by abundant Histosols, Gleysols, and Argillisols. Thick meandering stream and deltaic deposits suggest intense provenance weathering, large sediment production and transport by perennial rive flows, and over-filled lake conditions, all of which indicate a great surplus of surface water budget and a strongly wet–dry seasonality (Schumm, 1968; Miall, 1996). Similar conditions were reported by Brand et al. (1993) in a paleoclimatic study in Taodonggou based on oxygen and carbon isotopes of bivalve shells, and by Wartes et al. (2002) in a regional sedimentologic and stratigraphic study in the Bogda Mountains. Climate variations at the HC and IC scales are

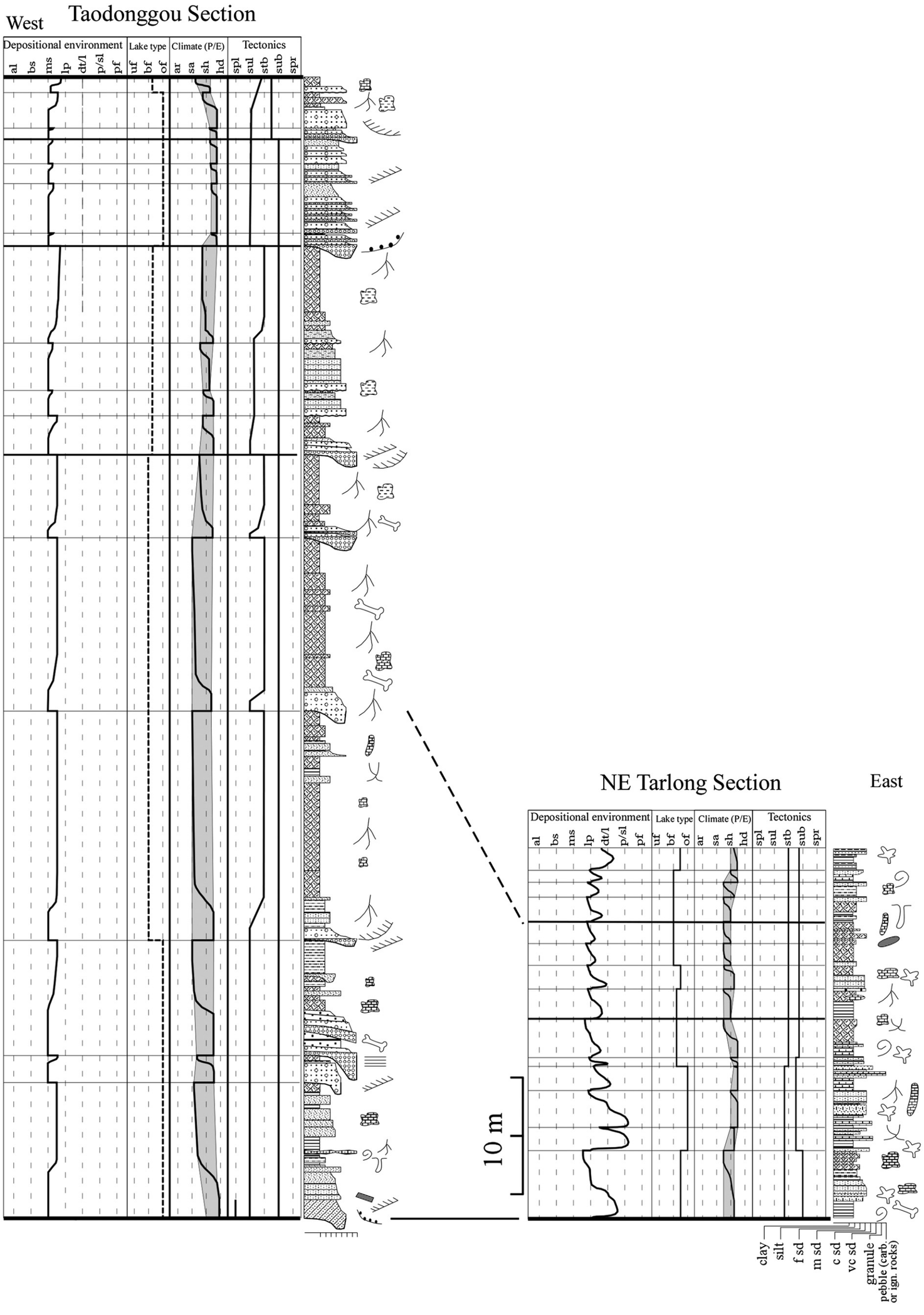

Fig. 10. Highly-simplified lithology and sedimentary structures, and interpreted depositional environment, lake type, climate, and tectonic movement of source area and depositional site and cyclostratigraphy of Induan Jiucaiyuan low-order cycle of the Taodonggou and NE Tarlong sections. See Fig. 4A for explanations.

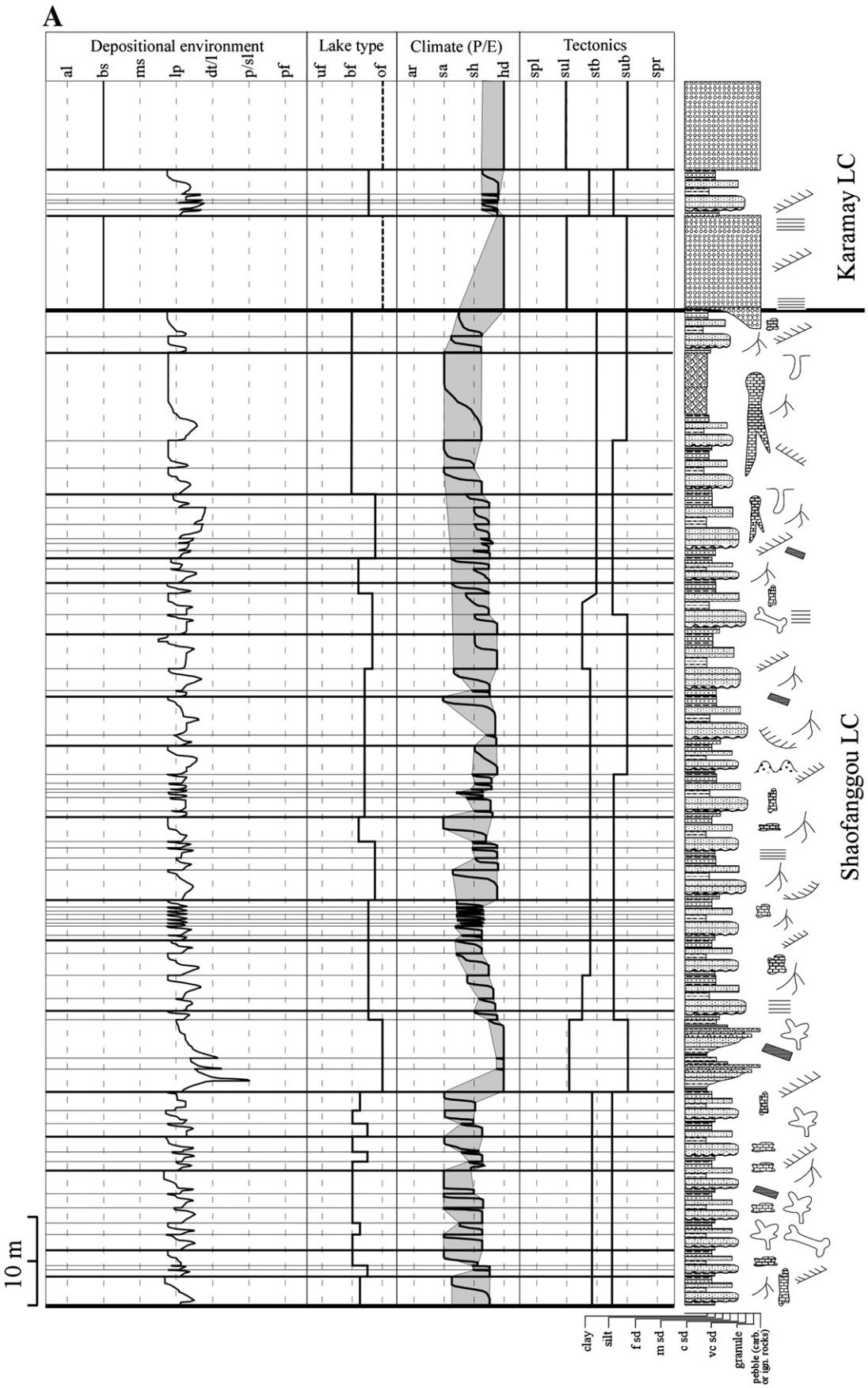
A
Depositional environment
al
bs
ms
lp
dt/l
p/sl
pf
Lake type
uf
bf
of
Climate (P/E)
ar
sa
sh
hd
Tectonics
spl
sul
stb
sub
spr
Karamay LC
Shaofanggou LC
10 m
clay
silt
f sd
m sd
c sd
vc sd
granule
pebble (carb. or ign. rocks)

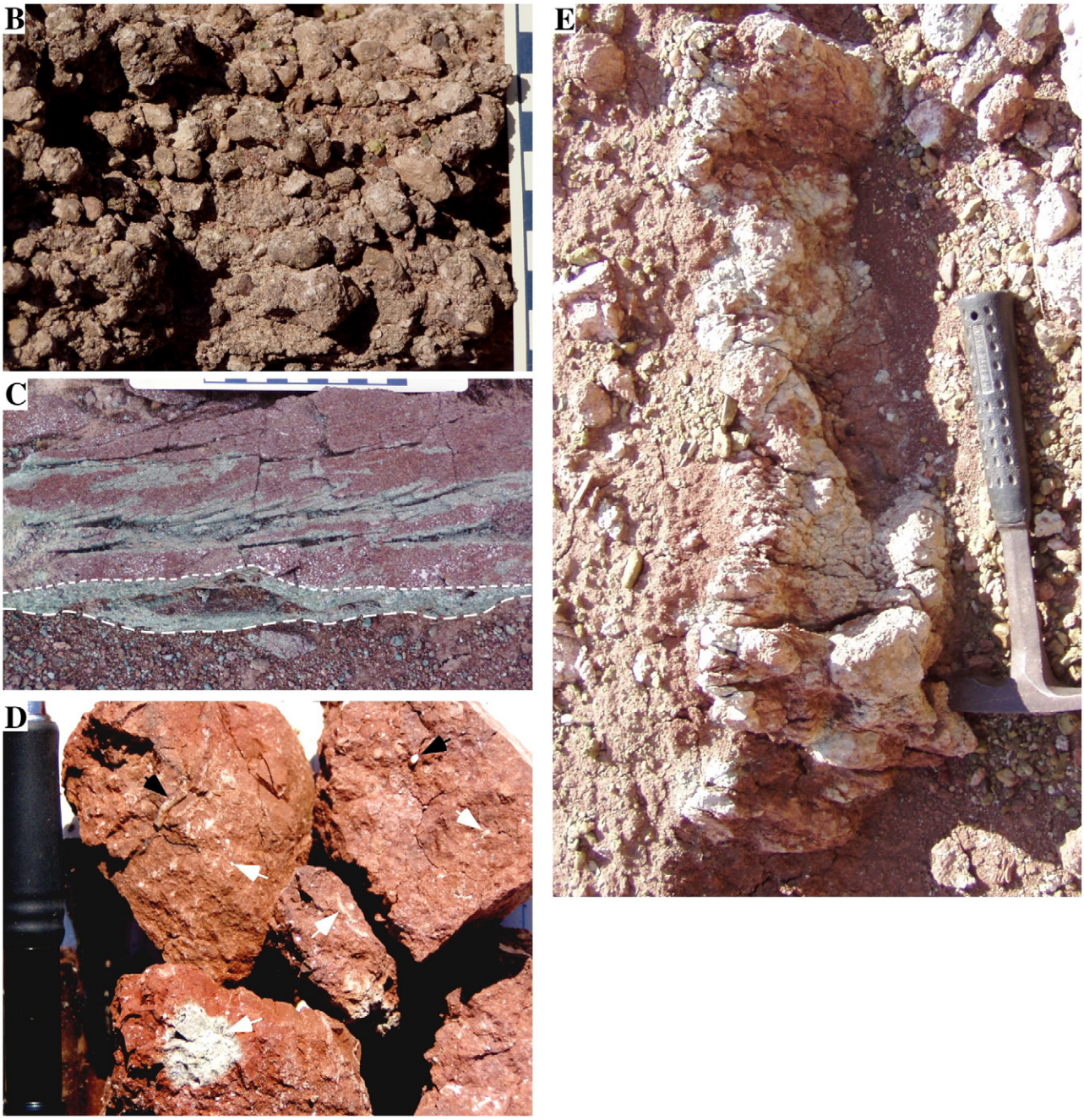

Fig. 11. (A) Highly-simplified lithology and sedimentary structure, and interpreted depositional environment, lake type, climate, and tectonic movement of source area and depositional site, and cyclostratigraphy of Olenekian Shaofanggou and the lower Anisian Karamay low-order cycles (LCs), Taodonggou. See Fig. 4 for explanations. (B) Close-up of a persistent, thin conglomerate (shoreline pebbles) composed of calcitic soil nodules, which overlies a Calcisol, uppermost Shaofanggou, SW Taodonggou. The nodules were probably derived from the underlying Calcisols. See Yang (2007) for an example of a similar origin. Scale bar is 1 cm long. (C) Field photo showing a calcareous Argillisol separated by an erosional transgressive cycle boundary (long dashed line) from an overlying lenticular layer of granule to fine-pebble conglomerate containing rip-up clasts of the Argillisol, which is overlain by high-angle tabular cross-bedded very coarse arenites. Short dashed line separates basal transgressive lag (i.e. conglomerate) from transgressive arenites, lower Shaofanggou, SW Taodonggou. Scale bar is 1 cm. (D) Field photo of oxidized calcareous Argillisol blocks containing mm-size green rounded to elongate steles (white arrows) and calcified rootlets (black arrows), middle Shaofanggou, SW Taodonggou. Pencil is 1 cm thick. (E) Field photo of a vertical calcitic rhizoconcretion in the Calcisol underneath the Olenekian–Anisian unconformity, SW Taodonggou. Hammer is 35 cm long.

common. The two Calcisols in upper Wutonggou in NE Tarlong indicate a subhumid–semiarid condition as a short but significant deviation from the prevalent humid–subhumid condition. A 1.5 m-thick coal interval ~70 m above the Calcisols occurs above the ~90 m-thick interval where the Permo–Triassic boundary is likely to be placed (Fig. 9A). It is the thickest in the studied sections and shows a return to the humid–subhumid condition after the end-Permian. Nevertheless, the occurrence of short-term shifts toward drier conditions becomes increasingly common upward in the upper Wutonggou LC, signaling a gradual change to a drier condition in the overlying Jiucaiyuan LC.

4.8. Jiucaiyuan low-order cycle

The Jiucaiyuan LC contains 17 HCs in 4 ICs and is 97.8 m thick in Taodonggou. It is incomplete (37.1 m thick) and contains 14 HCs in 3

Table 1
Characteristics, interpreted depositional environments, and occurrence of lithofacies in uppermost Carboniferous–Lower Triassic fluvial–lacustrine deposits, southern Bogda Mountains, NW China.

Lithofacies	Grain composition	Sedimentary texture	Sedimentary structure	Stratal geometry, boundary relationship, thickness	Fossils	Depositional environment	Occurrence[a]
1. Conglomerate							
a. Clast-supported conglomerate	Volcanic and shallow intrusive, marine and nonmarine sedimentary	Granule to boulder, subangular to well-rounded, mod-well-sorted, imbricated	Plane or low-angle x-bedded, normal graded.	1) Erosional base, channel form; 2) lenticular, convex top and concave base; 3) well thin-bedded, laterally persistent, 1–10 cm thick	Locally concentrated large tree trunks and plant remains	1) Channel-fill; 2) delta-front; 3) shoreline and littoral pebbles	Braided stream deposits mainly in DHY LCs; deltaic and lacustrine throughout. Decreasing upward Uncommon. DHY LCs
b. Matrix supported conglomerate	Same as above	Granule-boulder, very angular to sub-rounded, very poorly sorted, random oriented	Massive bedded.	Tabular, sharp base, gradational-sharp top, 1–10 m thick	None	Alluvial debris flow	Uncommon. DHY LCs
2. Sandstone							
a. Fluvial arenite, subarenite, wacke	Lithic, minor feldspar and quartz	Highly variable, c-silt to v. coarse sand, gravelly, angular to sub-rounded, poorly-well-sorted; upward-fining	Plane, trough, tabular x-beds	Accretionary sheets filling channel forms with erosional base or tabular beds; 0.1–10 m thick; thinning-upward	Common dissenated plant remains; local large plants	Meandering and braided stream channel-fill and overbank deposits	Meandering streams - L. DHY, basal HYC, QZJ, WTG, JCY LCs. Braided streams - M & U DHY basal HYCLCs
b. Littoral–lakeshore arenite and subarenite	Lithic, common feldspar and quartz	C-silt to v. coarse sand, sub-rounded-well-rounded, well-sorted, well-washed	Parallel and ripple lamination, high-angle tabular x-beds; HCS, upper part may be mottled	Tabular, sharp or slightly erosional base, sharp-gradational top, laterally persistent, 0.1–1 m thick	Local large plant remains and shell fragments	High-energy littoral and front deposits	Common in LCG, HYC, WTG, SFG, LCs; absent in M&U DHY, QZJ, JCY LCs
c. Deltaic arenite to wacke	Lithic, minor feldspar and quartz	C-silt to v. coarse sand, subangular-well-rounded, mod-well-sorted, upward-coarsening	Parallel and ripple lamination, large trough and tabular x-bed, convolute bedding	Concave sharp, gradational and/or contorted base, convex top, clinoforms 1–10 m thick	Common disseminated plants, rare petrified woods	Distal to proximal delta-front deposits	Some in L. DHY, LCG, HYC LCs. abundant in WTG LC, absent in M&U DHY, QZJ, JCY, SFG LCs
d. Turbidite arenite and subarenite	Lithic, minor feldspar and quartz	C-silt to medium sand, subangular-well-rounded, mod-well-sorted	Normal graded, parallel and ripple lamination	Tabular, even sharp base, sharp-gradational top, 1–10 cm thick	Common disseminated plants, shell debris	Sub-littoral to profudal turbidity flow deposits	M-U HYC LC in southern Tarlong
3. Mudrock							
a. Shale and siltstone	Mud, variably calcareous and sandy	Variable amount of fine coarse sand	Thick laminated, locally mottled and burrowed	Sharp or gradational top and base; upward-coarsening or fining or no grain size trend, 10–100 cm thick	Variable amount of plant remains and microfossils	Prodeltaic; overbank; or littoral to lakeplain	Rare in M–U DHY LCs; common in other LCs
b. Organic-rich shale	Clay, variably silty; black to dark gray	Clay-silt-organic laminae, TOC 5–22%, types I and II kerogens	mm to sub-mm interlaminated	Sharp top and base, 1–100 cm thick	Fish, microfossils, plant remains	Profundal, low-energy, prob. anoxic	Abundant in LCG & HYC LCs
c. Dolomitic shale	Dolomite, variable calcite, mit gypsum crystals	Heterogenous, silly	mm to sub-mm interlaminated	Sharp or gradational base and top, 1–10 cm thick	Fish, microfossils, sparse plant remains	low-energy, evaporative littoral, marginal mud flat, playa	Abundant in LCG and HYC LCs
d. Bentonite	Clay, minor quartz, feldspar, biotite, rare zircon	Variable amount of fine-coarse sand	Ductile, extensively slickensided, blocky	Sharp to gradational top and base. 1–10 cm thick	None	Low-energy lake	Rare in LCG, HYC, WTG, SFG LCs
e. Carbonaceous shale and coal	Mud, variably silty, sandy, and calcareous	Variable amount of fine-coarse sand	Thick laminated, locally mottled and burrowed	Sharp to gradational base and top, 1–10 cm thick	Locally rich microfossils	Low-energy littoral to swamp	L. DHY, WTG LCs; coal in WTG LCs
f. Massive mud-stone	Mud, variously silty, sandy, and calcareous	Variable amount of fine-coarse sand	Massive, thick bedded	Sharp or gradational base and top, 1–100 cm thick	Variable microfossils and plant remains	Low-energy littoral to lakeplain. Or paleosol	Absent in M–U DHY LCs. Common in other LCs
4. Carbonates							
a. Limestone	Skeletal fragment, ooid, intraclast,peloids, minor pisoids and oncoids. Variable amount of lithics and dolomite. Minor gypsum.	Grainstone, packstone, wackestone, mudstone, minor rudstone. Silicification, micritization, recrystllization, calcification	Parallel, algal, stromatolitic, lamination, massive and cross bedding, cone-in cone, microbrecciation, rare mudcrack and micro-karst	Well-bedded, sharp or gradational base and top, laterally persistent, local c linoforms; 1–10 cm thick	Fish, bivalve, microfossils, organic-rich, sparse plant remains	Lakeshore, littoral, sub-littoral, palustrine, low-high energy. Variably evaporative, minimal siliciclastic influx	LCG & HYC LCs. Rare in L DHY and WTG LCs
b. Dolomite	Dolomite, variable amount oflithics and allochems, mit gypsum crystals and nodules	Micritic, subhedral to euhedral spars. Silicification, recrystallization, calcification	Parallel and algal lamination, micro-brecciation, rare mudcracks & fenestrae	Well-bedded, sharp or gradational base and top, laterlly persistent; 1–10 cm thick	Fish, microfossils, organic-rich, sparse plant remains	Littoral to lakeshore, low-energy, evaporative, minimal siliciclastic influx	LCG & HYC LCs
5. Paleosols	See Table 3						

[a] Abbreviations for names of low-order cycles. DHY: Daheyan; LCG: Lucaogou; HYC: Hongyanchi; QZJ: Quanzijie; WTG: Wutonggou; JCY: Jiucaiyuan; SFG: Shaofanggou.

Table 2
Characteristics, type, and environmental and climatic interpretations of uppermost Carboniferous–Lower Triassic paleosols, southern Bogda Mountains, NW China.

Paleosol description			Environmental and climatic interpretations		
Structure and lithology	Horizons	Type	Soil drainage	Landscape type	Climate (P/E)[a]
1. Massive					
a. Red or brown sandstone	AC	Protosol	Variable	Variable	Variable
b. Gray sandstone, red, yellow or orange mottles	ACg	Protosol	Somewhat poorly to poorly drained	Lowland	Variable
c. Red or brown Mudstone	AC	Protosol	Variable	Variable	Variable
d. Gray mudstone, red, yellow or orange mottles, fine and few nodules	ACg	Protosol	Somewhat poorly to poorly drained	Lowland	Variable
2. Blocky					
a. Blocky red or Brown Mudstone	Bw	Protosol	Somewhat poorly to well-drained	Variable	Variable
b. Prismatic to blocky mudstone with Fe–Mn nodules	Bc(g)	Gleysol	Somewhat poorly to poorly drained	Lowland	Humid
c. Abundant oriented clays in blocks and along block surfaces	Bt	Argillisol	Well to somewhat poorly drained	Upland/topographic high; preferentially on fluvial or lacustrine sandstones	Humid
d. Abundant carbonate nodules and/or rhizoliths	Bk	Calcisol	Well-drained	Floodplain, lakeplain or playa	Semiarid to arid Arid
e. Containing bladed cathonate nodules, probably gypsum pseudomorphs	By	Gypsisol	Well-drained	Playa	Arid
3. Wedge-shaped aggregates					
a. Gray, green or red mudstone	Bss	Vertisol	Somewhat poorly drained	Lakeplain, deltaplain or floodplain	Seasonal variation in precipitation
b. Common carbonate nodules	Bkss	Calcic Vertisol	Somewhat poorly drained	Lakeplain, deltaplain or floodplain	Subhumid-semiarid; seasonal variation in precipitation
c. A varying amount of Fe–Mn concretions or nodules	Bcss	Ferric Vertisol	Somewhat poorly drained to poorly	Lakeplain, deltaplain or floodplain	Subhumid; seasonal precipitation
d. Gley features, matrix low chroma, olive gray, greenish yellow, Fe–Mn reduced and removed, with or without Fe–Mn concretions	Bgss	Gleyed Vertisol	Somewhat poorly drained to poorly drained	Low-lying lakeplain, deltaplain or floodplain	Seasonal precipitation
4. Coal, organic mudstone					
a. *In situ* organic matter accumulation	O	Histosol	Very poorly drained	Lowland, depression on delta or floodplain	Humid
b. Overlying gray blocky mudstone containing carbonate nodules	0, Bk	Calcic Histosol	Poorly drained	Lowland, marsh	Humid

[a] Climate was interpreted qualitatively with respect to the precipitation (P)/evaporation (E) ratio as arid (P/E<<1), semiarid (<1), subhumid (>1), and humid (>>1) in this study.

HCs in Tarlong (Fig. 10A and Table 4). Its base is a high-relief meandering stream channel base in Taodonggou and a sharp surface in Tarlong. The Taodonggou section consists exclusively of thick meandering stream HCs with well-developed channel-fill and overbank facies, whereas the NE Tarlong section consists entirely of lakeplain-littoral HCs. The Jiucaiyuan is variegated with a mixture of brown, red, purple, and gray colors. Many rocks are mottled and massive. Calcitic and dense clayey nodules are abundant. Calcisols, vertic Calcisols, and calcic Argillisols are common in floodplain and lakeplain deposits.

The lateral change from meandering stream HCs in Taodonggou to lakeplain–littoral HCs in Tarlong indicates a complete lake withdrawal from Taodonggou and shallowing in Tarlong. This is also indicated by the abrupt facies shift across the Wutonggou–Jiucaiyuan boundary, and may have been caused by a catastrophic lowering of lake spill-point as indicated by the fluvial channel incision in Taodonggou. The limited coarse-grained deposits in Tarlong suggest a balance-filled lake. Common fluvial channel incisions followed by thick overbank deposition in Taodonggou suggests episodic source uplift followed by periods of tectonic quiescence. Catchment basin was probably large and of a low relief. Subsidence was persistent to preserve thick fluvial and lake-margin deposits in the study area.

The climate condition ranged widely from subhumid–humid to semiarid–subhumid at intra-HC, HC and IC scales. However, a shift to a much drier condition from that of the Wutonggou time is clear. The well-developed meandering stream systems in Taodonggou suggest intense provenance weathering and large sediment production and transport by perennial river flows. Abundant root mottling and calcified and illuvial-clay-filled rootlets indicate well-vegetated floodplain and lakeplain. On the other hand, the calcareous paleosols and lack of preserved plant materials suggest periods of low groundwater table and soil moisture deficiency. Repetitive lake transgression and regression in Tarlong also suggest fluctuating supply of river water and sediment to the lake. The climate changed from semiarid–subhumid in the lower and middle Jiucaiyuan to subhumid–humid conditions in the upper part before returning to the semiarid–subhumid condition at the uppermost Jiucaiyuan (Fig. 10A).

4.9. Shaofanggou low-order cycle

The Shaofanggou LC is present only in Taodonggou and contains 64 HCs in 17 ICs (Fig. 11A and Table 4). It is 112.8 m thick. Its base is a sharp to broad, slightly erosional surface, and top is a fluvial erosional surface. Thin lakeplain–littoral HCs dominate and are laterally persistent for 100s m, except two conglomerate-rich deltaic HCs in the lower part. The lakeplain–littoral HCs commonly have a broad, slightly erosional base as a transgressive ravinement surface upon which thin conglomerates and arenites were deposited (Fig. 11B, C). The upper mudrocks are massive with pervasive root mottling, rhizoconcretions 1–100 cm long, and layers of coalesced calcitic and clayey nodules which are especially well-developed in the uppermost Shaofanggou. Most beds are moderately to strongly calcareous. Calcisols cap most HCs (Fig. 11A, E). Possible Gypsisols containing gypsum pseudomorphs are present. The Shaofanggou has a distinctive bright variegated color of red, purple, yellow, brown, and stringers of blue. The grain size and abundance of conglomerate decrease upward; and the uppermost 30 m is composed almost entirely of mudrocks.

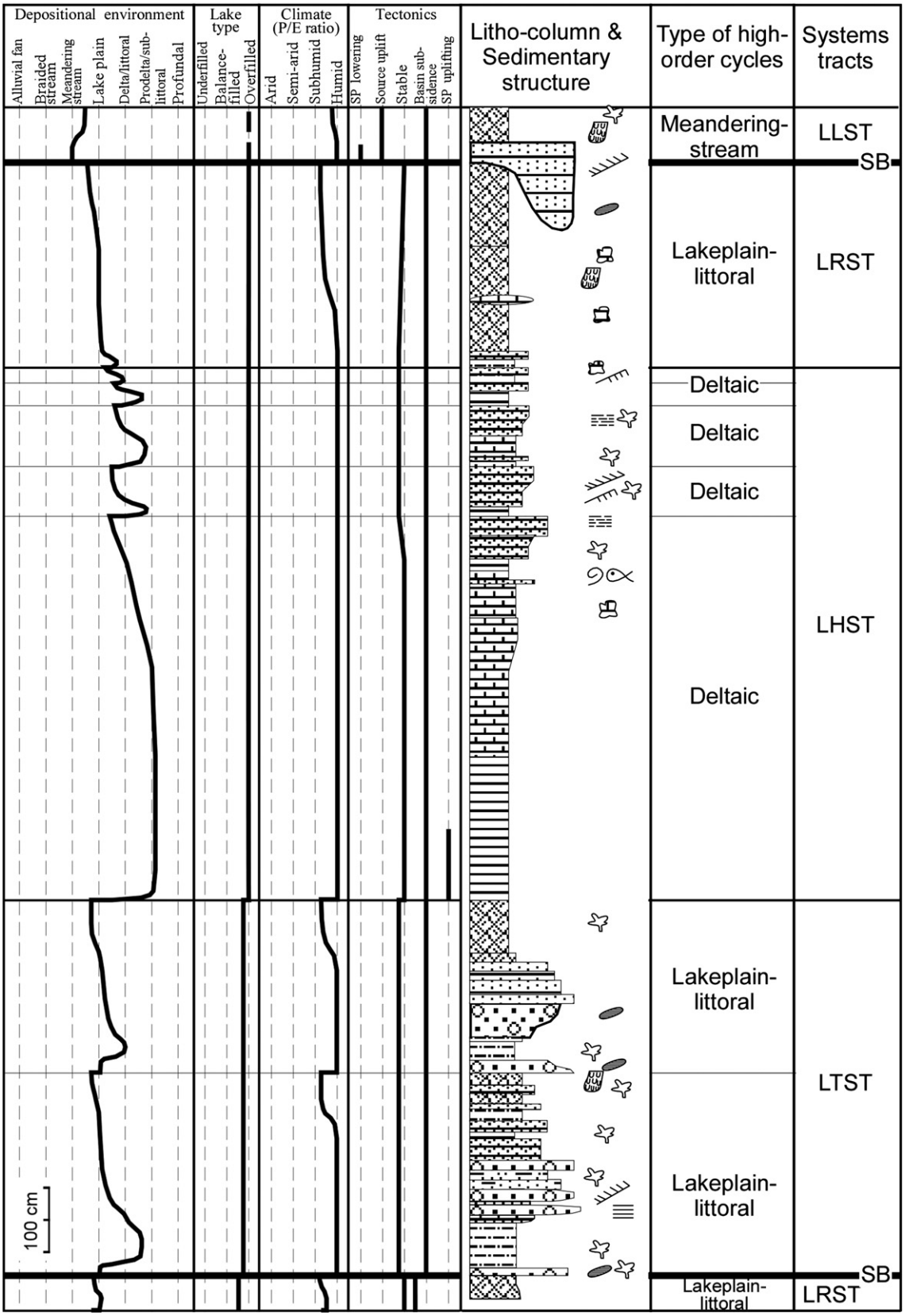

Fig. 12. An example showing the delineation of intermediate-order cycles/stratigraphic sequences in fluvial–lacustrine deposits formed under humid–subhumid climate. The base of the section is ~353 m below the top of the Wutonggou low-order cycle in the NE Tarlong section. Thin lines are high-order cycle boundaries; medium lines are boundaries of systems tracts; thick lines are sequence boundaries. LLST — lacustrine lowstand systems tract; LTST — lacustrine transgressive systems tract; LHST — lacustrine highstand systems tract; LRST — lacustrine regressive systems tracts; SB — sequence boundary. See Fig. 4A for explanations.

The abundant lakeplain–littoral HCs indicate frequent shoreline transgression and regression across a low-relief stable landscape, where broad mud-flat and shallow littoral environments shifted repeatedly. The balance-filled Shaofanggou lake received little coarse sediments. Source uplift was subdued; and subsidence was persistent to preserve abundant thin HCs. Calcisols and possible Gypsisols and minimal coarse clastics suggest a subhumid–semiarid condition during the Shaofanggou time.

The Shaofanggou LC separates from the Karamay LC (Fig. 11A) by a regional unconformity (Zhang, 1981; Wartes et al., 2002) with a relief up to ~25 m in Taodonggou. The basal 25 m of the Karamay LC contains two (~10 m thick each) braided stream HCs and five thin lakeplain–littoral HCs. The braided stream HCs contain thick, matrix-free, pebble–cobble conglomerates intercalated with very coarse arenites and large tabular cross-beddings. The regional unconformity (Zhang, 1981) and large influx of gravelly deposits suggest a major source uplift across the Shaofanggou–Karamay boundary. Well-washed conglomerates and the absence of Calcisols suggest a humid to subhumid condition in the early Karamay time.

5. Latest Carboniferous–Early Triassic terrestrial climatic variability — a synthesis

Climate and its changes are one of the important processes that formed the sedimentologic and stratigraphic characteristics of the studied strata in the Tarlong–Taodonggou half graben, as demonstrated in above observations and interpretations. This forms the basis for a synthesis on paleoclimatic variability. The synthesis is at a LC scale in the context of the most up-to-date chronostratigraphy (Figs. 2, 13).

The uppermost Carboniferous–Lower Triassic strata formed during a rifting–drifting tectonic cycle. The thick Upper Carboniferous volcaniclastics signify the initial unroofing of the northern Tianshan suture zone, upon which the three Daheyan LCs were deposited during initial rifting from late Gzhelian to middle Sakamarian (Figs. 1D, 13). The Daheyan deposition occurred initially in local valleys and then intensified to form thick alluvial fan complexes when rifting progressed. Fluctuating profundal sediments of the Lucaogou and Hongyanchi LCs were deposited in a narrow and deep half graben during intense rifting in Sakamarian and Artinskian. Intense pedogenesis and local deep fluvial incision at the Hongyanchi–Quanzijie unconformity indicate prolonged nondeposition and erosion, signifying the cessation of rifting and beginning of drifting (Figs. 1D, 13). The meandering stream deposits of the Capitanian Quanzijie LC may have been deposited during the rifting–drifting transition when the catchment topography began to shallow. The catchment area increased significantly during the deposition of the thick Wutonggou LC from Wuchiapingian to early Induan, signifying full-fledged drifting. In the middle Induan and Olenekian stages, both source uplift and graben subsidence stabilized, as indicated by persistent fluvial and lake-margin environments of the Jiucaiyuan and Shaofanggou LCs. Intense pedogenesis and deep fluvial incision, similar to those at the Hongyanchi–Quanzijie unconformity, occurred at the regional Shaofanggou–Karamay unconformity (Fig. 1D). The thick braided stream conglomerates in basal Karamay LC indicate rejuvenation of source uplift and graben subsidence, signifying the beginning of a new tectonic cycle.

The paleoclimatic signals were interpreted within the above tectonic framework. The graben fill recorded four levels of continental climatic variabilities at the east coast of mid-latitude NE Pangea (Figs. 1A, 13). The late Gzhelian climate was subhumid–humid, and shifted to subhumid, then highly-variable subhumid–semiarid conditions at the beginning of Sakamarian. The subhumid–semiarid conditions continued to the end of Sakamarian during the deposition of the Lucaogou LC. The climate changed from semiarid–subhumid to humid–subhumid in the lower part and to humid–semiarid in the upper part, and was highly variable, especially at the intra-HC and HC scales. Great climatic variability persisted during the deposition of the Hongyanchi LC during the Artinskian and, perhaps, into the Kungurian. The climate changed from dominantly humid–subhumid to highly variable humid–semiarid conditions. A shift from humid to semiarid climate is evident in the uppermost Hongyanchi LC; the semiarid condition probably culminated at the end of the Hongyanchi time and persisted during the Hongyanchi–Quanzijie unconformity. The Artinskian–Kungurian (?) Hongyanchi LC recorded the greatest climate variability at all scales in the latest Carboniferous–Early Triassic Tarlong–Taodonggou record.

Climate interpretation during the Kungurian, Roadian, and Wordian spanning ~10 million years is uncertain, because of the poorly-constrained duration of the Hongyanchi–Quanzijie unconformity. Nevertheless, a large, abrupt shift from semiarid–subhumid to humid–subhumid conditions occurred across the unconformity (Fig. 13). The Quanzijie fluvial successions suggest perennial river flow and surplus precipitation during Capitanian; but the intense oxidation and atypical overbank siltstones may indicate unique atmospheric conditions not related to precipitation, such as strong wind intensity and/or high atmospheric oxygen content. Alternative interpretations await future petrographic and geochemical studies.

The Capitanian subhumid to humid condition signals the beginning of a long (~10 m.y.), humid–subhumid climate from Late Permian to early Induan (Fig. 13). A stable humid condition dominated in the early Lopingian, gradually changed into variably humid to subhumid conditions in middle and late Lopingian. Evidence of a drier climate increases in the uppermost Wutonggou LC, indicating a gradual shift to a subhumid condition in the latest Permian and earliest Triassic. However, indicators of humid–subhumid conditions are still abundant in upper Wutonggou, such as the thickest coal interval above the Permo–Triassic boundary zone (Figs. 11A, 13), showing that the conditions persisted into early Induan.

A clear shift from subhumid–humid to subhumid–semiarid conditions occurred across the Wutonggou–Jiucaiyuan boundary in early–middle Induan and the conditions persisted to the end of Olenekian Stage (Fig. 13). Climate variability at all scales increases and are comparable to that in Sakamarian–Artinskian time. Two short humid–subhumid intervals in late Induan and early Olenekian interrupt the overall trend. The subhumid–semiarid conditions probably persisted during the Shaofanggou–Karamay unconformity and may extend into early Anisian, when intense pedogenesis occurred. Finally, humid–subhumid conditions returned at the beginning of the Anisian Stage. The climatic and environmental changes across the Shaofanggou–Karamay unconformity closely resemble those across the Hongyanchi–Quanzijie unconformity.

In summary, four prominent climatic shifts occur in the studied latest Carboniferous–Early Triassic continental records. They include: 1) the shift from humid–subhumid to highly-variable subhumid–semiarid conditions across the boundary between the middle and upper Daheyan LCs at the base of Sakamarian; 2) the shift from highly–variable subhumid–semiarid to humid–subhumid conditions across the Artinskian Hongyanchi–Capitanian Quanzijie unconformity; 3) the shift from humid–subhumid to highly-variable subhumid–semiarid conditions across the boundary between Wutonggou and Jiucaiyuan LCs in early Induan; and 4) the shift from highly-variable subhumid–semiarid to humid–subhumid conditions across the Olenekian Shaofanggou–Anisian Karamay unconformity (Fig. 13).

The above paleoclimatic interpretation raises two questions. First, a major change in P/E ratio across the Permo–Triassic boundary is absent (cf. Retallack et al., 1996). The climate in the 90 m interval in the NE Tarlong section where Permo–Triassic boundary is likely placed oscillates between humid and subhumid conditions at the HC and IC scales (Fig. 9A). This is also suggested by stable carbon isotope data of Thomas et al. (2007). The stable condition from Lopingian to early Induan implies that the end-Permian terrestrial mass extinction may not have been caused directly by a paleoclimatic change. In our

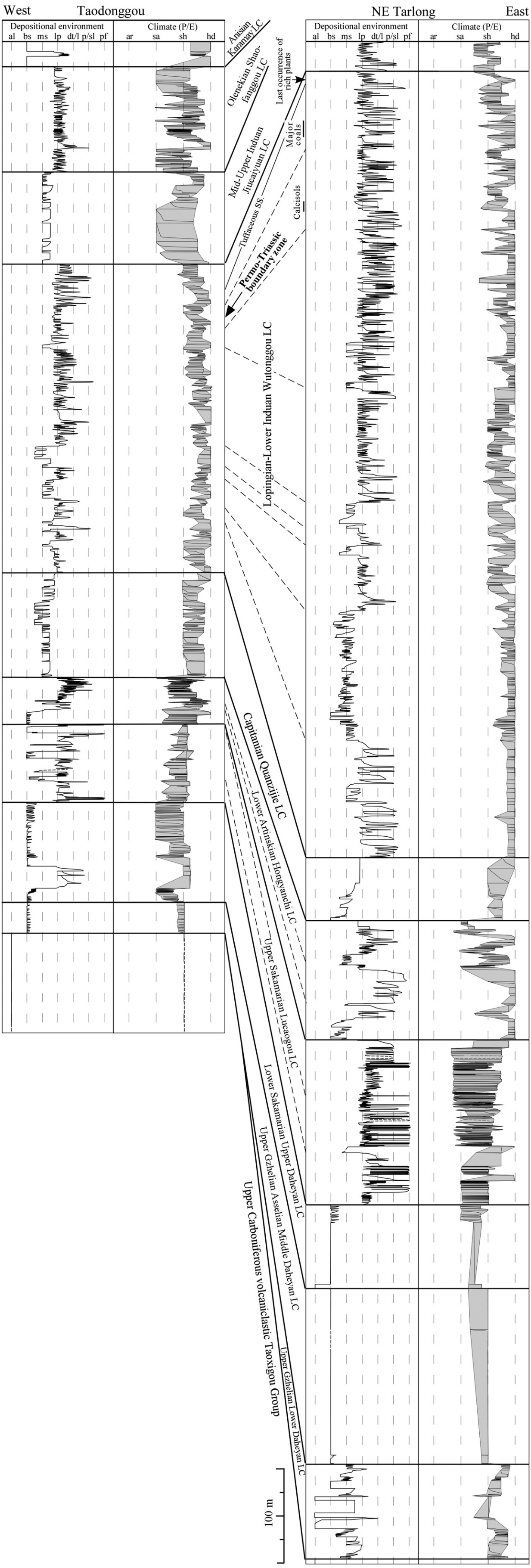

Fig. 13. Trends and correlation of late Gzhelian–Anisian depositional environments and climatic conditions within a cyclostratigraphic framework between Taodonggou and Tarlong sections. Thick correlation lines are for LCs; thin dashed lines are tentative correlations of ICs and stratigraphic markers. See Fig. 4A for other explanations.

Table 3
Characteristics and controlling processes of intermediate-order stratigraphic sequences in uppermost Carboniferous–Lower Triassic fluvial–lacustrine deposits, southern Bogda Mountains, NW China (Yang et al., 2007b, 2009).

Depositional setting	Setting tracts[a]	Typical lithofacies and type of high-order cycles	Sequence boundary	Stacking patterns		Despositional/architectural style	Controls
				Facies	Thickness		
Overfill Lake	LRST LHST LCS LTST LLST	Common; humid paleosol Deltaic deposit dominant Organic-rich shale and turbidite Thick shore and littoral Rare; meandering stream cycle	Sharp or low-relief erosional; High-relief erosional channel base if LLST present	Deepening-to-shallowing. Overall sand-stone rich	Overall thick. Thickening-upward LHST.	Progradational LHST, aggradational LRST, retrogradational LTST.	Climate and tectonic dominant, autogenic
Balance-filled to overfilled (shallow, silici-elastics-rich)	LRST LHST LCS LTST LLST	Common calcareous paleosol Shore-littoral ss and shale Rare; organic-rich shale and turbidite Ss overlying plant-rich shale Rare; meandering stream cycle	Sharp or low-relief erosional. High-relief erosional channel base if LLST present	Deepening-to-shallowing. Ss rich in LTST	Overall thin, Common thick LTST	Minor retrogradational LTST, aggradational LHST and LRST	Climate, autogenic, tectonic quies cence
Under-filled-Balance-filled Lake (profundal carbonate-rich)	LRST LHST LCS LTST LLST	Common calcareous paleosol Carbonate, organic-rich shale Organic-rich shale Siltstone, fine sandstone Rare; meandering stream cycle	Sharp or low-relief erosional. High-relief erosional channel base if LLST present	Deepening-to-shallowing. Shale rich and sandstone poor in LHST and LRST	Variable, overall thin. Relatively thick LHST	Retrogradational LTST, aggradational LHST and LRST	Climate, tectonic quies-cence
Meandering streams	LRST LHST LCS LTST LLST	Rare; common leached paleosol Thick sandstone, shale, paleosol Absent Absent Conglomerate and sandstone	High-relief erosional channel base	Thick, well-developed over bank facies in LHST	Thickening upward. Thin LLST, thick LHST	Dominantly erosional in lower part, aggradational in upper part	Tectonic, autogenic, climate
Alluvial fan to braided streams	LRST LHST LCS LTST LLST	Rare to absent; thin paleosol Thick conglomerate and sandstone Absent Absent Thin conglomerate and sandstone	Low-relief erosional channel base glomerate	Variably fining upward. More mature paleo-sols, less con-toward top	Thickening upward. Thin LLST, thick LHST	Dominantly erosional in lower part, aggradational in upper part	Tectonic, autogenic, climate

[a] Abbreviations: LLST — lacustrine lowstand systems tract; LTST — transgressive systems tract; LCS — condensed section; LHST — highstand systems tract; LRST — regressive systems tract; ss — sandstone.

Table 4
Characteristics and interpreted lake type and climatic and tectonic conditions of low-order cycles of uppermost Carboniferous–Lower Triassic fluvial–lacustrine deposits in NE Tarlong and Taodonggou sections, southern Bogda Mountains, NW China.

LC[1]	Thickness (m)		No. of HCs and ICs[2]		Types of HCs[3]					Nature of low-order cycle boundaries	Lake types[3]			Climate[4]				Tectonics	Correlation between Taodonggou and Tarlong
	TDG	NE TL	TDG	NE TL	BS	MS	DT	LL	FP		Under-filled	Balance-filled	Over-filled	Arid	Semi-arid	Sub-humid	Humid		
SFGLC	112.8		64, 17				●	●		Sharp, slightly erosional base, transgressive. Top is a regional unconformity, regressive		●	●		———			Dominantly tectonic quiescence in source area(s). Dominantly slow, episodically fast, subsidence	Not present in Tarlong. Persistent stable lake-margin environment
JCY LC	97.8	37.1	17, 4	14, 3	●	●		●		Base sharp in Tarlong, fluvial-erosional in Taodonggu, regressive. Sharp top, transgressive		●	●		———			Episodic source uplift followed by long periods of tectonic quiescence. Persistent fast subsidence	Only lower part present in Tarlong. Lake shrank to the Tarlong area, and became shallower. Large expanse of flood plain in Taodonggou area
WTG LC	329.3	828.6	121, 27	328, 49		●	●	●		Gradational to sharp base, transgressive. Sharp top in Tarlong, erosional top in Taodonggou, regressive		●	●				———	Variable but persistent uplift in source area. Persistent great basin subsidence. Enlarging catchment basin with a decreasing topographic gradient	Deltaic systems dominate in Tarlong, fluvial and lake-margin systems in Taodonggou. Drastic thinning from Tarlong to Taodonggou. Overall upward decrease in size of sand and gravel and occurrence of conglomerate.
QZJ LC	112.4	67.5	35, 5	8, 2 (minimum)	●	●	●	●		Sharp, disconformable base, locally erosional. Gradational to sharp top, transgressive			● (?)				——— (?)	Tectonic quiescence dominant with episodic active uplift in source area. Persistent basin subsidence	Similar meandering stream environments graben-wide. Similar thickness graben-wide; thinnest in NE Tarlong. Overall fining-upward trend with variable depocenters
HYC LC	50.6	116.7	53, 6	45, 5	●	●	●	●	●	High-relief erosional to sharp base, regressive. Disconformable, locally erosional top, regressive.		●	●			———		Active source uplift in lower part, stabilizing up section. Similar trend for subsidence in the graben. Common spill-point movement	Drastic thinning away from N. Tarlong. Basal part incised valley fill in N. Tarlong and Taodonggou but deltaic in S. Tarlong. Mature Calcisols at top, except severe erosion in SE Tarlong
LCG LC	83.2	179.6	45, 12	137, 31	●		●	●	●	Sharp base, transgressive. High-relief erosional to sharp top, regressive	●	●	●		———			Highly variable. Episodic source uplift and subsidence. Frequent spill-point movement	Drastic thinning away from Northern Tarlong. Common fluvial cycles in Taodonggou, common deltaic cycles in SE Tarlong.
U. DHY LC	91.1	108.8	39, 5	12, 1 (minimum)	●	●				Low-relief erosional base. Sharp top, transgressive		● (?)			———			Active source uplift and subsidence	Slight thickening to the west. The thick deltaic interval may or may not be present in the east.
M. DHY	33.2	188.6	15, 1	15, 1	●					Low-relief erosional base and top			● (?)		———			Active source uplift and subsidence	Drastic westward thinning. Thinner HCs in Taodonggou
L. DHY	0	106.5		31, 6			●	●		Sharp disconformable (?) base; low-relief erosional top		●	● (?)				———	Tectonic quiescence with episodic source uplift; active subsidence	Not present in Taodonggou. Dramatic lateral thickness change

1. LC — Low-order cycle; DHY — Daheyan; LCG — Lucaogou; HYC — Hongyanchi; QZJ — Quanzijie; WTG — Wutonggou; JCY — Jiucaiyuan; SFG — Shaofanggou.
2. HCs — High-order cycles; ICs — Intermediate-order cycles; TDG — Taodonggou section; NE TL — NE Tarlong section.
3. Large, intermediate, small dots indicate most, intermediate, and least occurrences of a HC type or a lake type. BS — Braided stream HC; MS — Meandering stream HC; DT — Deltaic HC; LL — Lakeplain–littoral HC; FP — Fluctuating profundal HC. Question marks indicate speculated lake types for fluvial HCs.
4. Bar length indicates range of climate conditions; thick and thin bars indicate common and rare occurrences of a climate condition, respectively. Question mark indicates tentative interpretation.

record, a major climatic shift before the end-Permian occurred across the Hongyanchi–Quanzijie unconformity, which is also demonstrated by organic carbon isotope data in the region (Foster and Metcalfe, 2002); the other after the end-Permian occurred across the Wutonggou–Jiucaiyuan boundary in early Induan. If climate change is a major cause of terrestrial mass extinction at the end-Permian, our results suggest that close documentation of the pace and timing of end-Permian mass extinction and exploration of other alternative climatic causes are needed in future studies (cf. Erwin, 2002; Retallack et al., 2003, 2006; Ward et al., 2005; Gastaldo et al., 2009).

Second, the semiarid–subhumid conditions had occurred over two long periods, one from Sakamarian to at least end of Artinskian (upper Daheyan to Hongyanchi LCs, ~19 m.y.), the other from early Induan to at least end of Olenekian (Jiucaiyuan to Shaofanggou LCs, minimum ~6 m.y.; Figs. 2, 13). These occurrences are in conflict with modern east coast macrothermal humid climate at mid-latitudes (cf. Carroll, 1998; Zhu et al., 2005). Extreme continentality, regional orographic effect, and/or abnormal circulation of Paleo-Tethys (e.g., Kutzbach et al., 1990; Parrish, 1993; Gibbs et al., 2002) may be possible causes. The intermontane setting of the study strata surrounded by several suture zones argues that orographic effect may have caused some climatic variability (Hendrix et al., 1992; Allen et al., 1995; Gibbs et al., 2002). Our work serves as a rare data point at mid-latitudes of NE Pangea for future climate modeling to seek explanations on the origin(s) of climate variability and conditions in NE Pangea.

6. Conclusions

Outcrop studies and new radiometric ages of fluvial–lacustrine strata in the Tarlong–Taodonggou half graben, southern Bogda Mountains, NW China, demonstrate that the strata comprise a relatively complete sedimentary and paleoclimatic record from latest Carboniferous to Early Triassic, and contain three orders of depositional cyclicity. Five types of high-order cycles (HCs) were identified as braided stream, meandering stream, lakeplain–littoral, lacustrine deltaic, and fluctuating profundal. The systematic stacking of HCs of different types and thicknesses forms intermediate-order cycles (ICs), which, in turn, comprise nine low-order cycles (LCs) formed under similar tectonic and climatic conditions.

The LCs formed during a rifting–drifting tectonic cycle. The late Gzhelian–middle Sakamarian lower, middle, and upper Daheyan LCs overlie upper Carboniferous volcaniclastics and form alluvial fan complexes during initial rifting. The middle Sakamarian–Artinskian Lucaogou and Hongyanchi LCs are composed of mainly fluctuating profundal, deltaic, and fluvial cycles, deposited in a narrow half graben during peak rifting. A major unconformity separates the Hongyanchi LC from the Capitanian fluvial Quanzijie LC deposited during the rifting–drifting transition. The thick Lopingian–lower Induan Wutonggou LC composed of deltaic, fluvial, and lakeplain–littoral HCs represents deposition in an enlarged catchment basin during the drifting phase. The middle–upper Induan Jiucaiyuan LC composed of meandering stream and lakeplain–littoral HCs formed during a major lake contraction. The Olenekian Shaofanggou LC is composed of lakeplain–littoral HCs deposited during a period of lake expansion and stabilization when source uplift was subdued. Intense pedogenesis followed by fluvial incision occurred at the Olenekian–Anisian unconformity. Finally, thick braided stream deposits of the Anisian Karamay LC represent the beginning of a new tectonic cycle.

Climate-sensitive sedimentary evidence indicates four levels of continental climate variability at the intra-HC, HC, IC, and LC scales at the mid-latitude east coast of NE Pangea during latest Carboniferous and Early Triassic. Four prominent climatic shifts occur in the studied record: 1) the shift from the humid–subhumid to highly-variable subhumid–semiarid conditions at the beginning of Sakamarian; 2) the shift from highly-variable subhumid–semiarid to humid–subhumid conditions across the Artinskian–Capitanian unconformity; 3) the shift from humid–subhumid to highly-variable subhumid–semiarid conditions at early Induan; and 4) the shift from the highly-variable subhumid–semiarid to humid–subhumid conditions across the Olenekian–Anisian unconformity.

The stable humid–subhumid conditions from Lopingian to early Induan imply that paleoclimatic change may not be the cause of the end-Permian terrestrial mass extinction. A close documentation of the pace and timing of end-Permian mass extinction and exploration of other alternative causes are needed to understand the dynamics of terrestrial mass extinction. In addition, the semiarid–subhumid conditions from Sakamarian to end of Artinskian with a ~19-m.y. duration and from middle Induan to end of Olenekian with a ~6-m.y. duration are in conflict with modern east coast meso- and macrothermal humid climate at mid-latitudes. Extreme continentality, regional orographic effect, and/or abnormal circulation of Paleo-Tethys may be possible causes. Our work serves as a rare data point at mid-latitudes of NE Pangea for future climate modeling to seek explanations on the origin(s) of climate variability in NE Pangea during the late Paleozoic icehouse–greenhouse climatic transition.

Acknowledgements

We thank W. Guan, B. Jeffrey, W.H. Ma, Z.J. Ouyang, M. Runnion, G.Z. Sun, P. Sun, D. Wang, H.Y. Wang, Y. Wang, H.Y. Wu, and Y. Yang for field assistance in a span of six summer seasons. The project was partially supported by three grants from Wichita State University, two grants from the Key Laboratory of Continental Dynamics, Northwestern University, China, and a grant from the Chinese Academy of Sciences, all to WY. WY also gratefully acknowledges the support of K. C. Wong Education Foundation, Hong Kong, obtained through the collaboration with Dr. X.R. Luo of Institute of Geology and Geophysics, Chinese Academy of Sciences. Acknowledgment is made to the Donors of the American Chemical Society Petroleum Research Fund, for partial support of this research. We are grateful to reviewers William A. DiMichele, Zhong Chen, Christopher Fielding, Shannon Mahan, and Krystal Pearson,whose critical and constructive comments have helped us make this paper publishable, and to Ezat Heydari (guest editor) for his patience and encouragement.

Appendix 1. Geochronological analysis

1.1. Data and methodology

Eight ages were obtained from five samples collected in four sections in the Tarlong–Taodonggou graben in this study (Fig. A). The samples are bentonites and volcanic ash-fall and ash-flow tuffs (Table A). Three methods were applied in the geochronological analysis of these samples: isotope dilution thermal ionization mass spectrometry (IDTIMS), $^{40}Ar/^{39}Ar$ geochronology, and Sensitive High-Resolution Ion MicroProbe-Reverse Geometry (SHRIMP-RG) (Tables B, C, D).

1.1.1. IDTIM analysis

The IDTIM analysis of samples TRN8, TRN40, TR10, and S8-15 was carried out in Boise State University Isotope Geology Laboratory. Zircon was subjected to a modified version of the chemical abrasion method of Mattinson (2005), reflecting a preference to prepare and analyze carefully selected single crystals. Zircon separates were placed in a muffle furnace at 900 °C for 60 h in quartz beakers. Single grains were then transferred to 3 ml Teflon PFA beakers and loaded into 300 µl Teflon PFA microcapsules. Fifteen microcapsules were placed in a large-capacity Parr vessel, and the crystals partially dissolved in 120 µl of 29 M HF for 12 h at 180 °C. The contents of each microcapsule were returned to 3 ml Teflon PFA beakers, the HF removed and the residual grains immersed in 3.5 M HNO_3, ultrasonically cleaned for an hour, and fluxed on a hotplate at 80 °C for an hour. The HNO_3 was removed and the grains were rinsed twice in

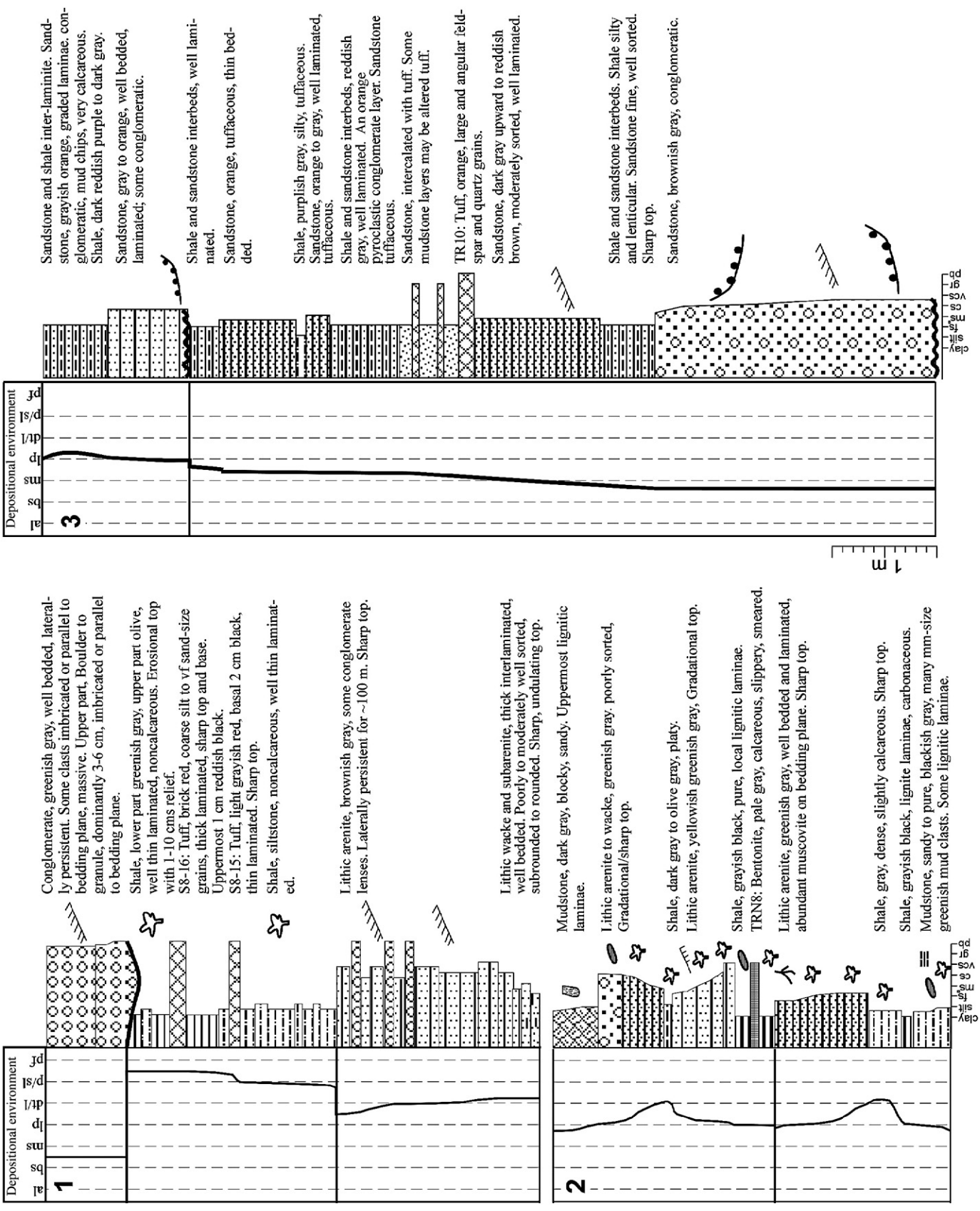
Depositional environment
al
bs
ms
lp
dl/l
p/sl
pf
1
Conglomerate, greenish gray, well bedded, laterally persistent. Some clasts imbricated or parallel to bedding plane, massive. Upper part, Boulder to granule, dominantly 3-6 cm, imbricated or parallel to bedding plane.
Shale, lower part greenish gray, upper part olive, well thin laminated, noncalcareous. Erosional top with 1-10 cms relief.
S8-16: Tuff, brick red, coarse silt to vf sand-size grains, thick laminated, sharp top and base. Uppermost 1 cm reddish black.
S8-15: Tuff, light grayish red, basal 2 cm black, thin laminated. Sharp top.
Shale, siltstone, noncalcareous, well thin laminated.
Lithic arenite, brownish gray, some conglomerate lenses. Laterally persistent for ~100 m. Sharp top.
Lithic wacke and subarenite, thick interlaminated, well bedded. Poorly to moderately well sorted, subrounded to rounded. Sharp, undulating top.
Mudstone, dark gray, blocky, sandy. Uppermost lignitic laminae.
Lithic arenite to wacke, greenish gray. poorly sorted, Gradational/sharp top.
Shale, dark gray to olive gray, platy.
Lithic arenite, yellowish greenish gray, Gradational top.
Shale, grayish black, pure, local lignitic laminae.
TRN8: Bentonite, pale gray, calcareous, slippery, smeared.
Lithic arenite, greenish gray, well bedded and laminated, abundant muscovite on bedding plane. Sharp top.
Shale, gray, dense, slightly calcareous. Sharp top.
Shale, grayish black, lignite laminae, carbonaceous.
Mudstone, sandy to pure, blackish gray, many mm-size greenish mud clasts. Some lignitic laminae.
2
clay
silt
fs
ms
cs
vcs
gr
pb
3
Sandstone and shale inter-laminite. Sandstone, grayish orange, graded laminae. conglomeratic, mud chips, very calcareous.
Shale, dark reddish purple to dark gray.
Sandstone, gray to orange, well bedded, laminated; some conglomeratic.
Shale and sandstone interbeds, well laminated.
Sandstone, orange, tuffaceous, thin bedded.
Shale, purplish gray, silty, tuffaceous.
Sandstone, orange to gray, well laminated, tuffaceous.
Shale and sandstone interbeds, reddish gray, well laminated. An orange pyroclastic conglomerate layer. Sandstone tuffaceous.
Sandstone, intercalated with tuff. Some mudstone layers may be altered tuff.
TR10: Tuff, orange, large and angular feldspar and quartz grains.
Sandstone, dark gray upward to reddish brown, moderately sorted, well laminated.
Shale and sandstone interbeds. Shale silty and lenticular. Sandstone fine, well sorted.
Sharp top.
Sandstone, brownish gray, conglomeratic.
1
m

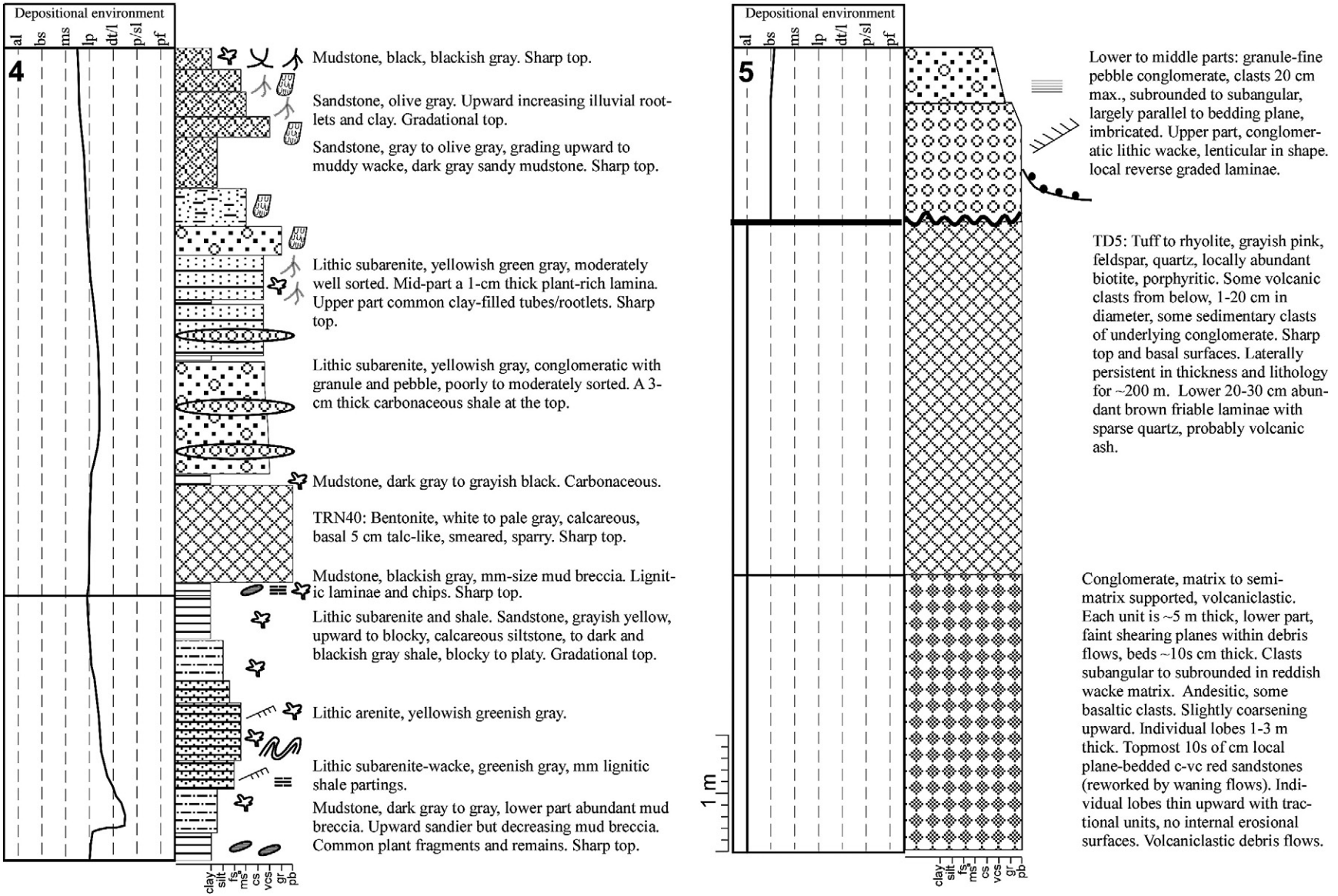

Fig. A. Measured sections around the radiometrically dated samples showing lithologic column, sedimentary structures, simplified field descriptions, depositional environment interpretation, and high-order cycle boundaries. 1) S8-15; 2) TRN8; 3) TR10; 4) TRN40; 5) TD5. See Fig. 4A for explanations Figs. 4E and 8D for field photos of TD5 and S8-15, respectively.

Table A
Characteristics, methods of geochronological analysis, and ages and dates of volcanic samples in the uppermost Carboniferous–Lower Triassic strata, southern Bogda Mountains, NW China.

Sample No.	Location	Lithology	Geochronological method	Ages and Dates (Ma)		Depositional age
				Previous	This study	
TRN-8	~241 m below top of cycle. NE Tarlong	Bentonite	IDTIMS, zircon	Lopingian	Earliest Changxingian (253.11 ± 0.05)	Earliest Changxingian
TRN-40	~249 m below the top of Wutonggou low-orde cycle at a location 300 m west of the NE Tarlong section	Bentonite	IDTIMS, zircon	Lopingian	Latest Wuchiapingian (253.63 ± 0.24, 254.22 ± 0.24)	Younger than latest Wuchiap ingian
S 8-15 (Fig. 8D)	Middle-upper Hong-yanchi low-order cycle. Right below Hongyanchi-Quanzijie unconformity. SE Tarlong	Ash-fall tuff	IDTJMS, zircon	Wordian	Early Artinskian (281.39 ± 0.10)	Early Artinskian
TR-10	~93 m above base, 8.5 m below the top of lower Daheyan low-order cycle. NE Tarlong	Ash-fall tuff	IDTIMS, zircon SHRIMP, zircon	Kungurian	Late Gzhelian (301.26 ± 0.05) Late Asselian (295.5 ± 2.6)	Late Gzhelian
TD-5 (Fig. 4E)	Underneath unconformity between Taoxigou Group and middle Daheyan low-order cycle. N. Taodonggou	Ash-flow tuff	Ar/Ar, biotite Ar/Ar, sanidine	Early Permian	Early-middle Gzhelian (301.61 ± 0.449, 303.8 ± 0.9) Latest Gzhelian (300 ± 3, 299.9 ± 0.6)	Late Gzhelian

ultrapure H_2O before being reloaded into the same 300 µl Teflon PFA microcapsules (rinsed and fluxed in 6 M HCl during crystal sonication and washing) and spiked with the EARTHTIME mixed ^{233}U–^{235}U–^{205}Pb tracer solution (ET535). These chemically abraded grains were dissolved in Parr vessels in 120 µl of 29 M HF with a trace of 3.5 M HNO_3 at 220 °C for 48 h, dried to fluorides, and then re-dissolved in 6 M HCl at 180 °C overnight. U and Pb were separated from the zircon matrix using an HCl-based anion-exchange chromatographic procedure (Krogh, 1973), eluted together and dried with 2 µl of 0.05 N H_3PO_4.

Pb and U were loaded on a single outgassed Re filament in 5 µl of a silica-gel/phosphoric acid mixture (Gerstenberger and Haase, 1997), and U and Pb isotopic measurements made on a GV Isoprobe-T multicollector thermal ionization mass spectrometer equipped with an ion-counting Daly detector. Pb isotopes were measured by peak-jumping all isotopes on the Daly detector for 100 to 150 cycles, and corrected for 0.18 ± 0.04%/amu mass fractionation. Transitory isobaric interferences due to high-molecular weight organics, particularly on ^{204}Pb and ^{207}Pb, disappeared within approximately 30 cycles, while ionization efficiency averaged 10^4 cps/pg of each Pb isotope. Linearity (to $\geq 1.4\times10^6$ cps) and the associated deadtime correction of the Daly detector were monitored by repeated analyses of NBS982, and have been constant since installation. Uranium was analyzed as UO_2^+ ions in static Faraday mode on 10^{11} Ω resistors for 150 to 200 cycles, and corrected for isobaric interference of $^{233}U^{18}O^{16}O$ on $^{235}U^{16}O^{16}O$ with an $^{18}O/^{16}O$ of 0.00206. Ionization efficiency averaged 20 mV/ng of each U isotope. U mass fractionation was corrected using the known $^{233}U/^{235}U$ ratio of the ET535 tracer solution.

U–Pb dates and uncertainties were calculated using the algorithms of Schmitz and Schoene (2007), $^{235}U/^{205}Pb$ of 100.206 and $^{233}U/^{235}U$ of 0.994746 for the ET535 tracer solution (Condon et al., 2007), and U decay constants recommended by Jaffey et al. (1971). $^{206}Pb/^{238}U$ ratios and dates were corrected for initial ^{230}Th disequilibrium using a Th/U[magma] = 3 using the algorithms of Crowley et al. (2007), resulting in an increase in the $^{206}Pb/^{238}U$ dates of ~0.09 Ma. All common Pb in analyses was attributed to laboratory blank and subtracted based on the measured laboratory Pb isotopic composition and associated uncertainty. U blanks are difficult to precisely measure, but are estimated at 0.07 pg.

Over the course of the experiment, analyses of the 500 Ma EARTHTIME standard solution that varied in size from 7–77 pg of radiogenic Pb yielded a weighted mean $^{206}Pb/^{238}U$ date of 499.97 ± 0.09 Ma ($n = 9$, MSWD = 0.6).

1.2. $^{40}Ar/^{39}Ar$ geochronology

The $^{40}Ar/^{39}Ar$ geochronological analysis of Sample TD5 was carried out in the U.S. Geological Survey $^{40}Ar/^{39}Ar$ Geochronology Laboratory at Denver, Colorado. The Sample was analyzed in a low blank resistance furnace. Mineral phases from the sample were prepared as described in Miggins et al. (2002, 2004). The samples were irradiated for 50 MW h in the central thimble of the U.S Geological Survey TRIGA reactor (Dalrymple et al., 1981). Neutron fluence was monitored using sanidine standard FCT-3 (Fish Canyon Tuff) with an internally calibrated age of 28.03 Ma. Argon isotopic compositions were measured at the U.S. Geological Survey Argon Geochronology Laboratory in Denver, Colorado. Analytical techniques are given in Table C and in general followed procedures given in Miggins et al. (2002, 2004). Standard methods were employed to produce $^{40}Ar/^{39}Ar$ age spectra and isochron diagrams (Snee, 2002).

Incremental heating results are given in Table C, and age spectra are shown in Fig. C. As used herein, the term "plateau" refers to two or more contiguous temperature steps with apparent dates that are indistinguishable at the 95% confidence interval and represent ≥50% of the total $^{39}Ar_K$ released (Fleck et al., 1977); $^{39}Ar_K$ is defined in Table C. A "weighted mean age" represents the best estimate of the apparent age for a sample that contains no plateau. Generally the term is restricted to a portion of the age spectrum that comprises between 90 and 40% of the released argon, or the included argon fractions have dates that overlap

Table B
U–Th–Pb isotopic data of samples in IDTIMS analysis in this study.

Sample	Radiogenic isotope ratios															Isotopic ages					
	$\frac{Th}{U}$	$^{206}Pb^{*}\times10^{-13}$ mol	mol % $^{206}Pb^{*}$	$\frac{Pb^{*}}{Pb_c}$	Pb_c (pg)	$\frac{^{206}Pb}{^{204}Pb}$	$\frac{^{208}Pb}{^{206}Pb}$	$\frac{^{207}Pb}{^{206}Pb}$	% err	$\frac{^{207}Pb}{^{235}U}$	% err	$\frac{^{206}Pb}{^{238}U}$	% err	corr. coef	$\frac{^{207}Pb}{^{206}Pb}$	±	$\frac{^{207}Pb}{^{235}U}$	±	$\frac{^{206}Pb}{^{238}U}$	±
(a)	(b)	(c)	(c)	(c)	(c)	(d)	(e)	(e)	(f)	(e)	(f)	(e)	(f)		(g)	(f)	(g)	(f)	(g)	(f)
TR-10																				
z2	0.505	6.5399	99.90%	301	0.54	18450	0.160	0.052463	0.049	0.346142	0.089	0.047852	0.045	0.938	305.6	1.1	301.82	0.23	301.32	0.13
z3	0.562	3.4034	99.73%	114	0.76	6898	0.178	0.052409	0.076	0.345801	0.112	0.047855	0.047	0.844	303.3	1.7	301.56	0.29	301.34	0.14
z4	0.528	1.3637	99.61%	78	0.44	4769	0.168	0.052707	0.042	0.351941	0.102	0.048428	0.042	1.223	316.2	0.9	306.18	0.27	304.87	0.12
z5	0.531	1.78%	99.71%	105	0.43	6404	0.168	0.052455	0.095	0.346104	0.127	0.047854	0.050	0.743	305.3	2.2	301.79	0.33	301.33	0.15
z6	0.637	0.7020	99.23%	41	0.45	2414	0.202	0.052414	0.209	0.345699	0.239	0.047835	0.051	0.645	303.5	4.8	301.48	0.62	301.22	0.15
z7	0.596	1.2373	99.54%	67	0.47	4027	0.189	0.052458	0.124	0.345933	0.154	0.047828	0.046	0.733	305.4	2.8	301.66	0.40	301.17	0.14
z8	0.499	1.3440	99.53%	65	0.52	3980	0.158	0.052432	0.134	0.345950	0.163	0.047853	0.050	0.683	304.3	3.0	301.67	0.42	301.33	0.15
z9	0.526	2.9080	99.78%	139	0.52	8499	0.167	0.052505	0.085	0.346249	0.115	0.047829	0.047	0.762	307.5	1.9	301.90	0.30	301.18	0.14
z10	0.468	1.7006	99.68%	93	0.45	5776	0.148	0.052423	0.094	0.345750	0.125	0.047834	0.046	0.780	303.9	2.1	301.52	0.33	301.21	0.13
TRN-8																				
z1	0.813	0.4700	98.48%	21	0.60	1222	0.258	0.051412	0.417	0.283944	0.458	0.040056	0.066	0.658	259.3	9.6	253.78	1.03	253.18	0.16
z2	1.193	0.5479	98.23%	20	0.81	1053	0.377	0.051149	0.469	0.282325	0.513	0.040033	0.083	0.587	247.5	10.8	252.50	1.15	253.04	0.21
z4a	0.688	1.5818	99.50%	63	0.65	3714	0.218	0.051221	0.153	0.282729	0.180	0.040033	0.047	0.664	250.8	3.5	252.82	0.40	253.04	0.12
z4b	0.690	0.8028	98.69%	24	0.88	1421	0.219	0.051347	0.344	0.283539	0.378	0.040050	0.053	0.671	256.4	7.9	253.46	0.85	253.14	0.13
z4c	0.709	1.0581	99.39%	52	0.53	3064	0.225	0.051333	0.173	0.283541	0.202	0.040061	0.058	0.600	255.8	4.0	253.46	0.45	253.21	0.14
z5	0.898	0.9458	98.83%	28	0.92	1590	0.285	0.051313	0.308	0.283223	0.339	0.040032	0.052	0.647	254.9	7.1	253.21	0.76	253.03	0.13
z6	0.975	0.4547	98.79%	28	0.46	1531	0.309	0.051326	0.322	0.283801	0.355	0.040103	0.055	0.649	255.5	7.4	253.67	0.80	253.47	0.14
z7	0.904	0.1975	95.63%	7	0.74	426	0.287	0.051303	1.246	0.283714	1.335	0.040109	0.120	0.761	254.5	28.7	253.60	3.00	253.51	0.30
z8	1.005	0.3320	97.84%	16	0.60	860	0.319	0.051268	0.573	0.283137	0.622	0.040054	0.068	0.738	252.9	13.2	253.14	1.39	253.17	0.17
TRN-40																				
z1	0.812	0.3838	98.94%	31	0.34	1762	0.256	0.051077	0.314	0.283263	0.349	0.040222	0.074	0.560	244.3	7.2	253.24	0.78	254.21	0.19
z2	0.783	0.3061	97.95%	16	0.53	905	0.248	0.051318	0.542	0.286671	0.589	0.040515	0.078	0.654	255.1	12.4	255.94	1.33	256.02	0.20
z3a	0.753	0.6861	99.15%	38	0.49	2176	0.238	0.051168	0.231	0.282953	0.260	0.040107	0.052	0.632	248.4	5.3	253.00	0.58	253.49	0.13
z3b	0.781	0.4761	98.82%	27	0.47	1580	0.248	0.051373	0.373	0.284233	0.407	0.040127	0.069	0.547	257.6	8.6	254.01	0.91	253.62	0.17
z3c	0.832	0.3173	97.95%	16	0.55	907	0.263	0.051217	0.620	0.283570	0.661	0.040156	0.099	0.482	250.6	14.3	253.49	1.48	253.80	0.25
z4	0.719	0.1941	97.17%	11	0.46	658	0.226	0.050913	0.759	0.282791	0.818	0.040285	0.083	0.734	236.9	17.5	252.87	1.83	254.60	0.21
z5	0.924	0.2109	97.18%	12	0.50	660	0.293	0.051334	0.780	0.284575	0.848	0.040206	0.139	0.546	255.8	17.9	254.28	1.91	254.11	0.35
z6	0.688	0.2826	94.64%	6	1.32	347	0.216	0.050771	1.456	0.281702	1.558	0.040242	0.125	0.832	230.4	33.6	252.01	3.48	254.33	0.31
z7	0.887	0.3202	97.96%	16	0.55	914	0.281	0.051299	0.533	0.284018	0.578	0.040154	0.068	0.686	254.3	12.3	253.84	1.30	253.79	0.17
S 8-15																				
z1	0.614	0.6231	99.18%	38	0.42	2263	0.194	0.051891	0.223	0.319212	0.254	0.044615	0.054	0.634	280.6	5.1	281.30	0.62	281.38	0.15
z2	0.646	0.8683	99.30%	45	0.50	2668	0.204	0.051862	0.209	0.319217	0.236	0.044641	0.051	0.606	279.3	4.8	281.30	0.58	281.53	0.14
z3	0.596	0.8334	99.13%	35	0.60	2129	0.189	0.051845	0.227	0.318854	0.258	0.044605	0.051	0.665	278.6	5.2	281.02	0.63	281.31	0.14
z5	0.729	0.5499	98.93%	30	0.49	1733	0.231	0.051935	0.297	0.319579	0.329	0.044629	0.054	0.650	282.6	6.8	281.58	0.81	281.46	0.15
z6	0.747	0.8225	99.06%	34	0.64	1969	0.237	0.051934	0.229	0.319369	0.264	0.044601	0.041	0.886	282.5	5.2	281.42	0.65	281.29	0.11
z7a	0.811	0.6233	99.22%	42	0.40	2390	0.257	0.051958	0.205	0.319776	0.237	0.044637	0.054	0.661	283.6	4.7	281.73	0.58	281.51	0.15
z7b	0.804	0.4781	98.39%	20	0.64	1154	0.255	0.052006	0.431	0.319858	0.470	0.044607	0.071	0.604	285.7	9.8	281.79	1.16	281.33	0.20
z8a	0.573	0.5673	98.14%	16	0.88	1002	0.181	0.051825	0.483	0.323082	0.525	0.045214	0.061	0.722	277.7	11.1	284.27	1.30	285.07	0.17
z8b	0.545	0.3319	97.58%	12	0.68	768	0.172	0.051970	0.640	0.324692	0.691	0.045312	0.076	0.698	284.1	14.6	285.51	1.72	285.68	0.21

(a) zl, z2, etc. are labels for analyses composed of single zircon grains that were annealed and chemically abraded (Mattinson, 2005). Analyses with letters following numbers denote fragments that are from the same grain. Bold labels denote analyses used in weighted mean calculations.
(b) Model Th/U ratio calculated from radiogenic $^{208}Pb/^{206}Pb$ ratio and $^{207}Pb/^{235}U$ date.
(c) Pb* and Pbc are radiogenic and common Pb, respectively. mol% $^{206}Pb^{*}$ is with respect to radiogenic and blank Pb.
(d) Measured ratio corrected for spike and fractionation only. Fractionation correction is 0.18 ± 0.02(1 sigma) %/amu (atomic mass unit) for single collector. Daly analyses, based on analysis ofNBS-981 and NBS-982.
(e) Corrected for fractionation, spike, common Pb, and initial disequilibrium in $^{230}Th/^{238}U$. Common Pb is assigned to procedural blank with composition of $^{206}Pb/^{204}Pb$ 18.60 ± 0.80%; $^{207}Pb/^{204}Pb$ 15.69 ± 0.32%; $^{208}Pb/^{204}Pb$ 38.51 ± 0.74% (1 sigma). $^{206}Pb/^{238}U$ and $^{207}Pb/^{206}Pb$ ratios corrected for initial disequilibrium in $^{230}Th/^{238}U$ using Tb/U [magma] = 3.
(f) Errors are 2 sigma, propagated using the algorithms of Schmitz and Schoene (2007) and Crowley et al. (2007).
(g) Calculations based on the decay constants of Jaffey et al. (1971). $^{206}Pb/^{238}U$ and $^{207}Pb/^{206}Pb$ dates corrected for initial disequilibrium in $^{230}Th/^{238}U$ using Th/U [magma] = 3.

within three standard deviations of the weighted mean. Isochron analysis (York, 1969) was used to assess if extraneous radiogenic argon components were trapped in any samples. A total gas age, analogous to a conventional K–Ar date, is calculated for each sample by taking the weighted mean of the dates for all gas fractions of the sample.

1.3. SHRIMP-RG

The SHRIMP analysis of Sample TR10 was carried out using the SHRIMP-RG housed in Green Hall at Stanford University and co-owned by the U.S. Geological Survey (SUMAC Facility). Zircon mineral separates were produced at the U.S. Geological Survey Argon Geochronology's mineral separation laboratory using conventional methods. Samples weighing between 1 and 5 kg were crushed, pulverized, sieved (less than 150 μm), washed, and magnetically-split to obtain a non-magnetic fraction. The non-magnetic fraction was then put through a heavy liquid (MeI-3.32) and/or Lithim Heteropoly Tungstate (LHT-2.85) and zircon concentrates were collected from the heavy fraction. After briefly cleaning with acetone, the analyzed zircon fractions were handpicked from this heavy concentrate, non-magnetic fraction.

SHRIMP-RG procedures used in this study are similar to those reported in Williams (1998) and Nourse et al. (2005). Briefly, zircons and chips of standard zircon R33 were mounted in Struers epoxy resin, ground to nearly half their thickness using 1500-grit, wet–dry sandpaper, and polished with 6- and 1 μm-grit diamond suspension abrasive. Transmitted- and reflected-light photos were taken of nearly

Table C
$^{40}Ar/^{39}Ar$ incremental heating data and ages of sample TD5 in the Ar/Ar geochronological analysis.

Temp (°C)	$^{40}Ar_R$[a]	$^{39}Ar_K$[a]	$^{40}Ar_K/^{39}Ar_K$[a, b]	$^{39}Ar/^{37}Ar$[c]	% $^{40}Ar_R$	% $^{39}Ar_R$	Apparent age[d] (Ma at ±1 sigma)
TD-5/#58/DD91, biotite; 51.2 mg; J-value = .011667 ± 0.1%							
650	0.33430	0.03667	9.115	9.10	72.5	1.1	182.32 ± 1.14
750	0.69394	0.05905	11.752	15.42	92.1	1.8	231.79 ± 0.79
800	0.99678	0.06435	15.489	19.68	91.0	1.9	299.68 ± 0.43
850	1.58548	0.10065	15.752	49.43	97.0	3.0	304.35 ± 0.44
900	2.76223	0.17624	15.673	68.68	98.3	5.3	302.95 ± 0.57
950	4.74371	0.30247	15.683	114.57	99.3	9.1	303.13 ± 0.45
000	5.87369	0.37581	15.630	112.11	99.4	11.4	302.18 ± 0.43
1050	4.60572	0.29588	15.566	123.47	99.2	8.9	301.05 ± 0.43
1100	4.35501	0.27563	15.800	63.52	99.3	8.3	305.21 ± 0.44
1150	12.03352	0.77649	15.497	68.46	99.8	23.5	299.82 ± 0.43
1200	7.73704	0.49625	15.591	70.76	99.7	15.0	301.49 ± 0.43
1250	4.26541	0.27485	15.519	19.59	99.3	8.3	300.20 ± 0.43
1400	1.13801	0.07312	15.564	5.63	98.2	2.2	301.01 ± 0.89
Total gas age:299.11 ± 0.47 Ma; weighted mean age (steps 3–13):301.61 ± 0.49 IVh; Isochron age (steps 3–9):303.8 ± 0.9 Ma;($^{40}Ar^{36}Ar$)1260 ± 22							
TD-5/#59/DD91, sanidine; 108.9 mg; J-value = .011615 ± 0.1%							
800	3.30968	0.21635	15.298	53.27	96.7	2.7	295.04 ± 1.03
850	2.27823	0.14727	15.469	171.46	99.4	1.8	298.10 ± 0.99
900	4.74052	0.30478	15.554	51.58	99.8	3.7	299.59 ± 0.97
950	6.62392	0.43131	15.358	1133.07	99.6	5.3	296.11 ± 1.24
1050	11.91842	0.78512	15.180	96.13	99.8	9.6	292.95 ± 0.63
1100	13.02305	0.89463	14.557	99.91	99.9	11.0	281.81 ± 0.41
1150	15.04395	0.97026	15.505	67.75	99.9	11.9	298.73 ± 0.43
1200	22.28623	1.43013	15.583	114.75	99.9	17.5	300.12 ± 0.43
1250	12.30499	0.79372	15.503	128.48	99.8	9.7	298.69 ± 15.86
1300	17.9828	1.15495	15.570	147.35	99.9	14.2	299.88 ± 2.18
1350	12.54225	0.79953	15.687	118.80	99.5	9.8	301.96 ± 0.47
1400	2.48965	0.15928	15.630	114.69	99.3	2.0	300.95 ± 0.43
1450	1.07777	0.06893	15.637	26.48	99.0	0.8	301.07 ± 1.26
Total gas age: 296.89 ± 2.24 Ma; weighted mean age (steps 3–13): 301.61 ± 0.49 Ma; Isochron age (steps 7–13): 299.9 ± 0.61 Ma; ($^{40}Ar/^{36}Ar$)1534 ± 122							

[a] Abundance of $^{40}Ar_R$ (radiogenic ^{40}Ar) and $^{39}Ar_K$ (K-derived ^{39}Ar) is measured in volts and calculated to five decimal places. Voltage may be converted to moles using 1.160×10^{-12} mol argon per volt signal. $^{40}Ar_R/^{39}Ar_K$ is calculated to three decimal places. All three are rounded to significant figures using analytical precision.

[b] Corrected for mass discrimination. Mass discrimination was determined by calculating the $^{40}Ar/^{36}Ar$ ratio of aliquots of atmospheric argon pipetted from a fixed pipette on the extraction line; the ratio during these experiments was between 298.5 and 299.1, which was corrected to 295.5 to account for mass discrimination. $^{40}Ar_R/^{39}Ar_K$ was also corrected for all interfering isotopes of argon including atmospheric argon. ^{37}Ar and ^{39}Ar, which are produced during irradiation, are radioactive, and their abundances were corrected for radioactive decay. Abundances of interfering isotopes from K and Ca were calculated from reactor production ratios determined by irradiating and analyzing pure CaF_2 and K_2SO_4 the K_2SO_4 was degassed in a vacuum furnace prior to irradiation to release extraneous argon. Corrections for Cl-derived ^{36}Ar were determined using the method of Roddick (1987). Production ratios for this experiment were determined for $(^{40}Ar/^{39}Ar)_K$, $(^{38}Ar/^{39}Ar)_K$, $(^{37}Ar/^{39}Ar)_K$, $(^{36}Ar/^{37}Ar)_{Ca}$, $(^{39}Ar/^{37}Ar)_{Ca}$, and $(^{38}Ar/^{37}Ar)_{Ca}$; measured values are available upon request.

[c] To calculate apparent K/Ca ratios, divide the $^{39}ArK/_{37}Ar_{Ca}$ by 2. The accuracy of apparent K/Ca ratios is dependent upon fast to thermal neutron ratios in the particular reactor. In the U.S. Geological Survey TRIGA reactor the correction factor has not been determined since Dalrymple et al. (1981). Because reactor fuel in the USGS TRIGA has been changed since 1981, this ratio must be viewed as approximate but is internally consistent for each sample and reveals within-sample variability.

[d] Apparent ages and associated errors were calculated from raw analytical data and then rounded using associated analytical errors. Apparent ages of each fraction include the error in *J* value (0.11%), which was calculated from the reproducibility of splits of the argon from several standards. Apparent ages were calculated using decay constants of Steiger and Jäger (1977). All apparent age errors are cited at is. Uncertainties in the calculations for apparent age of individual fractions were calculated using equations of Dalrymple et al. (1981) and the critical value test of McIntyre (1963).

all mounted grains (not shown) to aid in the spot selection to perform the SHRIMP analyses. In addition, scanning electron microscope-cathodoluminescence images (SEM-CL) of all zircons (not shown) were obtained at the U.S. Geological Survey Ion Microprobe Facility using a JEOL 6000 instrument and at Stanford University using a JOEL 5600 instrument prior to analysis, and used to reveal internal zoning

Table D
U–Th–Pb analytical data for SHRIMP spot analyses on zircon grains in sample TRiO.

Spot name	Comments core/rim?	Common ^{206}Pb	U (ppm)	Th (ppm)	Th/U	$^{238}U/^{206}Pb^*$	Error (%)	$^{207}Pb/^{206}Pb^*$	Error (%)	$^{206}Pb/^{238}U^{\#}$	Error (%)	$^{206}Pb/^{238}U^{\#}$ Age (Ma)	Error (%)
TRiO-1	Core	0.21	430	172	0.41	21.6	±0.52	0.0536	±1.58	0.0464	±0.51865	**291.9**	±1.5
TR1O-2	Core	0.11	353	167	0.49	21.2	±0.57	0.0541	±1.73	0.0472	±0.56746	**296.4**	±1.7
TR1O-3	Core	0.60	122	85	0.72	21.0	±0.95	0.0552	±2.85	0.0476	±0.94870	**298.6**	±2.8
TR1O-4	Discordant; core	0.32	123	61	0.51	20.6	±1.12	0.0501	±3.06	0.0486	±1.11975	**306.8**	±3.4
TR1O-5	Core	0.31	339	150	0.46	21.4	±0.56	0.0529	±1.71	0.0466	±0.56380	**293.6**	±1.7
TR1O-6	Core	0.97	92	42	0.48	21.1	±1.10	0.0514	±3.41	0.0473	±1.09929	**298.5**	±3.3
TR1O-7	Core	0.44	394	181	0.47	21.2	±0.55	0.0524	±1.68	0.0472	±0.54963	**297.3**	±1.6
TR1O-8	Core	−0.20	153	82	0.55	21.0	±0.86	0.0514	±2.68	0.0475	±0.86294	**299.6**	±2.6
TR1O-9	Discordant; core	−0.18	273	122	0.46	20.8	±0.64	0.0526	±1.96	0.0481	±0.64156	302.8	±2.0
(2 sigma; MSWD = 2.17); mean 206Pb/238U age = 295.5 ± 2.6 Ma													

*Uncorrected atomic ratios.
#Atomic ratios and ages corrected for initial Pb using the amount of 207Pb.
Individual zircon ages in bold were used to calculate the weighted average 206PbP38U age and its MSWD (mean square of weighted deviates).
All errors given are at the 1 sigma level except for the weighted average $^{206}Pb/^{238}U$ age reported at 2 sigma.

related to chemical composition in order to avoid possible problematic areas within grains. The mounts were cleaned in 1 N HCl and distilled water to minimize surface related common lead, and gold-coated for maximum surface conductivity.

The U–Th–Pb analyses were made on variable amounts of individual zircon grains per sample (between 22 and 25). The primary oxygen ion beam (O_2-), operated at about 2–4 nA, excavated an area of about 20–40 μm in diameter (adjustable depending on grain size) to a depth of about 1–2 μm; sensitivity ranged from 5 to 30 cps per ppm Pb. Data for each spot were collected in sets of five scans through the mass range. Nine peaks are measured sequentially for zircons with a single collector: $^{90}Zr2^{16}O$, ^{204}Pb, background (0.050 mass units above ^{204}Pb), ^{206}Pb, ^{207}Pb, ^{208}Pb, ^{238}U, $^{248}Th^{16}O$, and $^{254}U^{16}O$. The reduced ratios were normalized to the zircon standard R33 (418.9 ± 0.4 Ma, U–Pb ID-TIMS age at 2σ; from monzodiorite, Braintree Complex, Vermont; Black et al., 2004). For the closest control of Pb/U ratios, one standard was analyzed after every four to five unknown samples. Uranium concentrations were monitored by analyzing a standard (MAD) with ~4200 ppm U composition. U and Pb concentrations are accurate to about 10–20%.

Isotopic data were reduced and plotted using the Squid 1.02 and IsoplotEx 3.00 programs of Ludwig (2001, 2003). Ages are ^{207}Pb-corrected $^{206}Pb/^{238}U$ ages. The preferred weighted mean $^{206}Pb/^{238}U$ ages in Table C are calculated at 2σ.

2. Results, discussions, and interpretations

2.1. IDTIMS results

Concordant U–Pb dates were obtained by the IDTIMS method from 35 of 36 analyses composed of single grains and fragments of grains from four samples of volcanic ash (Table B and Fig. B). The $^{206}Pb/^{238}U$ dates are used to calculate weighted mean dates, based on 3–8 analyses per sample that are equivalent in age, with Isoplot 3.0 (Ludwig, 2003). Errors on the weighted mean dates are internal errors based on analytical uncertainties only, including counting statistics, subtraction of tracer solution, and blank and initial common Pb subtraction. They are given at the 95% confidence interval, which is the internal 2σ error for samples with MSWD < 1.2 and the internal 2σ error expanded by the square root of the MSWD and the Student's T multiplier of n-1 degrees of freedom for samples with MSWD > 1.2. These errors should be considered when comparing our dates with $^{206}Pb/^{238}U$ dates from other laboratories that used the same EARTHTIME tracer solution or a tracer solution that was cross-calibrated using EARTHTIME gravimetric standards. When comparing our dates with those derived from other decay schemes (e.g., $^{40}Ar/^{39}Ar$, ^{187}Re-^{187}Os), systematic uncertainties in the tracer calibration and ^{238}U decay constant (Jaffey et al., 1971) should be added to the internal error in quadrature.

2.1.1. TR10

Eight analyses from sample TR-10 yielded a weighted mean of 301.26 ± 0.05 Ma (MSWD = 1.1), which is interpreted as the age of deposition. Including systematic uncertainties in the tracer calibration and ^{238}U decay constant increases the error to ± 0.67 Ma. One other grain that is 3.5 Ma older is thought to be detrital or inherited in the magma that produced the volcanic ash.

2.1.2. TRN8

Seven analyses from five grains from sample TRN-8 yielded a weighted mean of 253.11 ± 0.05 Ma (MSWD = 1.2), which is interpreted as the age of deposition. Including systematic uncertainties in the tracer calibration and ^{238}U decay constant increases the error to ± 0.57 Ma. Three of these analyses are fragments from one grain that yielded a weighted mean of 253.12 ± 0.21 Ma (MSWD = 1.8). Two other grains that are slightly older are thought to be detrital or inherited in the magma that produced the volcanic ash.

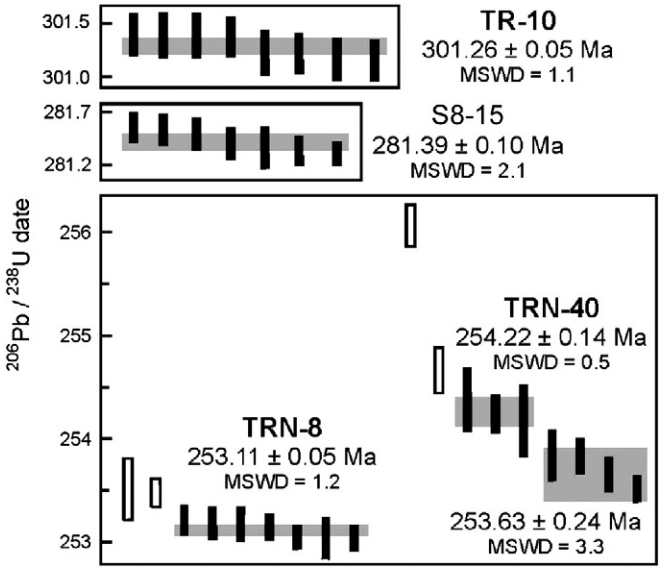

Fig. B. Plot of $^{206}Pb/^{238}U$ dates from single grains and fragments of zircon analyzed by the IDTIMS method. Plotted with Isoplot 3.0 (Ludwig, 2003). Error bars are at the 95% confidence interval. Weighted mean dates are shown and represented by the gray boxes behind the error bars. Error bars shown in white were not used in the weighted mean calculations. Three older grains are not plotted.

2.1.3. TRN40

Four analyses from two grains from sample TRN-40 yielded a weighted mean of 253.63 ± 0.24 Ma (MSWD = 3.3). Including systematic uncertainties in the tracer calibration and ^{238}U decay constant increases the error to ± 0.58 Ma. Three other analyses yielded a weighted mean of 254.22 ± 0.24 Ma (MSWD = 0.5). Including systematic uncertainties in the tracer calibration and ^{238}U decay constant increases the error to ± 0.58 Ma. Two other grains are slightly to moderately older. A depositional age cannot be interpreted due to the possibility that all dated grains are detrital or inherited in the magma that produced the volcanic ash; deposition occurred after crystallization of the youngest two grains that yielded a weighted mean of 253.63 ± 0.24 Ma.

2.1.4. S8-15

Seven analyses from six grains from sample S8-15 yielded a weighted mean of 281.39 ± 0.10 Ma (MSWD = 2.1), which is interpreted as the age of deposition. Including systematic uncertainties in the tracer calibration and ^{238}U decay constant increases the error to ± 0.63 Ma. Two fragments from one grain that are ~4 Ma older are thought to be from a grain that is detrital or inherited in the magma that produced the volcanic ash.

2.2. Ar/Ar results (Fig. C)

2.2.1. TD5 (biotite)

The age spectrum for this sample indicates that there was little chlorite present. This sample did not produce a plateau age. However, we assign a weighted mean age of 301.61 ± 0.449 Ma. An Isochron for this sample yielded a slightly older age of 303.8 ± 0.9 Ma.

2.2.2. TD5 (sanidine)

Sanidine from the ash-flow tuff is discordant. It is impossible to determine if the discordant spectrum is related to the presents of xenocrystic sanidine, or from instability of the instrument at the time of analyses as suggested by step #9, which yielded uncertainties of 15 Ma. This sample needs to be reanalyzed to determine the nature of the discordancy. However, despite the discordance nature of the age spectrum, we assign an Isochron age of 299.9 ± 0.6 Ma. This age is similar to the weighted mean age of 300 ± 3 Ma for the last 7 heating steps, but the uncertainty is larger.

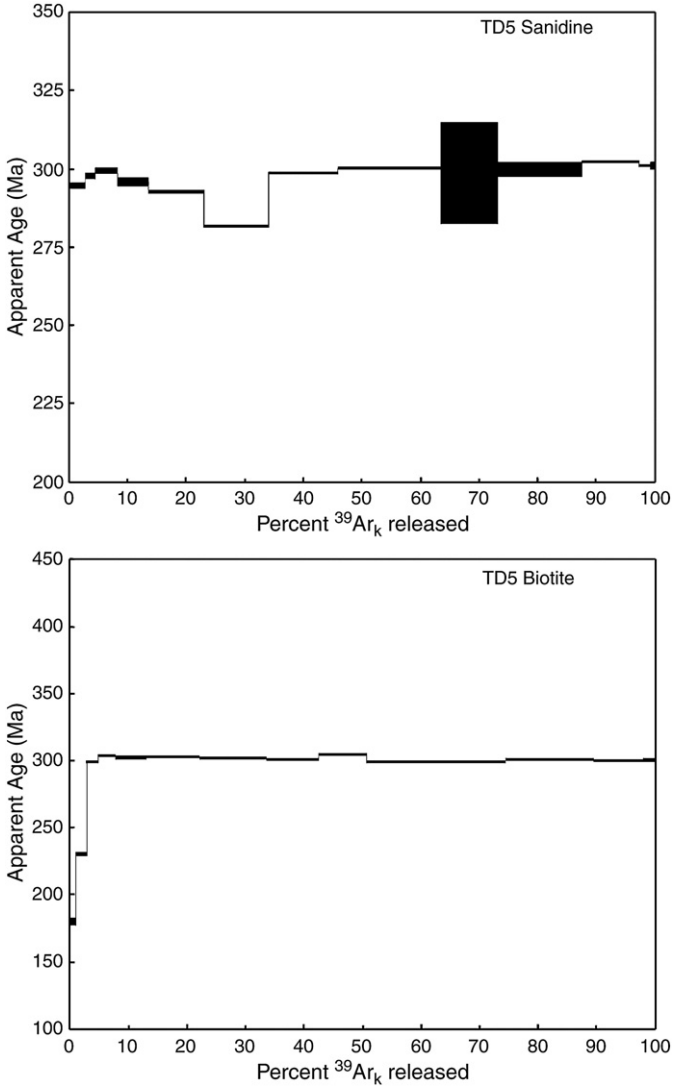

Fig. C. Age spectra of sanidine (upper) and biotite (lower) in Sample TD5 obtained through $^{39}Ar/^{40}Ar$ geochronological analysis in this study.

2.3. SHRIMP results

2.3.1. TR10

Zircons analyzed at the USGS/Stanford SHRIMP-RG facility yielded a mean $^{206}Pb/^{238}U$ age of 295.5 ± 2.6 Ma. Spot numbers 4 and 9 were not included in the mean age (Fig. D and Table D).

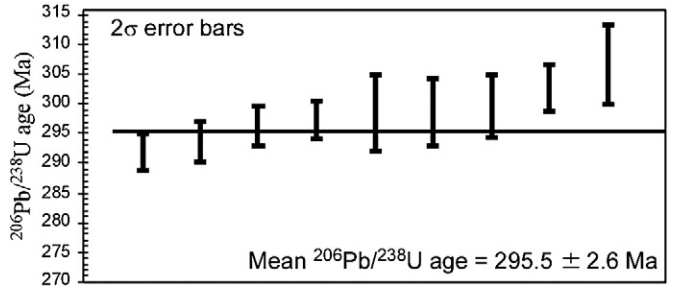

Fig. D. Plot of $^{206}Pb/^{238}U$ dates from single grains and fragments of zircon in Sample TR10 analyzed by the SHRIMP-RG method. Plotted with Isoplot 3.0 (Ludwig, 2003). See Table D for details.

Appendix A. Supplementary data

Supplementary data associated with this article can be found, in the online version, at doi:10.1016/j.gloplacha.2010.03.008.

References

Allen, M.B., Sengor, A.M.C., Natal'in, B.A., 1995. Junggar, Turfan and Alakol basins as Late Permian to ?Early Triassic extensional structures in a sinistral shear zone in the Altaid orogenic collage, Central Asia. J. Geol. Soc. London 152, 327–338.

Black, L.P., Kamo, S.L., Allen, C.M., Davis, D.W., Aleinikoff, J.N., Valley, J.W., Mundil, R., Campbell, I.H., Korsch, R.J., Williams, I.S., Foudoulis, C., 2004. Improved $^{206}Pb/^{238}U$ microprobe geochronology by the monitoring of a trace–element-related matrix effect; SHRIMP, ID-TIMS, ELA-ICP-MS and oxygen isotope documentation for a series of zircon standards. Chem. Geol. 205, 115–140.

Brand, U., Yochelson, E.L., Eagar, R.M., 1993. Geochemistry of Late Permian non-marine bivalves: implications for the continental paleohydrology and paleoclimatology of northwestern China. Carbonates Evaporites 8, 199–212.

Brown Jr., L.F., Fisher, W.L., 1977. Seismic-stratigraphic interpretation of depositional systems: examples from Brazilian rift and pull-apart basins. In: Payton, C.E. (Ed.), Seismic Stratigraphy — Applications to Exploration: Mem. Am. Assoc. Pet. Geol., 26, pp. 213–248.

Carroll, A.R., 1998. Upper Permian lacustrine organic facies evolution, southern Junggar Basin, NW China. Org. Geochem. 28, 649–667.

Carroll, A.R., Bohacs, K.M., 1999. Stratigraphic classification of ancient lakes: balancing tectonic and climatic controls. Geology 27, 99–102.

Carroll, A.R., Graham, S.A., Hendrix, M.S., Ying, D., Zhou, D., 1995. Late Paleozoic tectonic amalgamation of northwestern China: sedimentary record of the northern Tarim, northwestern Turpan, and southern Junggar Basins. Geol. Soc. Am. Bull. 107, 571–594.

Cheng, Z.-W., Lucas, S.G., 1993. A possible nonmarine GSSP for the Permian–Triassic boundary. Albertiana 12, 39–44.

Cheng, Z.W., Wu, S.Z., Fang, X.S., 1996. The Permian–Triassic sequences in the southern margin of the Junggar Basin and the Turpan Basin, Xinjiang, China. In: Hongfei, Hou, Jinsong, Zhou (Eds.), Field Trip Guide; Volume 1, Stratigraphy, Paleontology, Sedimentology, Petroleum and Coal Geology. 30th International Geological Congress. Geological Publishing House, Beijing, China.

Condon, D., et al., 2007. EARTHTIME; isotopic tracers and optimized solutions for high-precision U–Pb ID-TIMS geochronology: eos, transactions. Am. Geophys. Union 88 (52 Suppl.) Abstract V41E-06.

Crowley, J.L., Schoene, B., Bowring, S.A., 2007. U–Pb dating of zircon in the Bishop Tuff at the millennial scale. Geology 35, 1123–1126.

Dalrymple, G.B., Alexander Jr., E.C., Lanphere, M.A., Kraker, G.P., 1981. Irradiation of samples for 40Ar/39Ar dating using the Geological Survey TRIGA reactor. U.S. Geological Survey Professional Paper 1176. 55 pp.

Erwin, D.H., 1993. The great Paleozoic crisis: life and death in the Permian. In: Bottjer, D.J., Bambach, R.K. (Eds.), Critical Moments in Paleobiology and Earth History Series. Columbia University Press, New York, pp. 23–44.

Erwin, D.H., 2002. Testing alterative scenarios for the end-Permian extinction. Geol. Soc. of Australia, Abstracts Number 68, First Inter. Palaeontological Congress (IPC2002), p. 50.

Fielding, C.R., Frank, T.D., Birgenheier, L.P., Rygel, M.C., Jones, A.T., Roberts, J., 2008. Stratigraphic imprint of the Late Palaeozoic Ice Age in eastern Australia: a record of alternating glacial and nonglacial climate regime. J. Geol. Soc. London 65, 129–140.

Fleck, R.J., Sutter, J.F., Elliot, D.H., 1977. Interpretation of discordant 40Ar/39Ar age spectra of Mesozoic tholeiites from Antarctica. Geochim. Cosmochim. Acta 41, 15–32.

Foster, C., Metcalfe, I., 2002. Carbon isotopic composition of organic matter from non-marine Permian–Triassic boundary sections at Dalongkou and Lucaogou, Xinjiang, NW China. Geol. Soc. of Australia, Abstracts Number 68, First Inter. Palaeontological Congress (IPC2002), pp. 56–57.

Garner, H.F., 1959. Stratigraphic–sedimentary significance of contemporary climate and relief in four regions of the Andes Mountains. Bull. Geol. Soc. Am. 70, 1327–1368.

Gastaldo, R.A., Neveling, J., Clark, C.K., Newbury, S.S., 2009. The terrestrial Permian–Triassic boundary event bed is a non-event. Geology 37, 199–202.

Gerstenberger, H., Haase, G., 1997. A highly effective emitter substance for mass spectrometric Pb isotope ratio determinations. Chem. Geol. 136, 309–312.

Gibbs, M.T., Rees, P.Mc., Kutzbach, J.E., Ziegler, A.M., Behling, P.J., Rowley, D.B., 2002. Simulations of Permian climate and comparison with climate-sensitive sediments. J. Geol. 110, 33–55.

Lake basins through space and time. In: Gierlowski-Kordesch, E.H., Kelts, K.R. (Eds.), Geologists Studies in Geology. : Am. Assoc. Petrol., 46. Tulsa, Oklahoma.

Gradstein, F., Ogg, J., Smith, A. (Eds.), 2004. A Geologic Time Scale. Cambridge University Press, New York. 589 pp.

Greene, T.J., Carroll, A.R., Wartes, M., Graham, S.A., Wooden, J.L., 2005. Integrated provenance analysis of a complex orogenic terrane: Mesozoic uplift of the Bogda Shan and inception of the Turpan-Hami Basin, NW China. J. Sed. Res. 75, 251–267.

Guan, W., Yang, W., Jeffrey, B., Feng, Q., Liu, Y.Q., Zhao, W., Wang, Q.Y., 2010. Distinguishing source areas of Upper-Permian fluvial-lacustrine deltaic sediment fills of a half graben through petrographic study, southern Bogda Mountains, the Greater Turpan-Junggar basin, NW China: Abstract Volume, Am. Asso. Petrol. Geologists Annual Meeting, New Orleans, 95 pp.

Hendrix, M.S., Graham, S.A., Carroll, A.R., Sobel, E.R., McKnight, C.L., Schulein, B.J., Wang, Z., 1992. Sedimentary record and climatic implications of recurrent deformation in the Tian Shan: evidence from Mesozoic strata of the north Tarim, south Junggar, and Turpan basins, northwest China. Geol. Soc. Am. Bull. 104, 53–79.

Isozaki, Y., 1997. Permo–Triassic boundary superanoxia and stratified superocean: records from the lost deep sea. Science 276, 235–238.
Jaffey, A.H., Flynn, K.F., Glendenin, L.E., Bentley, W.C., Essling, A.M., 1971. Precision measurements of half-lives and specific activities of ^{235}U and ^{238}U:. Phys. Rev. C 4, 1889–1906.
Jeffrey, B., Yang, W., Feng, Q., and Liu, Y.Q., 2010, Nature and origin of a low-order cycle boundary in Lower–Permian fluvial–lacustrine deposits in a half graben, southern Bogda Mountains, NW China. Abstract Volume, Am. Assoc. Petrol. Geologists Annual Meeting, New Orleans, 121 pp.
Knoll, A.H., Bambach, R.K., Canfield, D.E., Grotzinger, J.P., 1996. Comparative Earth history and the Late Permian mass extinction. Science 273, 452–457.
Krogh, T.E., 1973. A low contamination method for hydrothermal decomposition of zircon and extraction of U and Pb for isotopic age determination. Geochim. Cosmochim. Acta 37, 485–494.
Kutzbach, J.E., Guetter, P.J., Washington, W.M., 1990. Simulated circulation of an idealized ocean for Pangaean time. Paleoceanography 5, 299–317.
Liao, Z., Lu, L., Jiang, N., Xia, F., Song, F., Zhou, Y., Li, S., Zhang, Z., 1987. Carboniferous and Permian in the western part of the east Tianshan Mountains. Eleventh Congress of Carboniferous Stratigraphy and Geology, Guidebook Excursion 4. Beijing, China, 50 pp.
Liu, Zhaosheng, 2000. The Permo–Triassic boundary at the northern margin of Tu–Ha Basin. J. Stratigr. 24, 310–314 (in Chinese with English abstract).
Ludwig, K.R., 2001. SQUID, version 1.02, A User's Manual. Berkeley Geochronology Center, Special Publication 2. 17 pp.
Ludwig, K.R., 2003. ISOPLOT, version 3.00, A Geochronological Toolkit for Microsoft Excel. Berkeley Geochronology Center, Special Publication 4. 70 pp.
Mack, G.H., James, W.C., 1994. Paleoclimate and the global distribution of paleosols. J. Geol. 102, 360–366.
Mack, G.H., James, W.C., Monger, H.C., 1993. Classification of paleosols. Geol. Soc. Am. Bull. 105, 129–136.
Mattinson, J.M., 2005. Zircon U–Pb chemical abrasion ("CA-TIMS") method: combined annealing and multi-step partial dissolution analysis for improved precision and accuracy of zircon ages. Chem. Geol. 220, 47–66.
McIntyre, D.B., 1963. Precision and resolution in geochronometry. In: Albritton Jr., C.C. (Ed.), The Fabric of Geology. Addison-Wesley, Reading, Massachusetts, pp. 112–134.
Metcalfe, I., Foster, C.B., Afonin, S.A., Nicoll, R.S., Mundil, R., Xiaofeng, Wang, Lucas, S.G., 2008. Stratigraphy, biostratigraphy and C-isotopes of the Permian–Triassic non-marine sequence at Dalongkou and Lucaogou, Xinjiang Province, China. J. Asian Earth Sci. 36, 503–520.
Miall, A.D., 1996. The Geology of Fluvial Deposits: Sedimentary Facies, Basin Analysis, and Petroleum Geology. Springer, New York. 582 pp.
Miall, A.D., 2006. Reconstructing the architecture and sequence stratigraphy of the preserved fluvial record as a tool for reservoir development: a reality check. Am. Assoc. Petrol. Geol. Bull. 90, 989–1002.
Miggins, D.P., Thompson, R.A., Pillmore, C.L., Snee, L.W., Stern, C.R., 2002. Extension and uplift of the northern Rio Grande Rift: evidence from $^{40}Ar/^{39}Ar$ geochronology from the Sangre de Cristo Mountains, south-central Colorado and northern New Mexico. In: Menzies, M.A., Klemperer, S.L., Ebinger, C.J., Baker, J. (Eds.), Volcanic Rifted Margins: Geological Society of America Special Paper, vol. 362, pp. 47–64.
Miggins, D.P., Blome, C.D., Smith, D.V., 2004. Preliminary 40Ar/39Ar geochronology of igneous intrusions from Uvalde County, Texas: defining a more precise eruption history for the southern Balcones Volcanic Province. U.S. Geological Survey Open File Report 2004–1031. 31 pp.
Mitchum Jr., R.M., Van Wagoner, J.C., 1991. High-frequency sequences and their stacking patterns: sequence-stratigraphic evidence of high-frequency cycles. Sed. Geol. 70, 131–160.
Montañez, I.P., Tabor, N.J., Niemeier, D., DiMichele, W.A., Frank, T.D., Fielding, C.R., Isbell, J.L., 2007. CO-forced climate and vegetation instability during Late Paleozoic Deglaciation. Science 315, 87–91.
Nourse, J.A., Premo, W.R., Iriondo, A., Stahl, E.R., 2005. Contrasting Proterozoic basement complexes near the truncated margin of Laurentia, northwestern Sonora–Arizona international border region. In: Anderson, T.H., Nourse, J.A., McKee, J.W., Steiner, M.B. (Eds.), The Mojave–Sonora Megashear Hypothesis: Development, Assessment, and Alternatives: Geological Society of America Special Paper, vol. 393, pp. 123–182.
Olsen, P.E., 1997. Stratigraphic record of the Early Mesozoic breakup of Pangea in the Laurasia–Gondwana rift system:. Annu. Rev. Earth Planet. Sci. 25, 337–401.
Parrish, J.T., 1993. Climate of the supercontinent Pangea. J. Geol. 101, 215–233.
Retallack, G.J., 1990. Soils of the past — an introduction to paleopedology. Unwin Hyman, Boston. 520 pp.
Retallack, G.J., Veevers, J.J., Morant, R., 1996. Global coal gap between Permian–Triassic extinction and Middle Triassic recovery of peat-forming plants. Geol. Soc. Am. Bull. 108, 195–207.
Retallack, G.J., Smith, R.M.H., Ward, P.D., 2003. Vertebrate extinction across Permian–Triassic boundary in Karoo Basin, South Africa. Geol. Soc. Am. Bull. 115, 1133–1152.
Retallack, G.J., Metzger, C.A., Greaver, T., Jahren, A.H., Smith, R.M.H., Sheldon, N.D., 2006. Middle–Late Permian mass extinction on land. Geol. Soc. Am. Bull. 118, 1398–1411.
Roddick, J.C., 1987. Generalized numerical error analysis with applications to geochronology and thermodynamics. Geochim. Cosmochim. Acta 51, 2129–2135.
Scheffler, K., Buehmann, D., Schwarck, L., 2006. Analysis of late Palaeozoic glacial to postglacial sedimentary successions in South Africa by geochemical proxies — response to climate evolution and sedimentary environment. Palaeogeogr. Palaeoclimatol. Palaeoecol. 240, 184–203.
Schmitz, M.D., Schoene, B., 2007. Derivation of isotope ratios, errors and error correlations for U–Pb geochronology using ^{205}Pb–^{235}U–(^{233}U)-spiked isotope dilution thermal ionization mass spectrometric data. Geochem. Geophys. Geosyst. 8, Q08006. doi:10.1029/2006GC001492 (G3).
Schumm, S.A., 1968. Speculations concerning paleohydrologic controls of terrestrial sedimentation. Geol. Soc. Am. Bull. 79, 1573–1588.
Scotese, C.R., 2001. Atlas of Earth History, Volume 1, Paleogeography. PALEOMAP Project, Arlington, Texas. 52 pp.
Sengor, A.M.C., Nat'lin, B.A., 1996. Paleotectonics of Asia: fragments of a synthesis. In: Yin, A., Harrison, T.M. (Eds.), The Tectonic Evolution of Asia. Cambridge University Press, New York, pp. 486–640.
Shanley, K.W., McCabe, P.J., 1994. Perspectives on the sequence stratigraphy of the continental strata. Am. Asso. Petrol. Geol. Bull. 78, 544–568.
Shao, L., Stattegger, K., Li, W., Haupt, B.J., 1999. Depositional style and subsidence history of the Turpan Basin (NW China). Sed. Geol. 128, 155–169.
Shao, L., Stattegger, L., Garbe-Schoenberg, C.-D., 2001. Sandstone petrology and geochemistry of the Turpan Basin (NW China): implications for the Tectonic evolution of a continental basin. J. Sediment. Res. 71, 37–49.
Snee, L.W., 2002. Argon thermochronology of mineral deposits — a review of analytical methods, formulations, and selected applications. U.S. Geol. Surv. Bull. 2194 39 pp.
Steiger, R.H., Jäger, E., 1977. Subcommission of geochronology: convention on the use of decay constants in geo- and cosmochronology. Earth Planet. Sci. Lett. 36, 359–362.
Stollhofen, H., Stanistreet, I.G., Bangert, B., Grill, H., 2000. Tuffs, tectonism, and glacially related sea-level changes, Carboniferous–Permian in southern Namibia. Palaeogeogr. Palaeoclimatol. Palaeoecol. 161, 127–150.
Tabor, N.J., Montanez, I.P., Steiner, M., Schwindt, D., 2007. The δ13C values of Permo–Triassic carbonates from South Africa reflect a stinking, sulfurous swamp, not atmospheric conditions. Palaeogeogr. Palaeoclimatol. Palaeoecol. 252, 370–381.
Talbot, M.R., Allen, P.A., 1996. Lakes. In: Reading, H.G. (Ed.), Sedimentary Environments: Processes, Facies and Stratigraphy. Blackwell Science, London, pp. 83–124.
Thomas, S., Tabor, N., Yang, W., 2007. Evaluation of pedogenic calcite nodules from the Jiucaiyuan Fm, NW China: implications for earliest Triassic atmospheric pCO_2. Geol. Soc. Am. Abstract with Programs, v. 39, Annual Meeting, p. 497. Denver.
Ward, P.D., Botha, J., Buick, R., De Kock, M.O., Erwin, D.H., Garrison, G.G., Kirschvink, J.L., Smith, R., 2005. Abrupt and gradual extinction among Late Permian land vertebrates in the Karoo Basin, South Africa. Science 307, 709–714.
Wartes, M.A., Carroll, A.R., Greene, T.J., 2002. Permian sedimentary record of the Turpan–Hami Basin and adjacent regions, Northwest China; constraints on postamalgamation tectonic evolution. Geol. Soc. Am. Bull. 114, 131–152.
Williams, I.S., 1998. U–Th–Pb geochronology by ion microprobe. In: McKibben, M.A., Shanks, W.C. (Eds.), Applications of Microanalytical Techniques to Understanding Mineralizing Processes: Reviews in Economic Geology, vol. 7, pp. 1–35.
Yang, W., 2007. Transgressive wave ravinement on an epeiric shelf as recorded by a soil–nodule conglomerate-sandstone unit, the Upper Pennsylvanian Oread Cyclothem, southeastern Kansas and northeastern Oklahoma. Sed. Geol. 197, 189–205.
Yang, W., 2008. Depositional Systems Analysis within a Seismic Sequence Stratigraphic Framework, Turpan-Hami Basin, NW China. Tu-Ha Oil Company Internal Report, PetroChina. 49 pp.
Yang, W., Liu, Y., Feng, Q., Lin, J., Zhou, D., Wang, D., 2007a. Sedimentary evidence of Early–Late Permian mid-latitude continental climate variability, southern Bogda Mountains, NW China. Palaeogeogr. Palaeoecol. Palaeoclimatol. 252, 239–258.
Yang, W., Feng, Q., Liu, Y.Q., Tabor, N., Thomas, S., Yang, Y., Sun, G.Z., Sun, B., 2007b. Promises and problems of two-dimensional nonmarine sequence stratigraphic analysis using hierarchical depositional cycles — an example from outcrop Lower Permian to Lower Triassic fluvial–lacustrine deposits, Southern Bogda Mountains, Turpan Intermontane Basin, NW China. Am. Assoc. Petrol. Geologists Annual Meeting, Abstracts Volume, p. 154.
Yang, W., Guan, W., Wang, Y., Feng, Q., Liu, Y.Q., Tabor, N., 2008. Limestone–sandstone clinoforms in Middle-Permian lacustrine deposits, Bogda Mountains, NW China — implications for progradational infilling of intermontane Lake Basins. Am. Assoc. Petrol. Geologists Annual Meeting, Abstracts Volume, p. 226. San Antonio, Texas.
Yang, Wan, Feng, Q., Guan, W., Lin, J., Liu, Y.Q., 2009. Wither nonmarine sequence stratigraphy? sequence stratigraphic correlation of Lower Permian fluvial–lacustrine deposits in a half graben, Bogda Mountains, NW China. Am. Assoc. Petrol. Geologists Annual Meeting, Abstracts Volume, p. 226. Denver, Colorado.
Yin, H.F., Zhang, K., Tong, J., Yang, Z., Wu, S., 2001. The global stratotype section and point (GSSP) of the Permian–Triassic Boundary. Episodes 24 (2), 102–114.
York, D., 1969. Least squares fitting of a straight line with correlated errors. Earth Planet. Sci. Lett. 5, 320–324.
Zhang, X., 1981. Regional Stratigraphic Chart of northwestern China, Branch of Xinjiang Uygur Autonomous Region. Geological Publishing House, Beijing. 496 pp. (in Chinese).
Zhou, T., Li, X., Yang, J., Hou, J., Liu, S., Cheng, Z., Wu, S., Li, Y., 1997. Research on Chinese nonmarine Permo–Triassic GSSP sections. Xinjiang Geology 15, 211–225 (in Chinese with English abstract).
Zhu, H.-C., Ouyang, S., Zhan, J.-Z., Wang, Z., 2005. Comparison of Permian palynological assemblages from the Junggar and Tarim basins and their phytoprovincial significance. Rev. Palaeobot. Palynol. 136, 181–207.
Ziegler, A.M., Hulver, M.L., Rowley, D.B., 1997. Permian world topography and climate. In: Martini, I.P. (Ed.), Late Glacial and Postglacial Environmental Changes: Pleistocene, Carboniferous–Permian, and Proterozoic. Oxford University Press, Oxford, pp. 111–146.